NUMERICAL SIMULATION AND EXPERIMENTAL STUDY OF ROOT ANCHORAGE

ABDOLHOSSEIN KHALILNEJAD

THESIS SUBMITED IN FULLFILMENT

OF THE REQUIREMENTS

FOR THE DEGREE OF DOCTOR OF PHILOSOPHY

FACULTY OF ENGINEERING

UNIVERITY OF MALAYA

KUALA LUMPUR

2013

UNIVERSITY OF MALAYA
ORIGINALITY LITERARY WORK DECLORATION

Name of Candidate: **ABDOLHOSSEIN KHALILNEJAD**

Registration/Matric No: **KHA 080084**

Name of Degree: **DOCTOR OF PHILOSOPHY**

Title of Thesis:

NUMERICAL SIMULATION AND EXPERIMENTAL STUDY OF ROOT ANCHORAGE

Field of study: **CIVIL ENGINEERING-GEOTECHNICAL ENGNINEERING**

I do solemnly and sincerely declare that:

(1) I am the sole author/writer of this work;

(2) This work is original;

(3) Any use of any work in which copyright exists was done by way of fair dealing and for permitted purposes and any excerpt or extract from, or reference to or reproduction of any copyright work has been disclosed expressly and sufficiently and the title of the work and its authorship have been acknowledged in this work;

(4) I do not have any actual knowledge nor do I ought reasonably to know that the making of this work constitutes an infringement of any copyright work;

(5) I hereby assign all and every rights in the copyright to this work to the University of Malaya (UM), who henceforth shall be owner of copyright in this work and that any reproduction or use in any form or by any means whatsoever is prohibited without the written consent of UM having been first had one obtained;

(6) I am fully aware that if in the course of making this work I have infringed any copyright whether intentionally or otherwise, I may be subject to legal action or any other action as may be determined by UM.

Candidate signature   Date

Subscribed and solemnly declared before,

Witness's signature   Date

Name:

Designation

I hereby declared that this thesis is based on the results found by myself. Material and work found by other researchers are mentioned by references. This thesis is neither in whole nor in part has been previously submitted for any degree.

Date   Signature

                                                                        ABDOLHOSSEIN KHALILNEJAD

ABSTRACT

Understanding the mechanism of root anchorage in soil slope is important in order to study the effects of vegetation roots on land sliding, especially in the subtropical and tropical areas with the dense herb coverage. A generic 3D finite element model has been widely used in recent years to characterize the anchorage mechanisms by the pulling out where each component of the anchorage can be tested individually. Despite the common usage of finite element simulation, few restrictions are causing inaccuracy in simulation result. To overcome those restrictions, in this research the root system was simulated and alternative root soil interaction was evaluated. In order to achieve a better understanding of pulling out effect on soil, the Mises stress and logarithmic strain distribution curve was studied. The effect of root architect and soil parameters such as soil cohesion and soil friction angle using improved root model were also examined.

Simulation during this study was carried out using FEM software ABAQUS 6.10.ef and analysis method chosen was Explicit (semi static) method.

To achieve the comparable result to reality, the root and soil mechanical properties were identified and measured during laboratory tests and pulling out process for *Melastoma malabathricum*.

Based on the experimental results, the uplifting force is higher for plants with higher root volumes and thicker lateral roots. According to the simulation results, it is found that the distribution of Mises stress and logarithmic strain in soil is highly dependent on the depth and width range of the roots. The main factor affecting the Mises stress and the logarithmic strain distribution is the rooting length and root geometry. The concentrations and amount of stress were more apparent in the model with long taproot. In the process of changing in root architecture, it appears that the

most insistent root architecture against the pull out is the root with branches of horizontal deviation angle that is equal to 53˚. By changing the soil properties, it is discovered that the friction angle is affecting roots pull out capacity even with small root inclination angle. The pull out resistance increases with increasing friction angle. In the case of changing the soil cohesion, it is found that the soil cohesion value denotes direct proportion to root anchorage. However, in soil with higher plasticity as CH (fat clay), the effect of soil cohesion is the maximum with the increase of the silt content. With the reduction of plasticity, the soil cohesion effect also decreases.

In conclusion, this study discovered that during the pulling out, Mises stress and consequently logarithmic strain distribution are more concentrated on root and soil effect is limited to almost 25% of final displacement. Therefore, the root architecture such as long taproot, root pattern and root branches deviation angle, playing more important role than soil characteristics such as soil cohesion and soil friction angle. Validation of the simulation result was carried out by comparing the simulation result with experimental pull out result and also with those in well control laboratory test.

ABSTRAK

Memahami mekanisme penambat akar dalam cerun tanah telah menjadi keutamaan disebabkan kesan akar tumbuh-tumbuhan di atas tanah runtuh, terutama di kawasan subtropika dan tropika dengan liputan herba padat. Untuk mencirikan mekanisme tempat penambat menarik keluar, model unsur terhingga 3D generik telah digunakan secara meluas dalam tahun-tahun kebelakangan ini di mana setiap komponen penambat boleh diuji secara individu. Walaupun penggunaan biasa simulasi unsur terhingga, banyak sekatan telah menyebabkan ketidaktepatan dalam keputusan penyelakuan. Untuk mengatasi masalah sekatan itu, kajian ini bertujuan untuk mensimulasikan akar dan interaksi tanah akar alternatif telah dinilai. Bagi mencapai pemahaman yang lebih baik kesun menarik keluar akar ke atas tanah, tekanan Mises dan lengkung taburan ketegangan logaritma telah dikaji. Kesan arkitek akar dan parameter tanah seperti perpaduan dan sudut geseran tanah dengan menggunakan model akar yang olitumbah-baik juga telah diperiksa.

Simulasi dalam kajian ini telah dijalankan menggunakan perisian FEM ABAQUS 6.10.ef dan kaedah analisis yang dipilih adalah kaedah 'Explicit' (separuh statik).

Untuk mencapai hasil yang setanding dengan realiti, sifat mekanikal akar dan tanah telah dikenal pasti dan diukur semasa ujian makmal dan proses tarik-keluar akar *Melastoma malabathricum*.

Berdasarkan keputusan-keputusan eksperimen, daya tarikan la atao adalah lebih tinggi bagi tumbuh-tumbuhan yang mempunyai isi padu akar yang lebih tinggi dan akar sisi yang lebih tebal. Menurut keputusan simulasi, didapati bahawa taburan tekanan Mises dan ketegangan logaritma dalam tanah adalah sangat bergantung kepada kedalaman dan julat lebar akar. Faktor utama yang mempengaruhi tekanan Mises dan taburan ketegangan logaritma adalah panjang dan geometri akar. Kepekatan dan jumlah

tekanan adalah lebih ketara dilihat dalam model dengan akar tunjang yang panjang. Dalam proses perubahan dalam corak jalinan akar, ternyata bahawa corak jalinan akar yang paling nyata terkesan terhadap penarikan keluar ialah akar dengan sudut sisihan mendatar 53°. Dengan menukar sifat-sifat tanah, didapati bahawa sudut geseran memberikesun ke atao kapasiti tarik keluar akar walaupun dengan akar sudut kecenderungan kecil. Rmtangan tarik keluar menjukat dengan peningkatan sudut geseran. Dalam hal mengubah perpaduan tanah, didapati bahawa nilai tanah perpaduan menandakan nisbah langsung tempat terhadap penombitan akar. Walau bagaimanapun, tanah dengan keplastikan tinggi sebagai CH (lemak tanah liat), kesan perpaduan tanah adalah maksimum dengan peningkatan kandungan kelodak. Dengan mengurangkan keplastikan, kesan tanah perpaduan juga berkurangan.

Sebagai kesimpulan, kajian ini mendapati bahawa semasa proses menarik keluar, akar, tekanan Mises dan seterusnya agihan ketegangan logaritma adalah lebih tertumpu pada akar dan kesan tanah yang terhad kepada hampir 25% daripada anjakan akhir. Oleh itu, corak jalinan akar seperti akar tunjang, corak akar dan sudut sisihan akar cawangan, memainkan peranan yang lebih penting daripada sifat-sifat tanah seperti perpaduan tanah dan sudut geseran tanah. Pengesahan keputusan simulasi telah dijalankan dengan membandingkan hasil simulasi dengan hasil eksperimen menarik keluar dan juga hasil ujian makmal ke atas kawalan.

ACKNOWLEDGEMENT

The grace of God has enabled the completion of this thesis.

The guidance and advice provided by Professor Dr. Faisal Haji Ali is much appreciated.

The author is grateful to Professor Dr. Roslan Hashim, Associate Professor Dr. Normaniza Osman and Dr. Saravanan Marapian for their guidance, support and comments in all aspects of this study.

Many thanks to those who supported me to finalize this thesis.

Finally, the support, love and understanding of my wife, Tala, and the apples of my eyes, Bahar & Baran was a great contribution.

TABLE OF CONTENTS

LIST OF TABLES

LIST OF FIGURES

LIST OF SYMBOLS AND ABBREVIATIONS

Ψ- Deliation angle

ϕ- Friction angle

c- Cohesion coefficient

σ- Total stress

u- Horizontal displacement

ua- Pore air pressure

uw- Pore water pressure

Cae- Extension for Abaqus modeling

TXT- Extension for word

Xls- Extension for Excel program

Φ'- Effective angle of internal friction

F- Slope Safety Factor

B- Slope slips surface angle

z- Slope slips surface depth

γ- Soil unit weight

h_w- water table level

c'- Effective cohesion coefficient

w- Surcharge weight

D- Wind load

T- Tensile root stress

A_r- Area of root reinforcement

Φ^b- The rate of change in soil shear strength with respect to matric suction

N_c, N_q, N_γ – Bearing capacity factor

E- Young modulus

I-.Moment of inertia

L- Length of tie

δ'- Effective stress

C_s- Compress ability of grain

C- Compress ability of granular skeleton

CHAPTER 1:

INTRODUCTION

1.1. Introduction

Landslide is a geotechnical event which includes a wide range of ground movement such as rock falls, deep failure of slope and shallow debris flows. This event can cause problems in various civil engineering projects such as roads, dams and others. In December 11, 1993, a 12-storey condominium in Hulu Klang-Malaysia collapsed due to slope failure behind the building, claiming 48 lives (Nordin, 1995). In June 30, 1995, the worst road failure happened in Genting Highlands, costing 21 lives (Audi Munir 2009). In December 10, 2007, the main route linking Gua Musang and Kota Baru via Kuala Krai, was closed due to a landslide at the 65th kilometre for more than a week (Landslides in Malaysia 2012). In February 12, 2009 - a contract worker was killed in a landslide at the construction site for a 43-storey condominium in Bukit Ceylon, Kuala Lumpur. In May 21, 2011 also (Landslides in Malaysia 2012), a landslides hit an orphanage nearby the Malaysian capital, Kuala Lumpur, killing 16 people (Landslides in Malaysia 2012). The above incidents are merely a small portion of the slope failures which happen every year, costing many lives and economic resources.

One of the most important factors for land sliding is gravity, which is the primary driving force for a landslide to occur. The gravitational force in slopes is divided into two components, one perpendicular to the failure surface and the other parallel to this surface which is the shear component. In spite of the fact that the normal component will prevent land from sliding, the shearing component will actually encourage it. Shear force in the mass soil can be overcome by different techniques, some of which are nailing, retaining wall, using geo textiles, vegetation and others.

Since the conventional methods are either too expensive or not applicable in many cases; attention has been drawn nowadays to the soil bioengineering by using vegetation as an environmental friendly method for slope stabilization. Soil bioengineering or vegetation usage in civil engineering projects is the most applicable method for shallow slope stabilization characterized by unstable slopes that have surface movement.

Soil and roots demonstrate several similarities in respect to the structure and ductile reaction to strain. Both deform to a great extent before they break. Their retaining capacity is not lost during deflection and subsidence of the relevant slope (Gray and Sotir , 1996). The roots mechanically reinforce the soil by transferring the shear stresses in the soil to tensile resistance in the roots via fibber reinforcement near the slope surface and deeper binding soil structure effect through tap or lateral root networks (Gray, 1973; Coutts, 1983 , 1986; Crock and Ennos, 1996; Nicoll and Ray, 1996; Matteck and Berloer, 1995; Stokes and Guitard, 1997; Stokes et al., 1995, 1998; Normaniza and Barakbah, 2006; Li et al., 2007; Wu, 2007; Chia-Cheng Fan and Chih-Feng Su, 2008).

Vegetation also has a salient role both in the soil moisture extraction by evapotranspiration process and in rain drop interception by foliage (Tsaparas et al., 2002). Foliage and plant residues absorb the rainfall energy and prevent soil detachment by raindrop splash. Root systems physically bind or restrain soil particles while the above-ground portions filter the sediment out of the runoff; therefore, the stems and foliage increase the surface roughness and slow the velocity of the runoff. Plants and their residues help to maintain the soil porosity and permeability, therefore delaying the onset to runoff.

The effect of root anchorage on slope stability during land sliding has become a well-researched topic over the last 25 years with a huge amount of field data available

(Schor and Gray, 1995; Nicoll et al., 2006, Stokes, 1999; Ruel et al., 2003; Achim et al., 2005; Danjon et al. 2005; Morgan, 2007; Moafian et al., 2009; Nordin et al. 2011, Normaniza et al. 2011 and Normaniza and Barakbah, 2011). However, only few numbers of researches are concentrated on effect of pulling out resistance in slope stability (Hamza et al., 2007). The weight of trees growing on a slope adds to the load on the slope but the roots of trees serve as soil reinforcement and can increase the resistance to instability. In order to ensure that the weight of the trees on the slope help to enhance its stability it is required that they are planted down-slope of the neutral point. Maximum contribution is produced if the trees are located at the slope toe. Considering a typical slip circle, at this location the direction of shear force acting on the trees may be considered as close-to-vertical (i.e. vertical pull out) for the purpose of analysis. In this situation trees behave like biological nails which give a stabilizing effect to the slope. Also it is not known which shape of root system is the best to increase the resistance against the pulling out. If optimal root architecture can be defined, it may then be achievable to control the root systems or soil properties to increase the resistance during the pulling out. Root anchorage resistance is regulated by several factors, e.g. root architecture, (Dupuy et al., 2005a, 2007) soil physical and mechanical characteristics (Ferdlound and Hardy, 2000; Moor, 2000; Dupuy et al., 2005b; Nicoll et al., 2006). However, it is believed that the pulling out resistance depends on the root system architecture and soil properties, but only few studies were accomplished to test this hypothesis. Field experiments on root anchorage for pulling out usually involve pulling the vegetation upside until failure and measuring the displacement and consequently the force required. Variables measured can then be included with the displacement occurred during the pulling out, performed force (Der-Guey Lin et al., 2010) and root system architecture (Khuder et al., 2007). However, although the pulling out test provides useful information, it is time-consuming and can

be difficult or even dangerous to conduct. Therefore, application of numerical modelling will assist us to execute the pulling out experiments and it is an ideal tool in studying the factors affecting root anchorage. Nevertheless, in most simulations done before for root anchorage (for instance to simulate overturning process), due to the small root diameter, the roots were modelled using beam element embedded in soil. Therefore the results found during the simulation were higher than the experimental results; hence due to the mixed model used in our simulation, obtained results were more accurate as they are proven by the comparison with experimental results.

Thus, to avoid this limitation in this study, a generic finite element model is developed using the ABAQUS6.10-EF1-Explicit with alternative interaction between the soil and root element, where real three-dimensional (3D) root system architectures are represented in a 3D soil.

In parallel, the field pulling out experiments were also conducted to validate the model by comparing the results of experimental and analytical data. Moreover, a number of models are developed to investigate how root architecture and soil engineering properties (e.g. friction angle and matric suction) contribute to the pulling out resistance. In this study, the mechanical properties of the roots and soil were identified and measured in the laboratory. Then, the in-situ pulling out test were conducted and at the same time the pressure distribution in soil during the pulling out process and soil matric suction were monitored, using the miniature pressure transducer and miniature tensiometer at a certain place and depth.

For the finite element analysis, the soil's material is considered to be a perfectly elastic plastic with the Mohr-coulomb failure criterion and root material which are considered to be elastic linear with a plastic threshold by a Von-Mises yield criterion.

Applications of this generic model include virtual uplifting experiments, where each component of the anchorage can be tested individually.

Finally, in order to verify the model accuracy comparisons with well control laboratory tests results (Siti Sara et al. 2010), were also made.

1.2. Research background

From time immemorial, it has been mentioned that the slope failure is hardly found in natural forests, in which drawing attentions to the good effects of vegetation on the slope stability. Although a lot of researches were conducted in the Australia, USA, Canada and European Union countries, only few studies were conducted in a Malaysian's geotechnical and geomorphologic situation.

It was discovered that vegetation can play an important role in the stabilization and maintenance of the slope. It is also cheap and able to control soil erosion simultaneously. It was also found that vegetation have important roles in both the improvement of soil mechanical and the hydrological properties.

Few studies were conducted to simulate the root anchorage process either on overturning or on pulling out such as Dupuy et al. 2005C; Fourcaud et al. 2008 and Der-Gueylin et al. 2010. A small number of studies were also conducted on the effect of ground water level and matric suction on the slope stability, such as Faisal et al., 1999; Faisal et al., 2006a b and c.

During the literature review of historical record of land sliding in Malaysia, it is obvious that most of the slope failures happened between Novembers to February which is the monsoon season. The annual rate of rainfall in Malaysia in this season is between 2500 to 3000 mm. It may indicate the importance of the effect of the ground water level and matric suction on the slope stability in Malaysia in which the subject has rarely

been investigated in other countries and vegetation is one of the influential factors to control the soil matric suction.

Faisal et al. (1999) revealed that reduction in soil matric suctions can be a possible case of land sliding. Despite this important fact that the soil above the ground water table is always partially saturated, most of the slope stability analyses where done so far are either totally dry or fully saturated soil. This is due to the difficulty in predicting the distribution of the soil matric suction in partially saturated soils.

In this case, the presence of negative pore water pressure, (soil matric suction) can arguably improve the shear strength of the soil (Li et al., 2010). Vegetations can increase the soil matric suction and consequently the shear strength in soil by reducing the soil moisture via respiration and transpiration. On the other hand, vegetations can also protect the soil from erosion by the surface coverage and can help to increase the soil shear strength via reinforcement.

1.3. The significance of the present research

Due to the complexity of pulling out process, only few researches are pertained to pulling out, and at the same time some restrictions are affecting root anchorage simulation in general.

With regard to that, this research is concentrated on evaluation of a 3D model for root – soil system in Malaysian geotechnical and geographical situation, using real root and soil mechanical properties to perform an accurate prediction for the root anchorage process. This model also can be used to estimate the effect of changing in root architecture and soil properties on root anchorage behaviour. In this research, there is an attempt to use a finite element model to analyze the interaction between the root and soil during the pulling out for a better understanding of this process and the factors influencing the pulling out force.

1.4. Research objectives

The primary focus of the present research is to investigate the influence of roots on the pulling out resistance in *Melastoma malabathricum*.

The objectives of the research are outlined as follows:

- To develop an alternative method to simulate the interaction between root and soil in root anchorage process.
- To obtain the distribution of stress and strain in the soil and root system during the pulling out process at failure.
- To identify the effect of root architecture (long taproot, branches form and angle) on the root anchorage
- To determine the effect of soil cohesion (c) and friction angle (Φ) on root anchorage

1.5. The Scope of the study

The study was carried out with the following scope:

1. Determination of the mechanical and physical properties of both soil and root of *Melastoma malabathricum*
2. 3D simulation of the root system
3. Validation of the prepared model by comparing the numerical analysis result against the experimental results.
4. Parametric studies to determine the following:
    a) Effect of soil mechanical parameter (c , Φ) on the pulling out resistance
    b) Effect of root architecture on the pulling out resistance

1.6. The outline of the research approach

This thesis is divided into seven chapters. The first chapter presents the Introduction, Research background, Significance of the present research, Research objectives and Scope of the study. It is followed by the Literature review chapter on the mechanism of root anchorage in soil slope and the three dimensional finite elements modelling. This literature review is vital in verifying the theory and the modification method used in the studies.

The core of this study is divided into two major parts namely experimental investigation and numerical simulation. Chapters 3 and 5 present the experimental research method and its output whilst chapters 4 and 6 present the numerical simulation method and its outputs. Chapter 3 and 5 emphasize the determination of laboratory parameters, the field testing outcomes while chapters 4 and 6 discuss about generation of three dimensional models for finite element analyses based upon the field and laboratories outcomes and model validation. In chapter 6, the parametric study has been discussed whereby the effect on soil parameter and root architecture resulted by pulling out process was being examined. Finally, in the seventh chapter, the conclusion of the findings from this study and recommendations for future related works is presented.

CHAPTER 2:

LITRATURE REVIEW

2.1 Introduction

A survey of the literature and research related to the mechanism of root anchorage in the soil slope and relevant three dimensional finite element models is carried out to ascertain the current research frontier. Soil bioengineering, i.e. using vegetation in civil engineering construction, is now an established practice in many parts of the world and is considered a practical alternative to the more traditional methods of soil stabilization such as soil nailing or geosynthetic reinforcement. These methods are the most applicable to shallow slope stabilization projects characterized by unstable slopes that have surface movement. To analyse the contribution of vegetation in the slope stability, one needs to think of its hydrological and biological role as well as its mechanical role. Throughout this study, the focus will be specifically focused on the mechanical role.

Soil reinforcement by roots is studied by considering the contribution of the tensile force in root segment that intersects with a potential slip surface in a root soil system, where the roots mechanically reinforce the soil by transferring the shear stresses in the soil to tensile resistance in the roots. Different types of root systems of plants provide different strengthening effects on the stability of the slope via fibres reinforcement near the slope surface and deeper binding soil structure effect through tap or lateral root networks. The anchorage of the roots and the improvement of the slope stability also depend on the properties of the root systems such as the root distribution and tensile strength (Nicoll and Ray, 1996; Stokes and Guitard, 1997; Stokes et al., 1998; Normaniza and Barakbah, 2006; Li et al., 2007) as well as the soil conditions.

Even root architecture has been long considered as a major component of root anchorage, but some researchers (Wu and Sidle, 1995, Waldron and Dakessian, 1981,

Greenwood et al., 2004) have suggested that the reinforcing effect of vegetation can be considered in conventional slope design by adding an additional root 'cohesion' term, C_R to the Mohr-Coulomb strength envelope for soil. When the soil is permeated by fibres (as in the case of roots), the displacement of soil, as a consequence of shear tension, generates friction between the soil grains and fibre surfaces, causing the fibres to deform and mobilize their tensile strengths. In such conditions, some of the shear tension can be transferred from the soil to the fibres, producing a reinforcement of the soil matrix itself. On the other hand, vegetation can predict soil erosion via foliage; they can also draw water from soil via respiration and transpiration and consequently cause an increase in the soil suction by reducing the soil moisture where it will help to increase the shear strength in soil, as elaborated by Faisal et al (1999).

2.2 Slope stability

"Sloping ground can be unstable if the gravity forces acting on a mass of soil exceed the shear strength available at the base of the mass and within it" (Barnes, 2000). Skempton and Hutchinson (1969) classified the types of land sliding, as shown in Figures 2.1
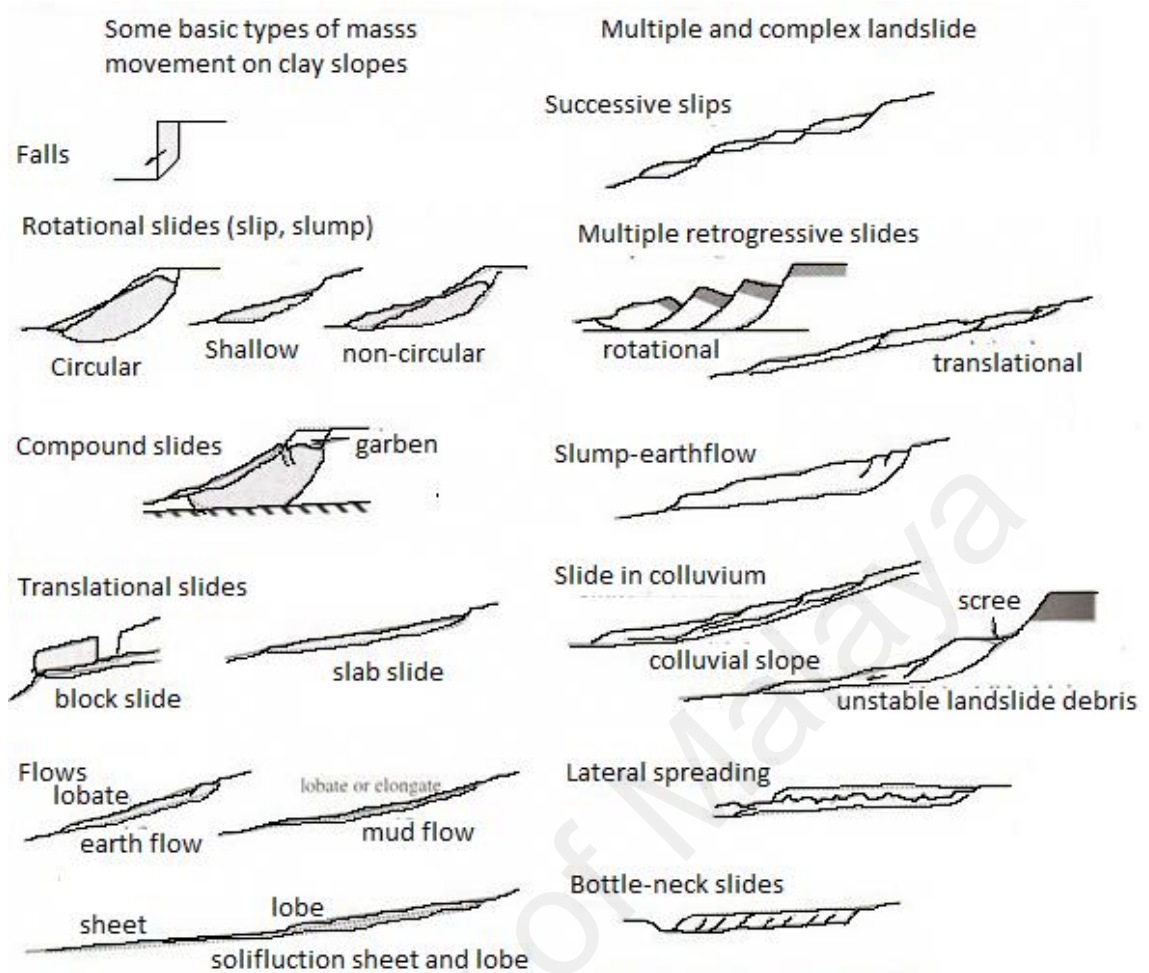
Figure 2.1: Type of mass movement (Skempton and Hutchinson, 1969)

Generally, land sliding occurred when shear stress (τ) in the slope overcomes the related shear strength (τf), and the safety factor F would be;

$$F = \tau_f / \tau \tag{2.1}$$

As mentioned in the introduction, different mechanical parameters can affect the shear strength of the soil and consequently the slope safety factor, e.g. pore water pressure; since the pore water pressure increases, the safety factor will decrease.

For analysis of the slope stability, there are different methods depending on the methods of movement.

2.2.1 Plane translational slide

As demonstrated in Figure 2.1, the translational slides are commonly controlled structurally by the surfaces of weakness such as faults, joints, bedding planes, and contacts between bedrock and etc.

This method can be employed when the slip surface (bedding planes) is parallel to the ground surface as illustrated in Figure 2.2.
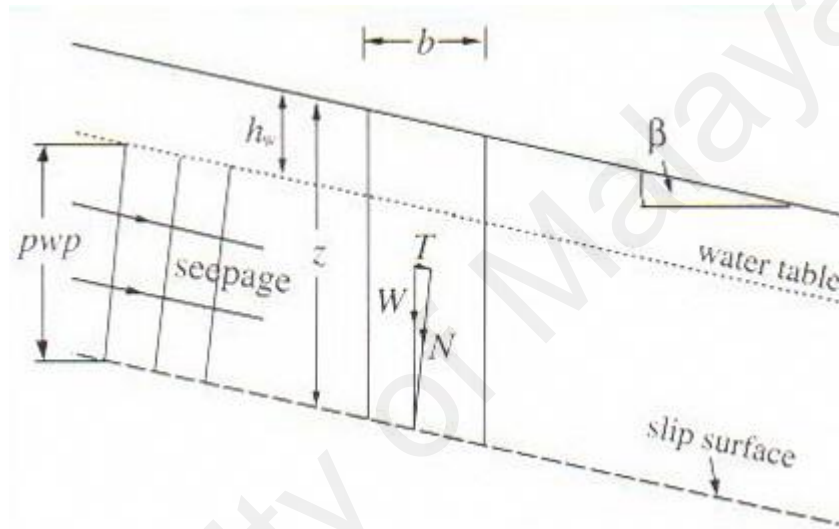
Figure 2.2: Plane translational slide (Barnes 2000)

Barnes (2000) proved that if the slip surface is under the water table, the safety factor will be:

$$F= (c'+tg\phi'\cos^2\beta \ (\gamma z-\gamma_w z+\gamma_h h_w))/\gamma z\sin\beta\cos\beta \tag{2.2}$$

Where β=slip surface angle, z= slip surface depth, γ=balk and saturated soil unit weight

h_w= water table depth, γ_w=water unit weight c'= effective cohesion impact and

ϕ'=effective angle of internal friction.

As mentioned earlier, the increasing c' and ϕ' can cause an increase in the safety factor F.

2.2.2 Circular arc analysis

This method assumes that the slip surface is an arc which cuts the ground surface in a certain point, as shown in Figure 2.3. The safety factor in this case can be presented as:

$$F= \text{shear resistance moment/overturning moment}$$

Over the turning moment, there is a moment caused by the weight of the soil over the slip surface and shear resistance moment caused by shear strength in the slip surface.
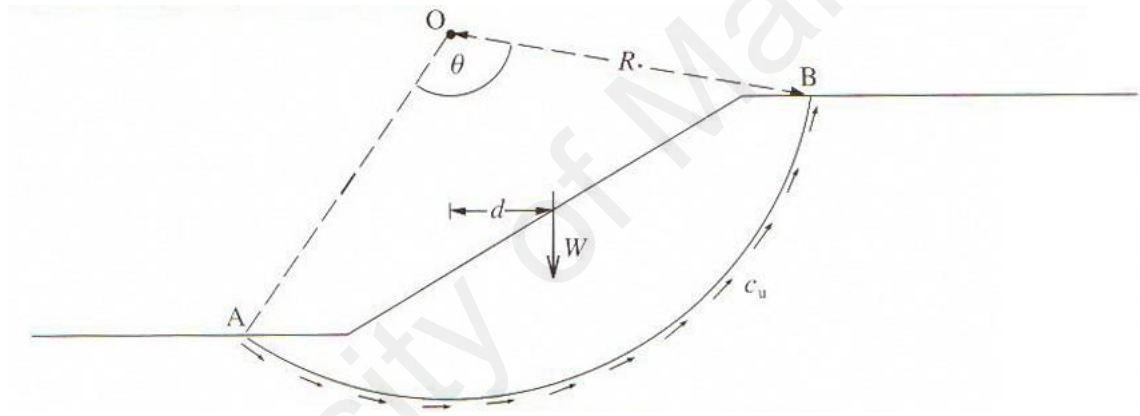
Figure 2.3: Circular arc analyses (Barnes 2000)

Barnes in 2000 shows that in this case safety factor will be:

$$F= c_u R^2 \Theta / Wd \tag{2.3}$$

2.2.3 Effective stress analysis

Bishop and Morgenstern (1960) discovered the relationship between the safety factor and pore pressure ratio r_u:

$$F=m-nr_u \tag{2.4}$$

Where: m and n are termed as the stability coefficient.

This method was adopted until Barnes (2000) discovered the relationship between the safety factor and ϕ':

$$F = a + b \, tg \, \phi' \qquad\qquad (2.5)$$

Where: a and b are the stability coefficients for the slope.

Coefficient a is related to (h_w/H) and b is related to both (h_w/H) and $(c'/\gamma H)$ where H is the slope height.

2.3 The influence of vegetation on the slope segment stability

In 1990, Coppin and Richards formulated the main influences of the vegetation on the slope segment stability. (Figure 2.4)
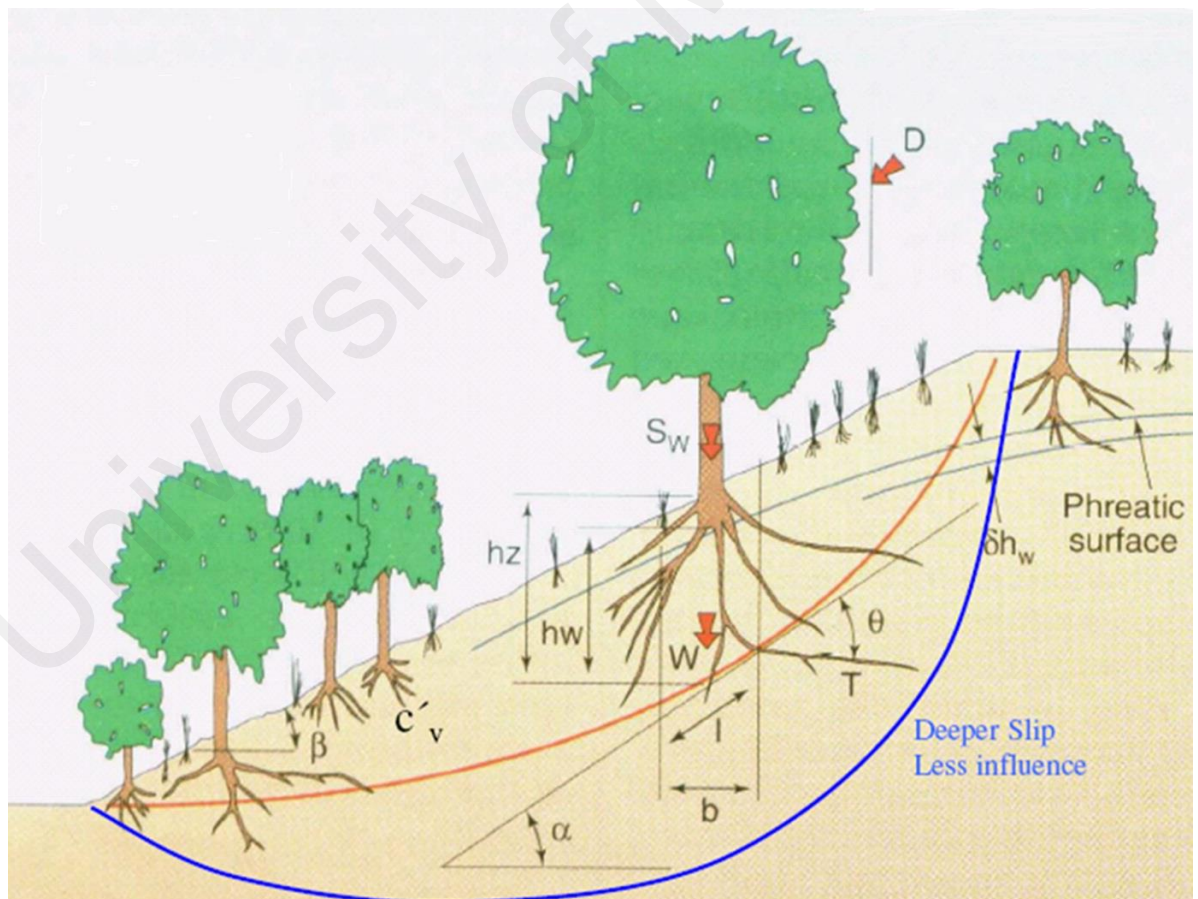
Figure 2.4: The main influences of the vegetation on the slope segment stability (Coppin and Richards, 1990)

They concluded a formula for the calculation of the safety factor as below:

$$F= ((c'+c_R') + (((\gamma Z-\gamma_w h_w) +W) \cos^2 \beta+T\sin\Theta) \, tg\phi'+T\cos\Theta)/ ((\gamma Z+W) \sin\beta+D) \cos\beta)$$

(2.6)

Where: γ=unite weight of soil (kN/m^3)

Z=vertical height of soil above the slip plane (m)

β=Slope angle (°)

γ_w =unit weight of water(9.81 kN/m^3)

h_w =vertical height of groundwater table above the slip plane(m)

c_R'=Enhanced effective soil cohesion due to root matrix reinforcement by vegetation along slip surface(kN/m^2)

c'= Enhanced effective soil cohesion due to soil suction due to evaporation by vegetation along slip surface(kN/m^2)

W=Surcharge due to weight of vegetation (kN/m)

D=wind loading force parallel to slope (kN/m)

T=Tensile root force acting at base of slice (kN/m)

As we could see from the formula above, safety factor have a direct relationship with effective soil cohesion coefficient as well as vertical height of ground water table above the slip plan. Both the overall weight of the soil located on top of the slip plan and vegetation located on slope surface have a destructive impact on safety factor. In general, this conclusion is expected because unlike the soil cohesion and deep ground water table helping to improve the slope stability, heavy load of located soil and vegetation above slip surface is causing further soil movement.

Greenway in 1987, also presented the hydro mechanical influence on the slope stability (Figure 2.5) as below;

No as per Figure 2.5	Hydrological Mechanisms	Influence
1	Foliage intercepts rainfall, causing absorptive and evaporative losses that reduce rainfall available for infiltration	Beneficial to stability
2	Root and stem increase the roughness of the ground surface and the permeability of the soil, leading to increased infiltration capacity	Adverse to stability
3	Roots extract moisture from the soil which is lost to the atmosphere via transportation, leading to lower pore-water pressures	Beneficial to stability
4	Depletion of soil moisture may accentuate desiccation cracking in the soil, resulting in higher in filtration capacity	Adverse to stability

No as per Figure 2.5	Mechanical Mechanisms	Influence
5	Roots reinforced the soil, increasing soil shear strength	Beneficial to stability
6	Tree roots may anchor into firm strata, providing support to the upslope soil mantle through buttressing and anchoring	Beneficial to stability
7	Weight of trees surcharges the slope, increasing normal and downhill force components	Adverse to stability/ Beneficial to stability
8	Vegetation exposed to the wind transmits dynamic force into the slope	Adverse to stability
9	Roots bind soil particles at the ground surface reducing the susceptibility to erosion	Beneficial to stability
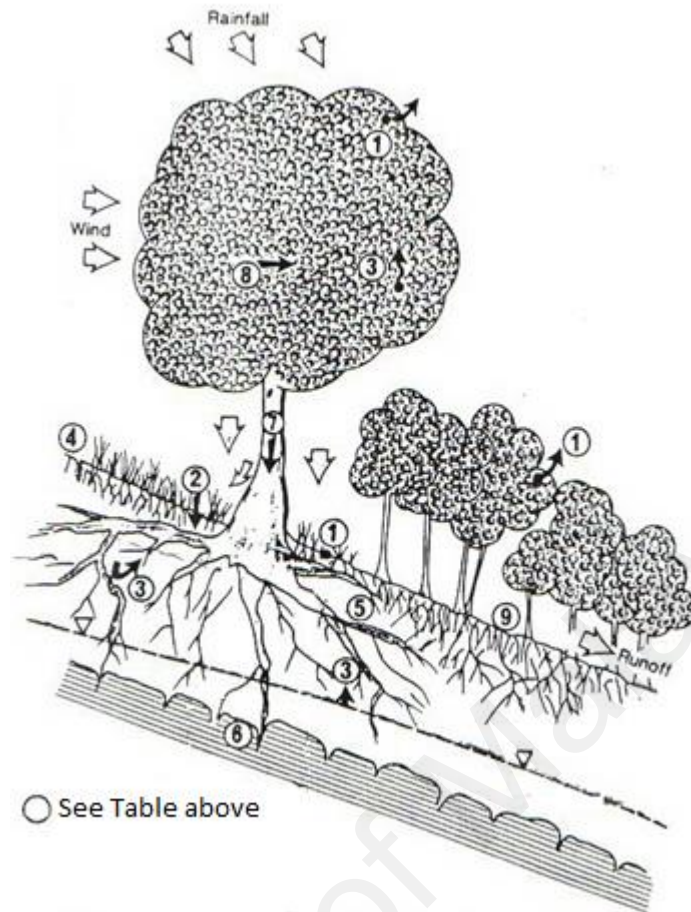
Figure 2.5: Hydro mechanical influence on the slope stability (Greenway, 1987)

2.4 The mechanism of root anchorage in the soil slope

"Vegetation affects both the superficial and mass stability of slopes in significant and important ways." (Gray , 1995) Soil and roots donate several similarities with respect to the structure and ductile reaction to strain. Both deform to a great extent before they break. Their retaining capacities are not lost during deflection and subsidence of the relevant slope. This fact of retaining capacity exist during the deflection protects the soil from overall collapses due to slope failure. It means that during the slope failure, soil shear strength is starting to fail only in slip surface rather than whole soil body.

The shear strength function is defined in the stress diagram by Mohr as the envelope of the circles rupture at different stress strain states/levels. It depicts obviously that the

common simplification of the function by a straight line is only valid for small extents of surcharge. The depth of the soil covered by roots is usually not longer than 1, 2 or 5 meters. On the soil surface, there is no surcharge and the stresses are too small compared to the deeper layers. The respective values are close to the values in the stress diagram mentioned above. The envelope is not a linear function of the shear parameter ϕ and c, which are only the parameters to simplify calculation and do not effectively describe the quality of the material.

Tobias (1995) described a data analysis with the supper position of passive stress state, where it is shown that shear strength in the root layer was 9% to 55% higher than the underneath depending on the type of the plant. By using a basic model for soil - root interaction, Gray et al (1980) elaborated that the shear strength increases in the reinforced soil by roots. The angle of the roots being 90˚ to the shear surface, the shear strength is contributed by root reinforcement, and S_r (limit equilibrium) requires that (Figure 2.6 a):

$$S_r = (T (\cos\alpha + \sin\alpha \, tg\phi))/A \tag{2.7}$$

$$S_r = (T_y + T_z \times tg\phi)/A \tag{2.7a}$$

Where T=tensile force in root reinforcement, α=inclination of T, A=area of the section under consideration and ϕ=angle of the internal friction of soil.
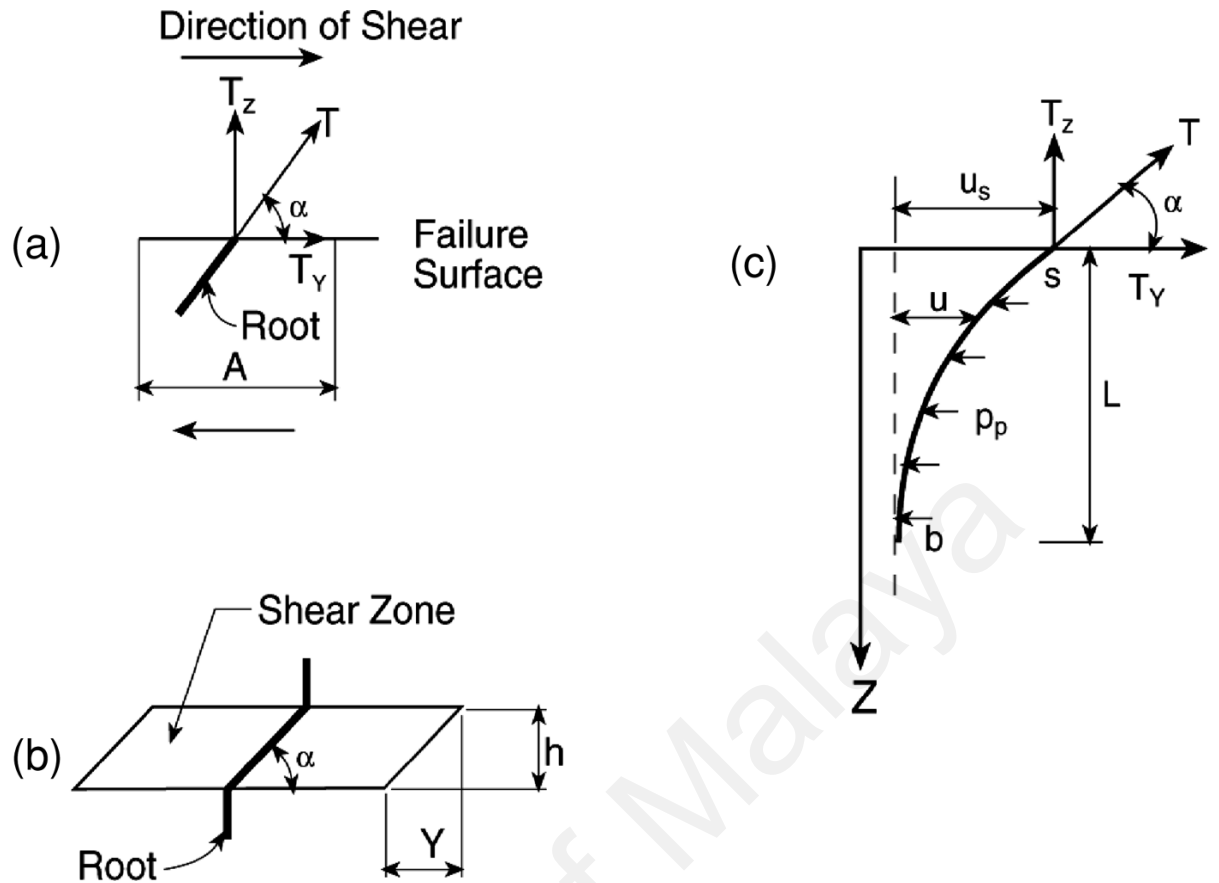
Figure 2.6: Simple models; a) limit equilibrium b) flexible reinforcement c) cable model (Tobias, 1995)

When written in terms of the stress (σ_r), Equation 2.7a becomes:

$$S_r = (\sigma_r A_r(\cos\alpha + \sin\alpha \, tg\phi))/A \qquad (2.7b)$$

Where A_r=Area of reinforcement.

Gray and Ohashi (1983) showed that for $48° < \alpha < 72°$ Equation 2.7b is applicable and $\cos\alpha + \sin\alpha \, tg\phi \approx 1.2$.

The simplest way is to assume that the root and soil will be deformed together or they have no influence on the shear deformation, where α is determined by the shear stress in the soil (Figure.2.6-b). In this case, the Equations 2.7, 2.7a and 2.7b are still valid provided that the correct value of T and σ_r is used.

Abe and Ziemer's experiment (1991) with the reinforced wall revealed that by increasing the bending stiffness, the thickness of the shear zone increases and reinforcement will no longer deform with the soil. To consider the deformation and bending resistance on the reinforcement, Oden et al. (1981) employed the following equation for the tie (Figure.2.6-C);

$$EI \left(d^4u/dz^4 \right) - T_z \left(d^2u/dz^2 \right) = q \tag{2.8}$$

Where E and I = Young modulus and moment of inertia of the root reinforcement, q=Soil reaction and u=displacement. This equation can be simplified to flexible cable if $\eta L > 2.5$ where $\eta = (Tz/EI)^{1/2}$ and L= Length of Tie (deformed portion of root reinforcement).

In this case:

$$T_z (0) = T (L) \tag{2.8a}$$

$$T_y (0) = q_y L \tag{2.8b}$$

$$u (0) = q_y L^2 / 2T_z (0) \tag{2.8c}$$

The amount of T is limited by the ultimate tension. For the roots that are perpendicular to the slope, small amounts of u; $\alpha \rightarrow 90°$ or $Tz \rightarrow 0$ can be used, which represent the initial failure when the root yields. If the root is ductile and does not fracture, u and T will increase continuously until the cable solution is applicable.

In addition, deep woody root is more effective to prevent shallow mass stability failures. "Roots mechanically reinforce a soil by the transfer of shear stress in the soil tensile resistance in the roots whereby anchored and embedded stems can also act as buttress piles or arch abutment to counteract down slope shear force. Moreover, the weight of vegetation may (in certain instance) increase the stability via increased

confining (normal) stress on the failure surface" .(Gray and Sotir, 1996) On the other hand, the roots provide better connection between particles in the soil body (tensile force on the surface) which resulted in some cementation forces of the mass of the soil.

However, a dense herbaceous cover is one of the best protections against superficial rainfall and wind erosion. Soil losses due to rainfall erosion can be decreased a hundred fold by maintaining a dense herbaceous cover (Smith, 1978). This protection has a salient role in both soil moisture extractions by the evapotranspiration process and rain drop interception by foliage. Foliage and plant residues absorb the rainfall energy and prevent soil detachment by raindrop splash. The root systems also physically bind or restrain the soil particles while the above-ground portions filter the sediment out of runoff; therefore, the stems and foliage will increase the surface roughness and slow the velocity of the runoff. Plants and their residues help to maintain soil porosity and permeability, therefore delaying the onset of the runoff.

Gray and Sotir (1996) described computed soil loss (e.g., tons) per acre for a given storm. The time interval (A) can be obtained by examining the Universal Soil Loss Equation (USLE):

$$A = R.K.LS.C.P \qquad (2.9)$$

Where: R = climatic factor, K = soil erodibility value, LS = topographic factor,

C = vegetation factor and P = erosion control practice factor.

The USLE equation provides a method to estimate the soil losses and range of variability of each of the parameters in order to change manage or limit the soil losses. In 1973, Brenner showed that evapo-transportation by vegetation can reduce pore water pressures within the soil mantle on the natural slopes, promoting stability.

2.4.1 The effect of vegetation at the toe of the slope on the slope stability

As displayed in Figure.2.7, the shear stress along the slope is converted into the pulling out force at the end of the slope (plane area).The roots in this area denote some resistance against this kind of force, as shown below.
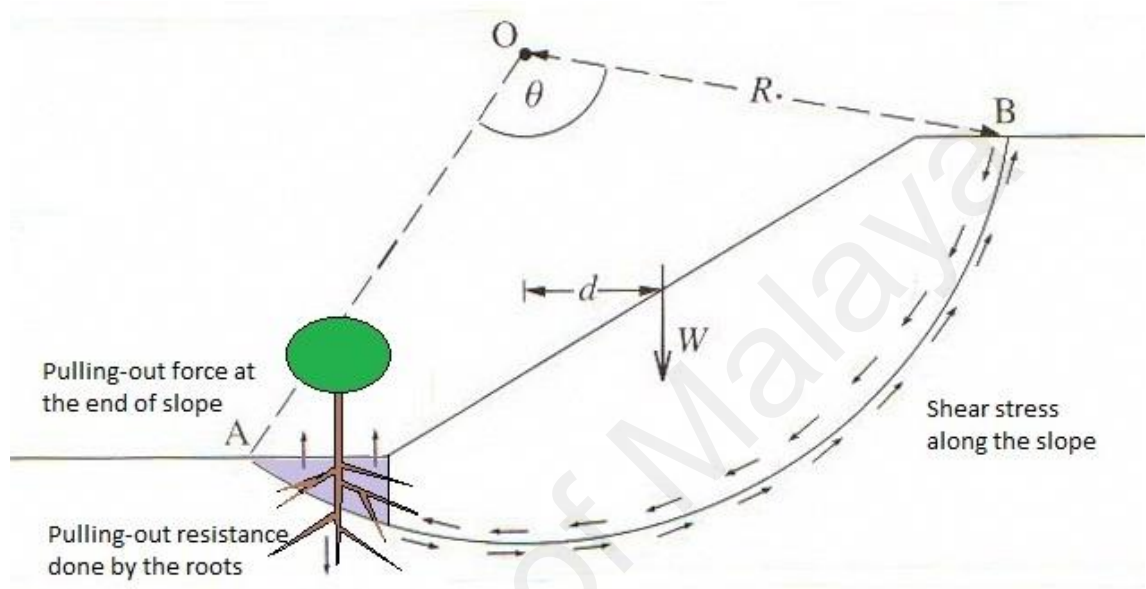
Figure 2.7: The effect of roots at the toe of the slope

Khalilnejad et al. (2012) stated that, this kind of resistance has an important role in the slope stability as the root protects the soil at the toe of the slope against the pulling out force. Roots reflect some kind of resistance against the slope failure by increasing the shear resistance directly (by tensile force in the roots) and indirectly by increasing the normal stress over the surface thus affecting the strength through Mohr-Coulomb criterion. The mechanism of this effect is fixing the plain part of the end of the slope by increasing the pulling out resistance in this part. In the other words, the roots work as biological nails to stabilize the slope. Hence this particular mechanism of the root anchorage is poorly investigated as this thesis is concentrated on the root anchorage modelling of pulling out.

2.5 Effect of soil matric suction on the root anchorage

As Ning Lu and Likos described (2006), the particle-scale equilibrium analyses are employed to distinguish three types of interparticle forces: 1) active forces transmitted through the soil grain; 2) active forces at or near interparticle contacts; and 3) passive, or counterbalancing, forces at or near the interparticle contacts. The second type of force includes physicochemical forces, cementation forces, surface tension forces, and the force arising from negative pore-water pressure; all these forces can be conceptually combined into a macroscopic stress called the suction stress.

In 1943, Terzaghi, regarding the saturated soil mentioned that:

$$\sigma' = \sigma - u_w \tag{2.10}$$

Where: σ'=effective stress, σ=total stress, u_w= pore-water pressure,

On the other hand, coulomb equation for shear strength in saturated soil is:

$$\tau = c' + \sigma' \, tg \, \phi' \tag{2.11}$$

Where: c'=effective cohesion impact and ϕ'=effective angle of internal friction.

With the replacement σ' from Equation 2.10 to Equation 2.11, we will have:

$$\tau = c' + (\sigma - u_w) \, tg \, \phi' \tag{2.12}$$

On the other hand, Skempton (1960) showed:

$$\sigma' = \sigma - (1 - (C_s/C)) \, u_w \tag{2.13}$$

Where: C_s=compressibility of the grain and C=compressibility of the granular skeleton.

As shown above, u_w is presented in both equations which caused capillary force in the soil moisture. This force in macroscopic engineering behaviour of the soil can be apparent by the associated increase in shear and tensile strength.

In 1959 Bishop added another parameter to the Terzaghi's equation:

$$\sigma' = \sigma - u_a + x(u_a - u_w) \qquad (2.14)$$

Where: $(\sigma - u_a)$ is the net normal stress, $(u_a - u_w)$ is the matric suction and x is the effective stress parameter (considered to vary between zero and unity).

Jennings and Burland (1962) stated that mechanical parameter in unsaturated soil is affected differently by changes in the net normal stress than by the matric suction. In other words, increase in the matric suction is caused by the increase in shear strength which we have described by the meaning ϕ^b.

As Fredlund and Morgenstern's independent stress variable approach incorporates Equation 2.12 and Mohr-Coulomb circle, the shear strength (τ) is:

$$\tau = c' + ((\sigma - u_a) + x(u_a - u_w))\, tg\phi' \qquad (2.15)$$

Fredlund and Morgenstern (1978) found that the effect of change in the total normal stress can be separated from the effect of change in pore water pressure as it is presented below:

$$\tau = c' + (\sigma - u_a)\, tg\phi' + (u_a - u_w)tg\phi^b \qquad (2.16)$$

Where: ϕ^b = Indicating the angle for the rate of increase in shear strength related to soil matric suction

When matric suction $(u_a - u_w)$ reaches zero (in saturated soil), Equation 2.16 will become Equation 2.12

They illustrated the Mohr-coulomb circles in three dimensional manners in the case of unsaturated soil as per Figure 2.8. In this model, they described the shear stress τ as the ordinate and $(\sigma - u_a)$ and $(u_a - u_w)$ as abscissas. $(\sigma - u_a)$ axis since the pore-air pressure becomes equal; the pore-water pressure (case of saturation) reverts to $(\sigma - u_w)$.
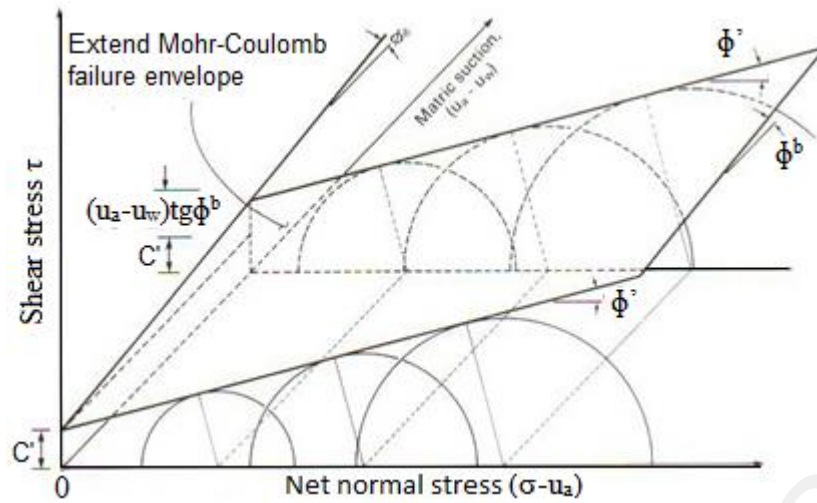
Figure 2.8: Extended Mohr-Coulomb failure envelope for unsaturated soil (Fredlund and Morgenstern 1978).

As it is pictured in Table 2.1 and also Figure 2.7, the value of ϕ^b is mostly less or equal to ϕ'. They revealed that shear stress has a direct relationship with the matric suction as illustrated in Figure 2.9
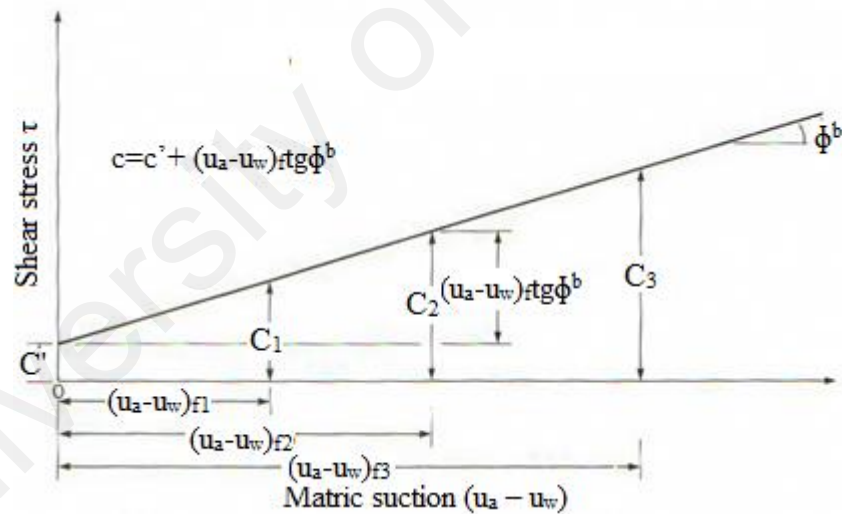
Figure 2.9: Line of intercepts along the failure plan on the τ vs (u_a-u_w) plane (Fredlund and Morgenstern 1978).

Table 2.1: Experimental Value of ϕ^b (Fredlund and Morgenstern 1978)

Soil Type	C' (kPa)	Φ' (degree)	Φ^b (degree)	Test procedure	Reference
Compacted shale w=18.6%	15.8	24.8	18.1	Constant water content triaxial	Bishop et al. (1960)
Boulder clay w=11.6%	9.6	27.3	21.7	Constant water content triaxial	Bishop et al. (1960)
Dhanauri clay w=22.2%, ρ_d=1580 kg/m^3	37.3	28.5	16.2	Consolidated drained triaxial	Satija, (1978)
Dhanauri clay w=22.2%, ρ_d=1478 kg/m^3	20.3	29.0	12.6	Consolidated drained triaxial	Satija, (1978)
Dhanauri clay w=22.2%, ρ_d=1580 kg/m^3	15.5	28.5	22.6	Consolidated drained triaxial	Satija, (1978)
Dhanauri clay w=22.2%, ρ_d=1478 kg/m^3	11.3	29	16.5	Consolidated drained triaxial	Satija, (1978)
Madrid grey clay w=29%	23.7	22.5	16.1	Consolidated drained direct shear	Escario (1980)
Undisturbed decomposed granite; Hong Kong	28.9	33.4	15.3	Consolidated drained multistage triaxial	Ho and Fredlund (1982a)
Undisturbed decomposed rhyolite; Hong Kong	7.4	35.3	13.8	Consolidated drained multistage triaxial	Ho and Fredlund (1982a)
Tappen-Notch Hill silt w=21.5%, ρ_d=1590 kg/m^3	0.0	35.0	16.0	Consolidated drained multistage triaxial	Krahn et al. (1989)
Compacted glacial till w=12.2%, ρ_d=1810 kg/m^3	10	25.3	7-25.5	Consolidated drained multistage direct shear	Gan et al. (1988)

As it is shown in the diagram, the equation for the line is:

$$c = c' + (u_a - u_w)_f \, tg\phi^b \qquad\qquad (2.17)$$

Where: c= total cohesion intercept and $(u_a - u_w)_f$ =matric suction on the failure plane at failure.

When the unsaturated soil is saturated parallel to the saturation process, c decreases as demonstrated in Figure 2.10.

The cohesion inspects c_1, c_2 and c_3 as total cohesion that have a direct relationship with the matric suction.
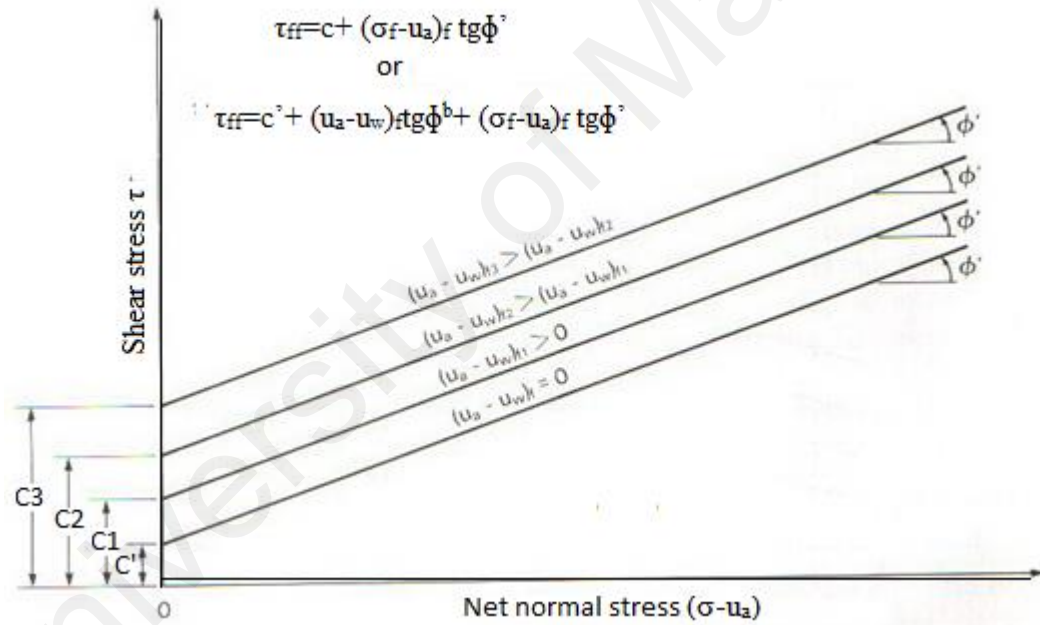
Figure 2.10: Horizontal projection of contour lines of the failure envelope onto the τ vs (σ-u_a) (Fredlund and Morgenstern 1978).

With the substitution of Equation 2.12 for Equation 2.11, the shear strength (τ_{ff}) will be:

$$\tau_{ff} = c + (\sigma - u_a)_f \, tg\phi' \qquad\qquad (2.18)$$

Faisal et al (2006a) announced that the soil water characteristic curve is another important relationship for unsaturated soil. SWCC is the relationship between soil water

content and matric suction. In this research, they found that the increase in matric suction in the unsaturated soil produces the same increase in the shear strength as it does in the increase in net normal stress; the increase in shear strength with respect to the matric suction becomes less than the increase with respect to the net normal stress. It is proven in this research that the stress state in an unsaturated soil can be represented by two independent stress tensors as (2.19 and 2.20).

They found that the increase by the matric suction causes an increase in the shear strength. However, this increase is not the result of increase in ϕ'. On the other hand, they found almost the same ϕ' for different matric suctions.

$$\begin{vmatrix} (\sigma_x - u_a) & \tau_{xy} & \tau_{xz} \\ \tau_{yx} & (\sigma_y - u_a) & \tau_{yz} \\ \tau_{xz} & \tau_{zy} & (\sigma_z - u_a) \end{vmatrix} \quad (2.19)$$

$$\begin{vmatrix} (u_a - u_w) & 0 & 0 \\ 0 & (u_a - u_w) & \\ 0 & 0 & (u_a - u_w) \end{vmatrix} \quad (2.20)$$

Matyas and Radhakrishna (1968) presented the volume change in a three dimensional surface with respect to the state parameter (u_a-u_w) and $(\sigma-u_a)$. Anderson and Lioyd (1991) in their model for slope/ hydrology stability used the effect of increasing the water table in tropical region due to infiltration but he ignored the increase in the soil strength through the suction effect.

Faisal et al (2006b) with the similar scheme as above simulated a change in the dynamic/ hydrological condition due to rainfall and discussed the responsibility of pure

water pressure change (negative and positive) in the slope stability analysis. They highlighted that in tropical regions, the soils involved are often residual soils and have deep water tables. The surface soils have negative pore water pressures that play a significant role in the stability of the slope.

Because of the heavy rain during the rainy season (November- February) in this region, the water table can changed in a short period of time, leading to slope instability (result of wet and dry cycle). However, in the slope stability analysis, the suction stress was often ignored. It is displayed in this study that for a given rainfall intensity $q_s = 1 \times 10^{-6}$ m/s, the factor of safety of the slope tends to decrease with the increase in the permeability (k_s) of the soil. The factor of safety of the slope also reduces with the increase in the slope height. It is also highlighted that in the simple soil section the factor of safety has a linear relationship with the rate of change in shear strength with respect to the suction stress, as shown below (Gasmo et al 2000):

$$F = f + s \tan \phi^b \tag{2.21}$$

Where: F=the factor of safety, f and s = stability coefficients, and $\tan \phi^b$ = the rate of change in the shear strength with respect to matric suction.

Faisal et al (2006b) stated that the vegetation in the soil surface not only decrease the infiltration but will also change the suction value. They discovered that the soil without surface cover appears to have a higher infiltration rate compared to the soil covered with grass. It appears that the presence of the grass encourages more water pounding. Besides, the root system assists in increasing the rate of water infiltration. Suction monitoring in this study reflects that the suction values at a steady state for the model with grass as its surface cover are generally marginally lower. This may be due to the effect of the roots that formed abnormal water passage for the water to infiltrate.

2.6 Method of soil slope improvement

As mentioned above, several soil parameters are involved in slope stability such as c and Φ. This parameter also affects the pulling out resistance. Some of these parameters depend on such environmental conditions as the matric suction affects c (as it was discussed before) and consequently affect the slope stability and pulling out process. Others will depend only on the soil structure (Such as Φ) but as it will be confirmed later that they also serve an important role in the pulling out resistance and consequently slope stability.

In this part, there is an attempt to review some of the soil improvement methods which can help to upgrade the soil structural characteristics (such as Φ) and consequently increase the pulling out characteristics of the soil-root matrix.

2.6.1 Using Vegetation

Graf et al. (2009) performed the triaxial test for three different soil types:

A) Planted soil,

B) Pure soil at low dry unit weight ($\gamma \approx 15.5 \text{kN/m3}$)

   and

C) Pure compacted soil at $\gamma \approx 19 \text{ kN/m3}$.

They used compacted soil for all samples whether planted or not. They found that there is a major discrepancy in the angle of internal friction (Φ) of about 5° between the samples of pure soil at low dry unit weight and those of both the compacted and planted soil. They explained it as increase in soil internal friction angle as the effect of vegetation presence.

Kirsten and Fourie (1999) justified on the influence of three different grass species on the shear strength of frictional (pure) sand and clayey sand applying drained triaxial compression tests. They found that there is an increase in the angle of internal friction Φ as well as on the apparent cohesion (c).

Michalowski (1997) signified that during experimental tests the angle of internal friction Φ of the composite is more than that of the granular matrix, while the applied model predicted changes only in the cohesion (c). The explanation for this is that the role of the filaments in the composite strength is included as a dissipation term independent of the composite stress state. Investigations of fine and coarse sand revealed that at small fibre concentrations (0.5 % Vol), the raise in the composite shear strength is more in the case of fine than coarse sand. Nevertheless, the effect of fibre concentration improvement for coarse sand is more than that of the fine sand.

The micro-mechanical behaviour of the fibre/matrix interface depends on the binding material properties in the soil, the normal stress around the fibre body, the effective contact area, and the fibre surface roughness. The interface roughness is known to serve an important role in the reinforced soil systems (Tang et al, 2007). The strain in a coarse matrix with a high fibre concentration (≈ 2 %) involves bending of the fibres to accommodate the change in the relative configuration of grains during the deformation process which, in turn, enhances the interaction between grains and fibres (Graf et al, 2009). The reinforcement effect is more effective on larger fibres compared to the size of the grains (Michalowski and Cermak , 2003).

2.6.2 Compaction Grouting

Compaction grouting is a technique whereby a slow-flowing water/sand/cement mix is injected under pressure into a granular soil. "The grout forms a bulb that displaces and hence densities the surrounding soil". (Johansson, 2000)

2.6.3 Drainage techniques

Drainage techniques include installation of drains of gravel, sand or synthetic materials. Synthetic wick drains can be installed at various angles, in contrast to the gravel or sand drains that are usually installed vertically. Drainage techniques are often used in combination with other types of soil improvement techniques for more effective liquefaction hazard reduction. (Johansson, 2000)

2.7 Effect of soil bearing capacity on root anchorage

Bearing capacity is the soil capability to carry the forces without undergoing shear failure or excessive settlement. Terzaghi (1943) was the first to declare the soil bearing capacity as a three-term expression incorporating the bearing capacity factors N_c, N_q and N_γ.

Values for N_q and N_c are derived from the Prandtl-Reissner expression giving:

$$N_q = e^{\pi tg\Phi'} tg^2(45° + (\Phi'/2)) \tag{2.22}$$

$$N_c = (N_q - 1)/tg\Phi' \tag{2.23}$$

Hansen (1961) stated that Value of N_γ is:

$$N_\gamma = 1.8(N_q - 1)tg\Phi' \tag{2.24}$$

He proposed the following equation for the ultimate bearing capacity of a long strip footing:

$$q_f = c.N_c + q_o.N_q + \frac{1}{2}\gamma BN_\gamma \tag{2.25}$$

Where the $c.N_c$ term is the contribution from soil shear strength, the $q_o.N_q$ term is the contribution from the surcharge pressure above the founding level and the $\frac{1}{2}\gamma BN_\gamma$ term is the contribution from the self-weight of the soil.

As Terzaghi demonstrated in the diagram below (Figure 2.11) and it is shown in the above mentioned equations, the bearing capacity factor is related to the drained angle of friction (Φ').

During root anchorage, soil bearing capacity (q_f) is one of the factors which are influencing the pulling out process (Figure 2.12).
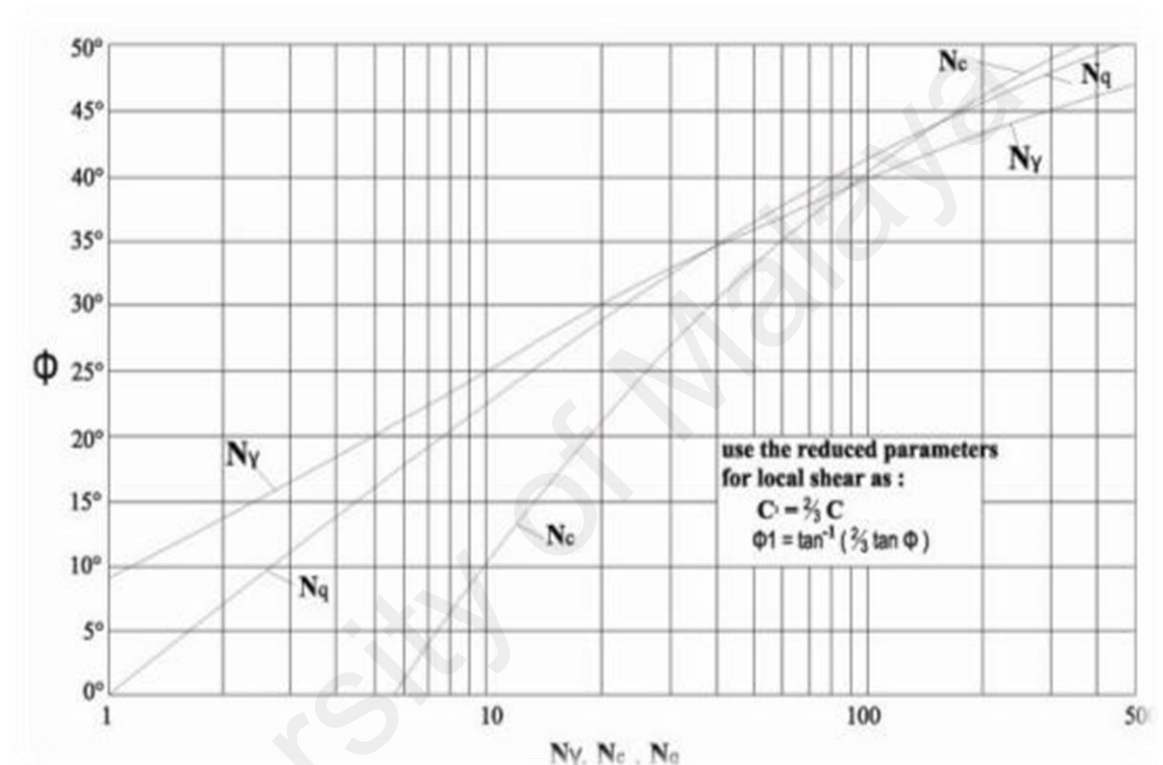
Figure 2.11: Bearing Capacity Factors for different ϕ (Trezaghi, 1943)
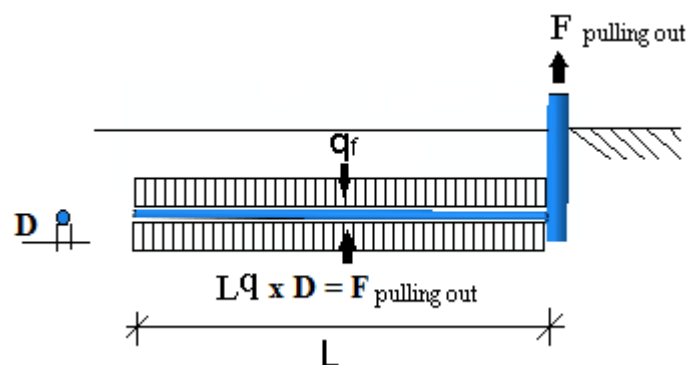
Figure 2.12: Effect of bearing capacity on pulling out process.

2.8 Root failure characteristics

Root material in this research is considered to be elastic linear with a plastic threshold by the Von-Mises yield criterion. Below were the explanations on some mechanical definitions which were used during this study such as logarithmical strain and Von Mises stress or yield criterion.

2.8.1 Strain

As it was discussed earlier, root and soil are subjected to large deformation material, which assumes small strains but large displacements. For this kind of material the engineering definition of strain is not applicable, e.g. typical engineering strains greater than 1%, thus other more complex definitions of strain are required, such as logarithmic strain (Mase and Mase, 2002). The logarithmic strain, ε, consider an incremental strain.

$$\delta_\varepsilon = \delta_l / l \tag{2.26}$$

The logarithmic strain is obtained by integrating this incremental strain

$$\delta_\varepsilon = \ln(1+e) \tag{2.27}$$

where e is the engineering strain.

The logarithmic strain provides the correct measure of the final strain when deformation takes place in a series of increments, taking into account the influence of the strain path.

2.8.2 Von-Mises yield criterion

The Von-Mises yield criterion suggests that the yielding of materials begins when:

$$(\sigma_1-\sigma_2)^2 + (\sigma_2-\sigma_3)^2 + (\sigma_3-\sigma_1)^2 = 2Q^2 \tag{2.28}$$

Where: Q= unconfined compressive strength.

In other words, materials start yielding when its Von-Mises yield criterion reaches a critical value known as the yield strength (Figure 2.13).
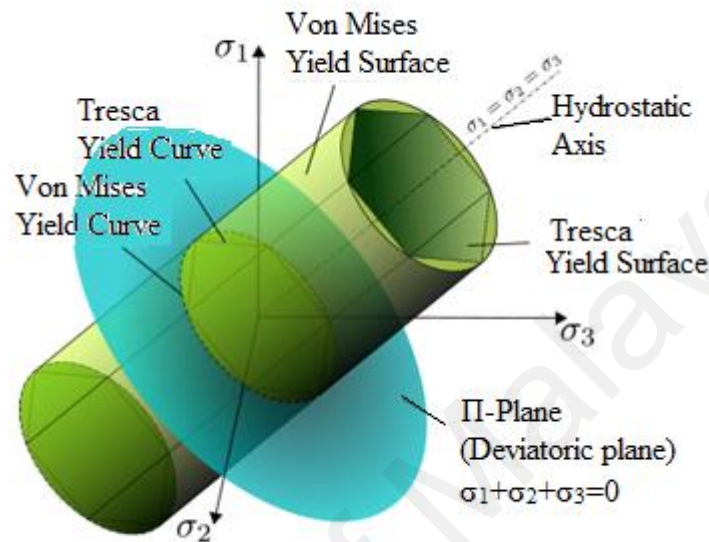
Figure 2.13: Von-Mises yield criterion (Kazimi, 1982).

The Von-Mises yield criterion is used to predict the yielding of materials under any loading condition from the results of simple uniaxial tensile tests (Kachanov, 2004).

2.9 Three dimensional finite element modelling

"The development of automatic and generic numerical methods that use accurate descriptions of plant morphology for biomechanical analyses can be extremely useful and such models have already been applied to both real and simulated architectures subjected to mechanical loading in different environments" (Fourcaud et al., 2003a, b; Sellier et al., 2006).

The finite element has been used to analyze different parts of the geotechnical engineering for more than three decades. The early codes such as NONSAP (Bathe and Wilson 1973), ADINA (Bathe and Wilson 1976) and AGGIE (Haisler et al. 1977)

possessed the capabilities such as three dimensional solid elements, non-conservative loading and so on. But commercial programs such as ABAQUS, ANSYS, ADIANA and MSC/NASTARAN also have graphical pre-and post-processors as well as many of the latest developments in element technology, solution scheme and many others.

The complex shape, small diameter and length of the roots from one side to the other, the complicated initial state in the contact zone between the soil and root (based upon root architecture), and change in the soil mechanical properties in different zones require a large amount of computer resources for finite element analysis, even on today's powerful and high performance computers.

2.9.1 Aliasing in simulation output

In simulation process aliasing occurs when a signal is sampled at a series of discrete points in time, but not enough data points are saved in order to correctly describe the signal.

Based on Nyquist- Shannon Sampling Theorom, a signal must be sampled at a rate that is greater than twice the signal's highest frequency in order to avoid alias distortions. Therefore, the maximum frequency content that can be described by a given sampling rate is half that rate (the Nyquist frequency). Sampling a signal with large-amplitude oscillations at frequencies greater than the Nyquist frequency of the sample rate may produce significantly distorted result due to aliasing. Any model characteristic that reduces the high-frequency response of the solution will decrease the analysis's susceptibility to aliasing.

The safest way to ensure that aliasing will not occur is to request output at every increment or use a run-time anti-aliasing filter. It is possible to create a user define filter or use a built in ABAQUS software anti-aliasing filter.

2.9.2 Energy Balance

An energy balanced equation can be performed to validate whether simulation is yielding an appropriated response.

In ABAQUS/Explicit the energy balance equation is illustrated as below:

EI+EVD+EFD+EKE-EW=ETOT

(2.29)

Where:

EI = Internal Energy

EVD = Energy absorbed by viscous dissipation

EFD = Frictional dissipation Energy

EKE = Kinetic Energy

EW = Work of external force

ETOT = Total Energy in system

In Explicit simulation internal Energy enhancement should be less than 1-2% and any excessive value of internal energy can be sign of mesh instability. In quasi-static simulation kinematic Energy should be a small fraction (5-10%) of work of the external force or internal Energy.

Furthermore, the energy balance diagram can be used to detect the model problem; in some instances, large value of work is possibly due to constraint conflict or in another case, too much mass scaling or large change in model total energy occurred as a result of exceeds in the stability limit.

2.9.3 The elements commonly used in root anchorage numerical analysis

In this section, the elements most probably used in root anchorage finite element analysis will be reviewed (Eight-node brick element (C3D8), ten-node tetrahedral element (C3D10) and beam element (B32)).

- **Eight-node brick element (C3D8)**

A typical eight-node element is illustrated in Figure 2.14. In this type of element, each of the nods has a three translational degree of freedom in x, y and z direction.
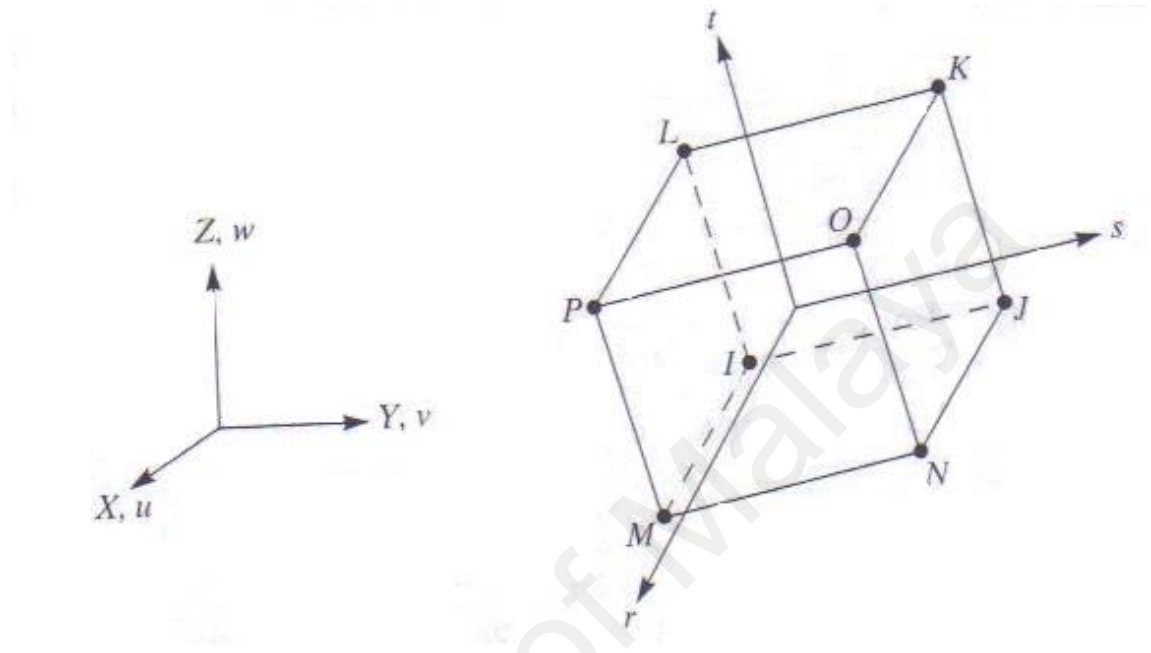
Figure 2.14: A typical eight-node brick element (Moaveni, 2008)

The element displacement for this type of element can be written as below;

$$u=1/8(u_1 (1-s)(1-t)(1-r)+u_J(1+s)(1-t)(1-r))+ 1/8(u_K (1-s)(1-t)(1-r)+u_L(1+s)(1-t)(1-r))+$$

$$1/8(u_M (1-s)(1-t)(1-r)+u_N(1+s)(1-t)(1-r))+ 1/8(u_O (1-s)(1-t)(1-r)+u_P(1+s)(1-t)(1-r)) \quad (2.30)$$

$$\upsilon=1/8(\upsilon_1 (1-s)(1-t)(1-r)+\upsilon_J(1+s)(1-t)(1-r))+ 1/8(\upsilon_K (1-s)(1-t)(1-r)+\upsilon_L(1+s)(1-t)(1-r))+$$

$$1/8(\upsilon_M (1-s)(1-t)(1-r)+\upsilon_N(1+s)(1-t)(1-r))+ 1/8(\upsilon_O (1-s)(1-t)(1-r)+\upsilon_P(1+s)(1-t)(1-r)) \quad (2.31)$$

$$w=1/8(w_1 (1-s)(1-t)(1-r)+w_J(1+s)(1-t)(1-r))+ 1/8(w_K (1-s)(1-t)(1-r) + w_L(1+s)(1-t)(1-r)) +$$

$$1/8(w_M (1-s)(1-t)(1-r)+w_N(1+s)(1-t)(1-r))+ 1/8(w_O (1-s)(1-t)(1-r)+w_P(1+s)(1-t)(1-r)) \quad (2.32)$$

This element type is commonly used for material with a relatively low Poisson ratio value. During this exercise, eight node elements with reduced integration (C3D8R) were used. The integration point is located in the middle of the element and effecting on

stress and strain value accuracy. These elements are required to capture the stress concentration in the element boundary.

- **Ten-node tetrahedral element (C3D10)**

    Ten-node tetrahedral element as illustrated in Figure 2.15 is a higher order version in the three-dimensional linear element.
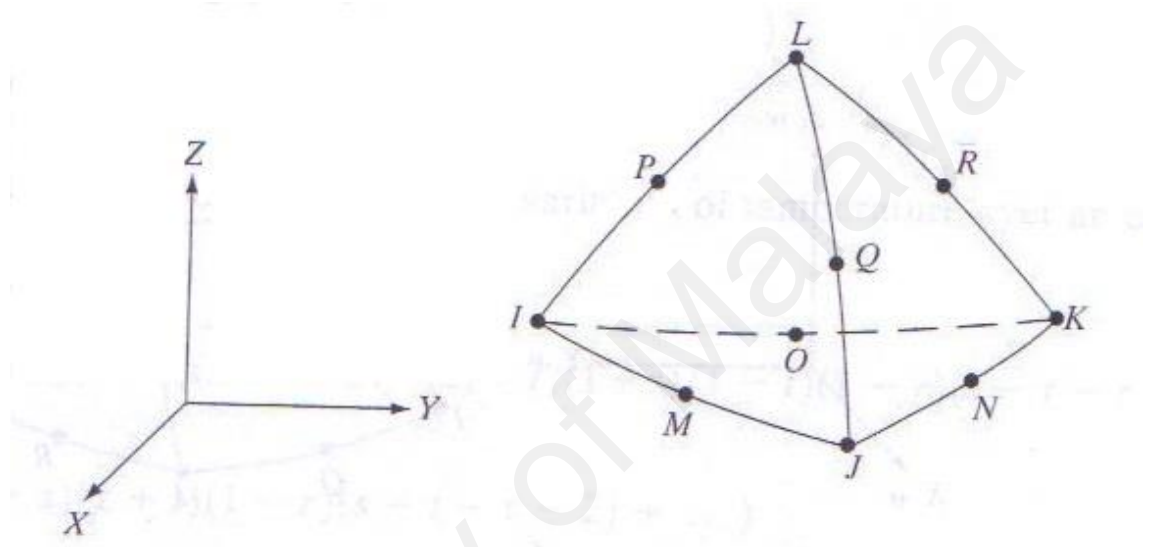
Figure 2.15: A typical ten-node tetrahedral element (Moaveni, 2008)

This element is better matched and more exact in modelling problem with curved borders. The displacement field for this type of element can be written as below;

$$u=u_I(2S_1-1)S_1+u_J(2S_2-1)S_2+u_K(2S_3-1)S_3+u_L(2S_4-1)S_4+$$

$$4(u_MS_1S_2+u_NS_2S_3+u_OS_1S_3+u_PS_1S_4+u_QS_2S_4+u_RS_3S_4) \qquad (2.33)$$

$$\upsilon=\upsilon_I(2S_1-1)S_1+\upsilon_J(2S_2-1)S_2+\upsilon_K(2S_3-1)S_3+\upsilon_L(2S_4-1)S_4+$$

$$4(\upsilon_MS_1S_2+\upsilon_NS_2S_3+\upsilon_OS_1S_3+\upsilon_PS_1S_4+\upsilon_QS_2S_4+\upsilon_RS_3S_4) \qquad (2.34)$$

$$w=w_I(2S_1-1)S_1+w_J(2S_2-1)S_2+w_K(2S_3-1)S_3+w_L(2S_4-1)S_4+$$

$$4(w_MS_1S_2+w_NS_2S_3+w_OS_1S_3+w_PS_1S_4+w_QS_2S_4+w_RS_3S_4) \qquad (2.35)$$

- **Beam element (B32)**

This element is classified as Timoshenko beam element. Hence, this kind of beam basically works in one direction (in tension and extension) as they can also be deformed in the perpendicular direction. The displacement field for this type of element can be written as follows;

$$w^{(e)} = N_1^{(e)} w_1^{(e)} + N_2^{(e)} w_2^{(e)} \qquad (2.36)$$

Where; $w_1^{(e)}$ and $w_2^{(e)}$ are the nodal lateral displacement at local nodes1 and 2 of element e and the shape function as it is displayed in Figure 2.16.
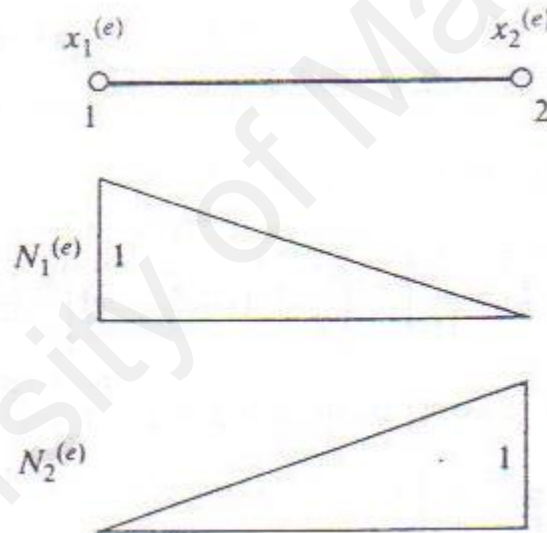
Figure.2.16: Beam element shape function (Owen and Hinton, 1986)

2.9.4 Stress formulation in elements

It is known from fundamental concepts that the displacement field and consequently nodal displacement are related to the strain component as follows:

$\varepsilon_{xx} = \eth u/\eth x$, $\varepsilon_{yy} = \eth u/\eth y$ and $\varepsilon_{zz} = \eth u/\eth z$

$\gamma_{xy}=(\eth u/\eth y)+(\eth \upsilon/\eth x)$, $\gamma_{yz}=(\eth \upsilon/\eth z)+(\eth w/\eth y)$ and $\gamma_{xz}=(\eth u/\eth z)+(\eth w/\eth x)$ \hfill (2.37)

On the other hand, stress components are characterized as below:

$[\sigma]^{T}= [\ \sigma_{xx}\quad \sigma_{yy}\quad \sigma_{zz}\quad \tau_{xy}\quad \tau_{yz}\quad \tau_{xz}\ ]$ \hfill (2.38)

Where; σ_{xx} , σ_{yy} and σ_{zz} are the normal stress and τ_{xy} , τ_{yz} and τ_{xz} are the shear stress component.

According to the Hookes low;

$\varepsilon_{xx} = (1/E)\ [\ \sigma_{xx} - \upsilon\ (\sigma_{yy} + \sigma_{zz}\ )]$

$\varepsilon_{yy} = (1/E)\ [\ \sigma_{yy} - \upsilon\ (\sigma_{xx} + \sigma_{zz}\ )]$

$\varepsilon_{zz} = (1/E)\ [\ \sigma_{zz} - \upsilon\ (\sigma_{xx} + \sigma_{yy}\ )]$

$\gamma_{xy} =1/G^{\tau xy}$, $\quad \gamma_{yz} =1/G^{\tau yz}$ and $\quad \gamma_{zx} =1/G^{\tau zx}$ \hfill (2.39)

In compact-matrix form, the above relationship transforms into;

$\{\sigma\} = [\upsilon]\ \{\varepsilon\}$ \hfill (2.40)

From (33) the compact-matrix form for strain energy Λ is;

$\Lambda^{(e)} = ½(\ \int_{v}[\varepsilon]^{T}[\upsilon]\{\varepsilon\}\ dV$ \hfill (2.41)

CHAPTER 3:

MATERIALS AND TEST METHODS

3.1 Introduction

The experimental part of this study was performed to determine the essential parameters and for comparisons with the numerical simulations. In other word, the main part of this study is numerical simulation and experimental examination is only an auxiliary part for finding the necessary input data for simulation and also helping to evaluate the simulation result (by comparing of the experimental results paradigm with the simulated ones). Therefore, small varieties of samples were chosen where only the major root diameters were examined. This part of study is divided into two major parts; laboratory and field testing.

The main purpose of laboratory testing is to determine the mechanical properties of the root and soil where the pulling out tests were performed, meanwhile field tests were performed to determine the pulling out characteristics as well as pulling out force, the vertical deformation and the stress distribution.

3.2 Laboratory tests

Material characteristics to be used in modelling of root anchorage were obtained from the laboratory test result. The laboratory tests were carried out on the root and soil samples collected from the site and the parameter determined included specific weight, mechanical properties and particle size distribution.

The test results are illustrated in chapter 5.

3.2.1 Soil properties test

The soil material was classified into sandy silt by the United Soil Classification System. This classification of the soil was determined based on the soil characteristics, obtained with the following tests:

a) Particle size distribution

This test was done based on BS 1377, 1990: part 2. As per as clause 9 BS 1377; 1990 part 2, whereby 'dry sieving' method was performed during this exercise. Soil sample for this test was dried in oven up to 105º and finally was sieved using the sieve shaker rotating at 15 rpm for 10 minutes. (Sieves assemble in the ascending order of sieve number 4 at the top and #200 sieve at the bottom).

b) Soil Young modulus and shear strength properties

- **Soil Young modulus and passion ratio**

The Young modulus and passion ratio is one of the most difficult soil parameter to estimate because they are depending on the variables. To obtain soil Young modulus (E) and Poisson ratio (ν) during this exercise, soil stress-strain curvature was extracted based on triaxial test result. Five set of Triaxial tests were performed based on BS 1377, 1975; Test 21. To do this, five undisturbed cylindrical soil standard samples were collected from the field of experiment and used for this test. To obtain young modulus and Passion ratio equation 3.1 to 3.3 was solved for 2 unknown values (E and ν)

$$\varepsilon xx = 1/E(\sigma 3 - \nu(\sigma 1 + \sigma 3)) \tag{3.1}$$

$$\varepsilon yy = 1/E(\sigma 3 - \nu(\sigma 1 + \sigma 3)) \tag{3.2}$$

$$\varepsilon zz = 1/E(\sigma 1 - \nu(\sigma 3 + \sigma 3)) \tag{3.3}$$

- **Direct shear test(shear Box test)**

This test was done based on BS 1377, 1990; Part 7(Soil Cohesion c, Internal friction angle Φ and Dilation angle Ψ was determine during this test). Five disturbed samples from the field were used for this test. Disturbed sample was chosen for this test to ignore the root effect on the soil shear characteristics (the remaining roots was removed from the soil sample before performing test)

3.2.2 The specious studied and roots mechanical properties test

The *Melastoma malabathricum* was chosen and marked for the pulling out test before testing. The species was chosen due to its outstanding physiological characteristics as a slope plant such as high growth rate, high plant-water relations and high aluminium accumulator (Normaniza, 2005).

The profile of the species studied was shown in Figure.3.1

Figure 3.1: Plant profile of *Melastoma malabathricum*

To determine the root material mechanical properties, ten series of each five specimen of pulled out root in the length of each 20 cm with different diameters (range 13mm to 30mm) were cut and used for tensile test based on ASTM D143-09. Instron 5565 test machine was used to perform the axial test for determination the root tensile

properties such as Young modulus E, poison ratio ν and yield stress. After tensile test, the failed specimens were used to determine the average of root density.

Fresh root sample after pulling out immediately was used for this test to reach acceptable accuracy in root mechanical characteristics used in simulation.

3.3 Field pulling out test

The site for the pulling out test was located in the campus of University of Malaya, Kuala lumpur, Malaysia. The pulling out equipment and its connection with the *Melastoma malabathricum* root system are illustrated in Figure 3. 2

Figure 3.2: The pulling out equipment and gripping system

In order to perform a better control on pulling out process, a DC motor was implemented in pulling out device (Figure 3.3). DC motor was chosen to perform a uniform force during whole pulling out process because as we know, changing in the performed force during the pulling out is affecting the root anchorage characteristics. To convert the motor torque to the vertical displacement a gear was employed with

performed rate of 1mm/minute. Performed displacement during the pulling out process is converted to pulling out force via load cell existing in pull out equipment.
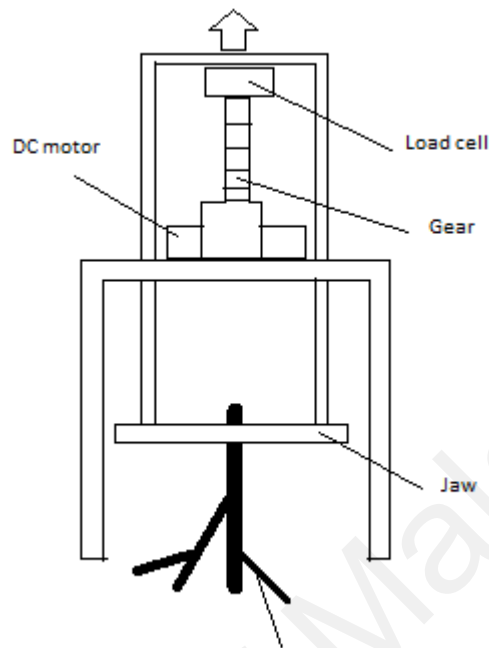
Figure 3.3: Schematic view of pulling out device

For this experiment, the load cell VMC model VLC-110s (50 kN) and LVDT model DP-500E (50 cm) were used. The load cell and LVDT were connected to the portable data logger Campbell Scientific model CR1000 which was connected to the laptop to record the data acquisition of the pulling out resistance and pulling out displacement.

Experimental site and area was chosen on a slope, near the entrance gate, Section 16, University of Malaya. The age of the plants ranged from 1 to 3 years, the stem diameters varied from 10 to 25 mm and the heights were up to 2 m.

From replicated performed tests, six sets of the pulling out tests in total were considered as index diameter to be as an average for all examined species. Considered diameter was chosen due to their multiplicity among all replication (13.4 mm, 15 mm, 16 mm, 20 mm, 24 mm, 25 mm and 30 mm). Based on the most commonly occurred replication during the test, three diameters (20 mm, 24 mm and 30 mm) were chosen for

simulation verification. These three samples were scan-modelled and simulation was performed on them (as shown in section 4.3.3).

The tests were performed during a rainy season; therefore, the matric suction was in the range of 7-12 kPa. The matric suction was measured using the miniature tensiometer with three sets of sensors (Figure 3.4) installed in the testing area (Figure 3.7)

Data logger   Sensor

Figure 3.4: Miniature tensiometer; the data logger and its sensor

To determine the stress distribution in the soil body, seven sets of the pressure transducer were used (Figure 3.5)

Figure 3.5: Pressure transducer

The tests were conducted until the root was pulled out completely. During the pulling out process some branches were ruptured and some of them were pulled-out. (Figure 3.6) The rapture locations differed from branch to branch in each test.

Figure 3.6: A sample of pulled-out roots.

3.3.1 Scheme for the installation of transducers and tensiometers for the experiment

To verify the trustable matric suction during the pulling out process, three nods of miniature tensiometers (shown in Figure 3.4) were employed in a triangle order placement. To determine the soil pressure in the soil during pulling out process, considering the root diameter, five nods ultra-miniature pressure transducer (shown in Figure 3.5) was located in circular plan in the equal distance in 10cm away from the species stem.

Scheme for the installation of pressure transducer and miniature tensiometer is depicted in Figure.3.7
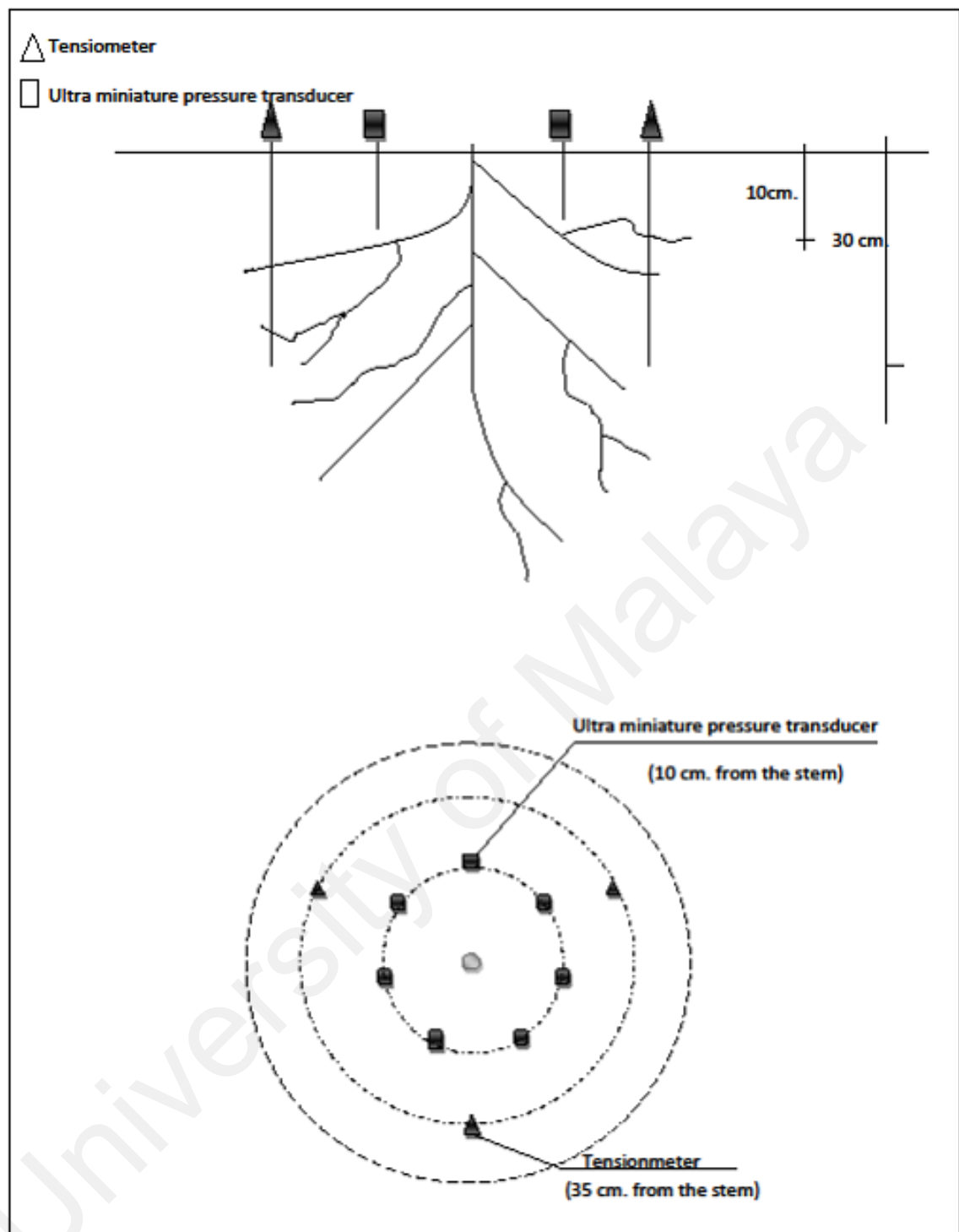
Figure 3.7: Scheme for the installation of pressure transducer and miniature tensiometer

CHAPTER 4:

NUMERICAL SIMULATION

4.1 General

Understanding how the pulling out forces are transferred to the soil via root system and what determines the anchorage resistance of the species is vital in predicting potential landslides in critical slopes. To date, our knowledge and ability to predict slope instabilities using vegetation has been limited by our capacity to comprehend the nature of the root–soil interaction in the context of real root system architectures. Root morphologies are usually very complex and their variability is poorly understood. Therefore current experimental approaches are also unable to measure the essential mechanical variables (e.g. strains, stresses, and displacement fields) in the roots during the in-situ pulling out tests. However finite element and other numerical methods applied in physics and engineering are potentially very powerful tools in obtaining quantitative and in depth information on such mechanisms, and the model presented here is an attempt to adopt such methods to understand the mechanical properties of the root–soil composites. In this study, the development and testing of the finite element method in the anchorage of the species studied were described. The developed model allowed us to simulate the pulling out process in the *Melastoma malabathricum* species while accounting for an accurate geometrical and topological description of their three distinct root system architectures located at the end of the slope during the slope failures.

4.2 Formulation of three dimensional finite element models

Contact algorithms incorporated in the finite element method are necessary to model the interaction between the root and soil during the pulling out process.

A number of commercial finite element codes which can deal with this kind of tasks are the ABAQUS, ADINA, ANSYS, ASAS, BERSAFE, CASTEM, LUSAS, MARC, MSC/NASTARAN/SYTRAN, and PAFEC (Mottershead and Stanway, 1986). Since the ABAQUS is powerful software for the finite element analysis in the case of dynamic problems and the implicit and explicit methods are combined together in one software, we chose the ABAQUS ver.6.10.Ef1 as the finite element code for the present research.

On the other hand, the explicit method was chosen (Quasi-static) for this study because of the fact that the failure in different branches occur separately in different time periods and the standard analysis job will be stopped with the first failure in the branches.

4.3 Root and soil modeling

This part explains the methods for modelling of the root and soil, not only about their geometry but also the technique which was adopted for this study.

4.3.1 Simulation restrictions

Root has a small cross section along a relatively long length and in the other hand possesses a complicated form. Lengthwise, root branches adjoin to other branches as well hair roots. These complicated roots form together with unpredictable soil characteristics causing complexity in simulation which consequently results in some restriction. Following some of this restrictions are maintained.

a) CPU run time

With regards to the technical aspects of the generic 3D model described here, the CPU run time is high (around 400,000 second), and perhaps the problem of convergence unable models to be compared readily to real data. Nevertheless, such a numerical tool is very promising and can be applied to any root architecture from which

the topology and geometry have been accurately described. The numerical approach developed in this study can also be adopted to explore in details the role of each of the structural elements involved in plant pulling out.

b) Root- Soil interaction and material characteristics

The embedded hair root in the soil body used in the model does not allow consideration for sliding or opening of the root–soil surface interaction during failure. Therefore, the rigid root–soil adhesion used in our model for hair root - soil constraint can be expected to artificially increase the uplifting resistance. Meanwhile, the material model used for the roots and soil is probably not suitable for large deformations. The highly anisotropic and fragile models can also lead to the failure of the individual root elements, which will realistically represent root breakage. However, the generic 3D uplifting model developed in this study does not include all the elements necessary to accurately predict the uplifting resistance. Despite all stated above, still FEM modell can provide useful information on how the root system structures interact within the soil.

4.3.2 Model Geometry

Based on the natural element size, the following units are used for modelling;

- Distances- meter (m)

- Force-Newton (N)

- Pressure- Pascal, Pa (N/m^2)

- Density- kg/m^3

- Angle-Degree (˚)

The root system of the *Melastoma malabathricum* consists of a shallow main vertical root, about 10 cm deep with a basal diameter of maximum 7 mm and long

horizontal root with the same basal diameter and the maximum 500 mm length. This central root bears numerous secondary laterals with an average density of 35l laterals/m and a mean diameter of 4.191 to 0.213 mm. The root system had a total volume of 30 cm^3 and had over 35 structural roots (50% were smaller than one mm in diameter), with a total root length of almost 2 m (Figure. 4.1).

Figure 4.1: One of the excavated *Melastoma malabathricum*

For the determination of root architecture, three samples of the root were excavated and dried in the oven at 85˚C for five days as shown in Figure 4.2. Then, they were scanned with a high definition scanner and the files were made in txt or xlsx extension by the WinRHizo program (ver. A). The root architecture data, which were recorded in the files, provided the topology and geometry of the whole root structure.

For this, each branch was cut from the main root and scanned individually. These data contain the length of each branch and the diameter, as denoted in Figure 4.2.

Figure 4.2: The branch scanned with the WinRhizo

The diameter of the roots (*Melastoma malabathricum*) was between 2-3 mm to 6 mm depending on the main or lateral root and the length was nearly 1000 mm. The soil block is supposed to be a cube with the dimensions 1000 mm x1000 mm x1000 mm which covers the root completely.

In this FEM model, the root systems were modelled as a combined system. As seen, the first order root branch was considered as a 3D solid element and the second order branches as 3D beam element available in the ABAQUS library. As in nature, the first order and second order branches (hair roots) are connected together with couple constrain using the ABAQUS predefine constrain (shown in Figure 4.3).Through this study, 1 mm branches (diameter) and less were considered as the second order branch and element with larger diameter branches were considered as the first order branches . The diameter of the branches was considered as the average diameter according to the branch biomass due to diameter change within the branches length.
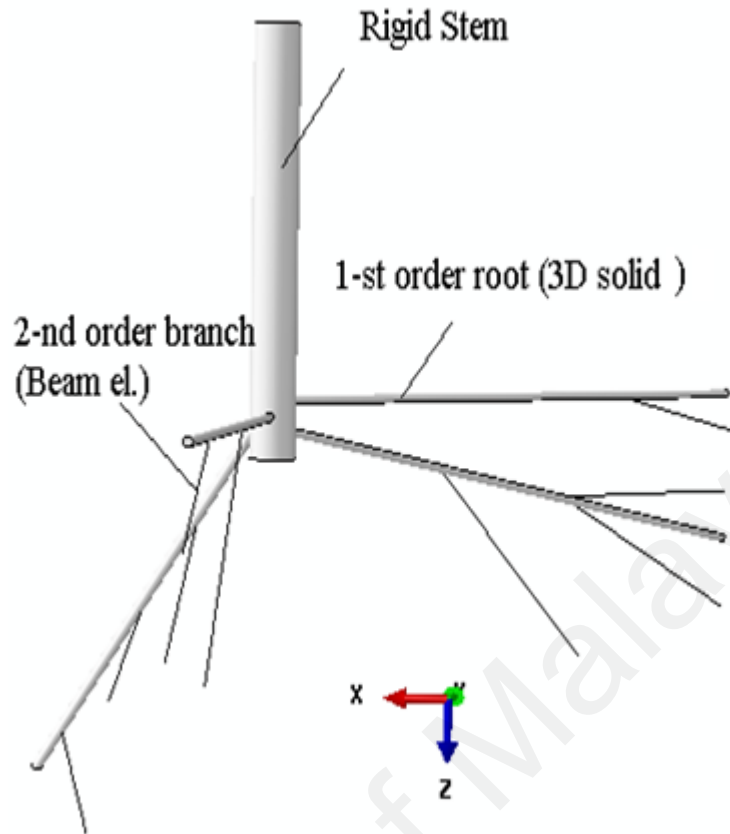
Figure4.3: Modelled root in Abaqus cae.

The above mentioned geometry was chosen to be in the natural root shape as much as possible. The stem was assigned as a rigid element with the Quad element shape and connected to the branches with the coupling constraint between rigid stem reference point and branches (0 degree of freedom). The reaction force and displacement are performed at this reference point. This displacement converts into the pulling out force in the soil (via roots), caused elastic strain and consequently caused plastic strain in the soil body.

4.3.3 Mesh generation and element type

Based on the small dimension and complicated shape of the model, 'free technique' was chosen for meshing during this study. The element type performed for the main roots (first order roots) and soil domain consisted of ten-node tetrahedral modified

element (C3D10M). On the other hand, the hair roots (second order roots) consisted of beam element (B32). The soil block was assumed to be fully integrated therefore adaptive mesh cannot be used for this particular element and since the main point of this exercise is to study the effect of pulling out on soil it's no point to choose root meshing as adapted mesh. Instead, the elements were chosen as quadratic element. Due to the root complex form the datum planes were identified along the root branch directions and section was drawn through this datum plans (as illustrated below).
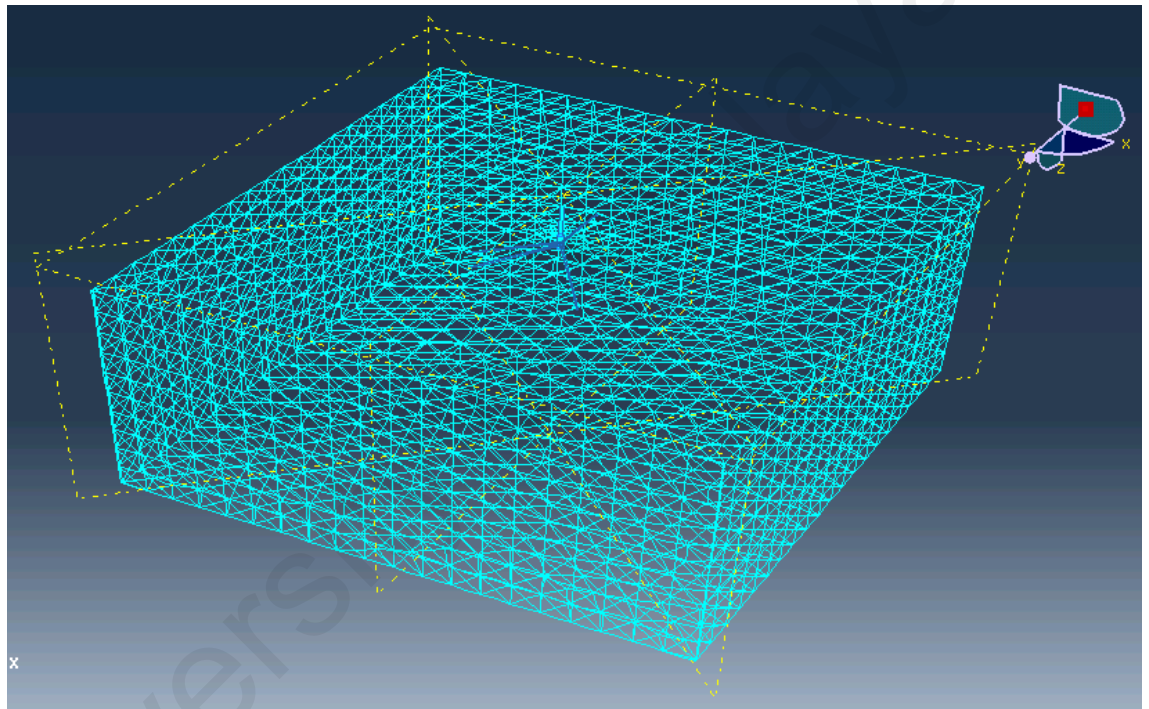
Figure4.4: Whole model including datum (cut) planes

The mesh size was chosen according to the model accuracy and CPU run time.

Besides, the numerical output demonstrated that result accuracy diminishes when the mesh size is larger, because some elements are being ignored with larger mesh. On the other hand, the calculation time (CPU) increased exponentially with the number of elements.

Therefore, a mesh with 8488 elements was finally used for the comparative analysis. Furthermore, in the explicit analysis the time period step can be determined,

which is effective on the CPU run time and consequently on the result accuracy (by the time of the load effect). Based on the experiment, 300 seconds was chosen for this research. This choice provided a good compromise between the accuracy of the numerical results and the calculation time required for the simulations. However, other techniques can also be used to decrease the CPU time such as the parallelization available in the ABAQUS software but we did not use them for this study.

In this study, mass scaling was also used in scaling the mass of critical elements (smallest and most distorted element when the structure impacts a fixed rigid body). The nodes associated with these elements often have very little mass and hence, contribute very little kinematic energy to the model (it was proved by changing the minimum target in mass scaling).

4.3.4 Boundary condition and interaction

The boundary condition was used to constrain portions of the model to remain fixed (no displacement) or to move by a prescribed amount. Specified boundary condition included the displacement and rotation. They could be given zero value as well as none zero value boundary condition.

In order to catch all the stress distribution contours, 1meter depth of the soil in the model was chosen. We assume that the stress is damping in this 1 m; therefore, the soil block is fixed in the base in 1 m (U1=U2=U3=UR1=UR2=UR3=0).

In order to limitless wide in natural, in this model, the absorbing boundary should be defined for the side boundaries (Poulos and Davis, 1974). Viscous boundary method was chosen where the connection was characterized as springs to distinguish the geometrical damping border as illustrated in Figure 4.4. In this model the damping coefficient is determined as below (Rahmanian and Maleki, 2007);

$$F_d = \rho V_s A \tag{4.1}$$

Where; ρ is soil density, V_s is S wave velocity and A is element cover surface.

To simulate the soil reaction in the lateral side, the dynamic spring was employed where the K coefficient was found from the damping coefficient as mentioned above. Based on the Soil classification mentioned in section 5.2.1.a and Terzaghi's diagram mentioned in Figure 2.11, the values for $N\gamma$, Nc and Nq corresponding to the soil friction angle mentioned in section 5.2.1.c were obtained while the value of qf was extracted using equation 2.25. S wave velocity is obtained using Imai and Yoshimura proposed empirical equation as given below (Tezcan and Ozdemir, 2011);

$$qf = Vs2.4 \ / \ (1590) \ (kPa) \tag{4.2}$$

All the nodal points at the bottom of the test specimen were fixed, as shown in Figure 4.5.
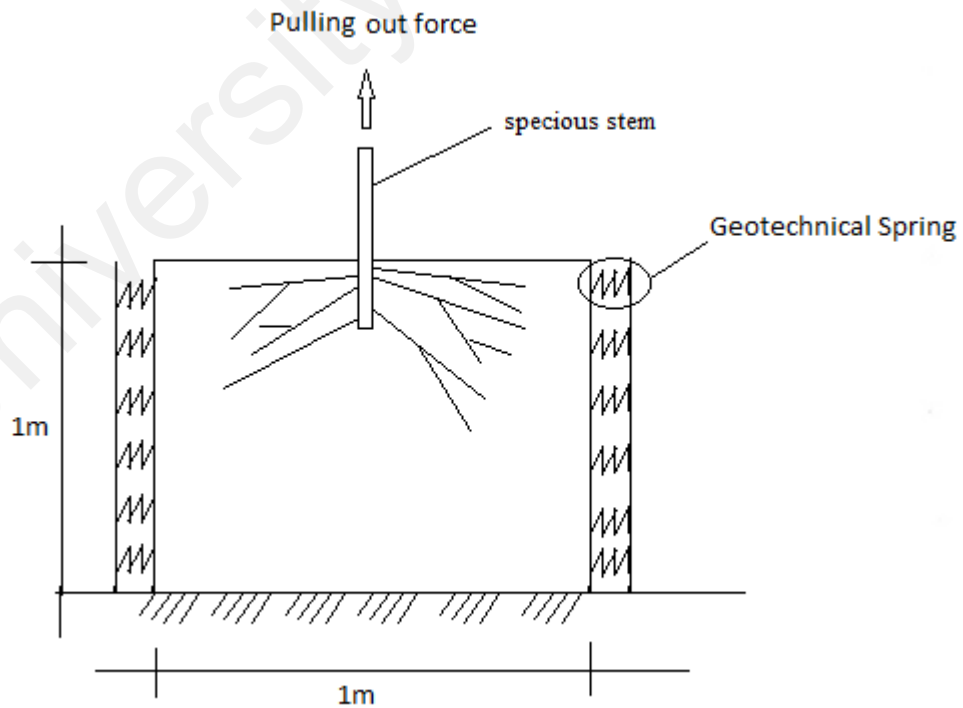
Figure 4.5: Simulation of pulling out performed on the finite element model.

4.3.5   Initial condition

Based on the combined system used during this study, two types of contact were employed in this model. The experimental results donate most of the raptures occurred in the second order branches therefore surface to surface with the frictional tangential behaviour was chosen for the first order root branches. The friction coefficient chosen was 0.4 based on the previous work (Dupuy L. Et al. 2007).

For the second order roots branches to show their rapture, it was assumed that the second order root branches are embedded in soil; therefore they are carrying the load until their rupture (comparison with experimental results will indicate the accuracy of this hypothesis).

4.3.6   Material properties

The material properties taken from the result of laboratories test as described in 3.2.

4.3.7   Loads applied for simulation

In this analysis, the displacement applied at the top of the rigid stem became the pulling out force in the soil (via roots) and caused elastic strain and consequently plastic strain in the soil body (as per as section 3.3).

The results from the pulling out test are used to compare with the pulling out concentrated reaction force reporting from numerical simulation (based on the maximum allowed vertical displacement in the performed model). This compression is helping us to validate the simulated model.

The maximum driving force for our pulling out test was the final load which caused pulling out for the species. However, in order to have a complete picture, we utilized the

maximum displacement on root anchorage failure point for the maximum reaction force fixation in our simulation (as per as section 4.2.6)

4.4 Three dimensional finite element model for root anchorage

Using the information above, several three dimensional models were carried out to elaborate a method to simulate an accurate 3D model for root anchorage during pulling out process which demonstrate maximum matching to actual case. As second step to validate the used models and hypothesis, the result of pull out reaction force from field experiments (obtained in section 3.3) was compared with the corresponding result from the finite element simulation. Moreover, well controlled laboratory test done by Siti Sara et al. 2010 were also modelled and the obtained results were compared with stated results to verify the model accuracy. In last stage of this research, those model were adopted again with different root architectures and soil mechanical properties to analyse its effect on the root anchorage (the following sections, a more detailed description in connection with the proposed models will be provided)

4.5 Pull out simulation of *Melastoma malabathricum*

As mentioned in section 3.3, after pulling out, three different root geometries were chosen out of a wide variety of geometry. These roots were prepared and modelled for this study. Each root has its own geometry with difference in their width and depth, as shown in Figure 4.6. The measured root length was around 40 cm for sample 1, 50 cm for sample b and 30 cm for sample c respectively.
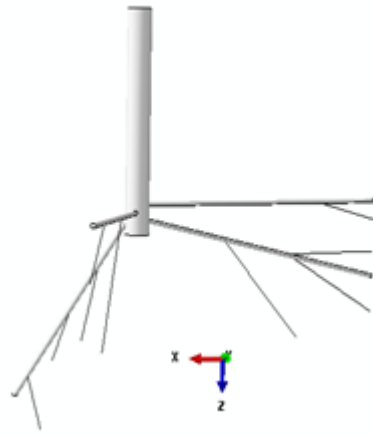
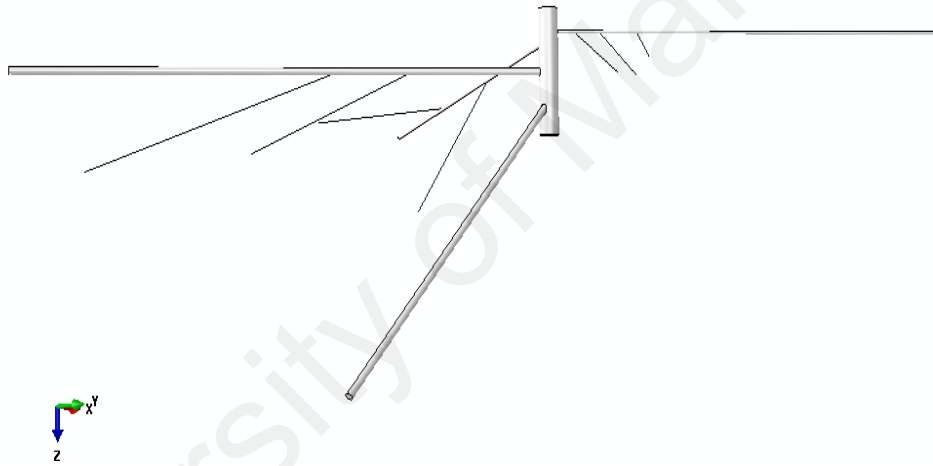Sample (1)   Sample (2)   Sample (3)

Figure 4.6: Three *Melastoma malabathricum* samples used for root geometry modelling

From each sample, a geometrical model was prepared (in the same way as 4.3), as displayed in Figure 4.7.

Sample (1)

Sample (2)

Sample (3)

Figure 4.7: Geometrical models for each sample

The laboratory test results for material properties demonstrate in chapter 5 and the maximum displacement obtained in field pulling out tests were used as input data for the simulation work.

4.6 The pulling out simulation for different root architecture

In this part of the study the effect of root architecture on the root anchorage was considered in different term such as long taproot, various root pattern and root deviation angle.

4.6.1 The effect of taproots on pulling out process

To justify the effect of taproots on the pulling out process, modelled sample (2) was modified by adding a long taproot (almost 1 m in length), and both the original and modified models were placed under the pulling out process as described before. To simplify the simulation, the root branches were considered as beam elements embedded in the surrounding soil. This simplified model ignored any root movement in the soil which can cause inaccuracy in the result. However, as shown in Figure 4.7, root form can be modelled more realistically than the method described in section 4.3. This is because, one dimensional element such as beam elements are employed for modelling, these elements do not complicate the mesh form for the soil body therefore their various curved forms can be modelled realistically. On the other hand, for three dimensional elements applied in root modelling (as per section 4.3), all movement and interaction between soil and roots are considered but the complicated root form cannot be modelled in exactness. In this particular case this inaccuracy can be ignored because we are going to compare similar cases where the only change is in the existence of the long taproot. Therefore the simplified model is sufficient for this part of the study.

In each case the long taproot (1m) was introduced as shown in the Figure 4.8.
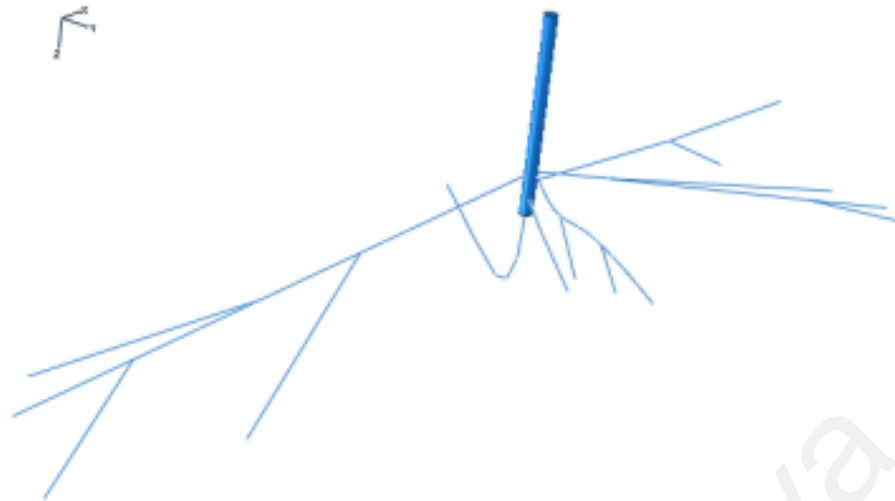
Simplified model for sample (2)
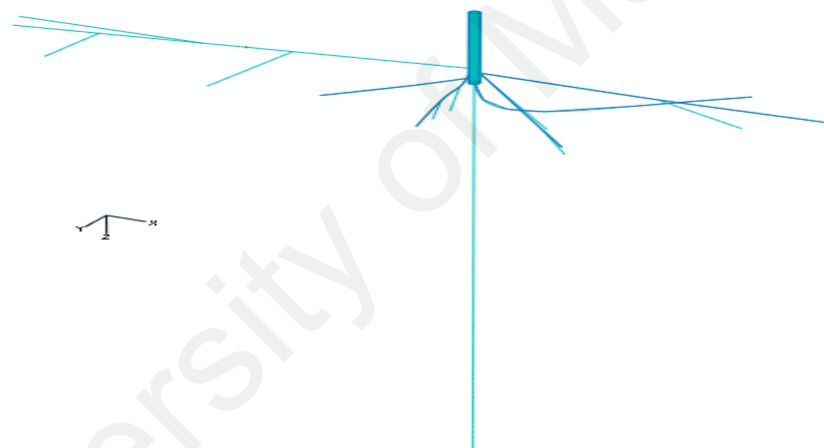
Simplified model for sample (2) adding long taproot

Figure 4.8: The geometry of the modified root

4.6.2 Effect of root pattern and angle of inclination on pulling out

It is still unknown how the root pattern and inclination angle affect the pulling out characteristics. If optimal root architecture can be defined, it may then be achievable to control the root systems or soil properties to increase the resistance when pulling out. However, it is believed that the pulling out resistance depends on the root system architecture and soil properties, but only few studies have been accomplished to test this

hypothesis. To predict the importance of root geometry especially the root form and angle to the maximum stress distribution on soil and consequently performed force during the pulling out process, a 3-D FEM model was formulated which permitted the pulling out of analytical root systems with different branching patterns and inclination angles to be simulated in the soil type similar to the unsaturated sandy silt. The soil and root mechanical characteristics and boundary condition were employed from the real root and soil condition (as per as section 5.2.1 and section 5.2.2).

In this part of the study, the simulation was done to study the effect of different parameters on the pulling out resistance where the first order roots are to perform the main role. Therefore, separate root models were employed where the second order root branches were ignored. To approach this effect, root models used were 3D cylinder elements (C3D10). During this simulation, friction coefficient 0.4 was utilized in the interaction to reach a more realistic result. Boundary conditions were such that the lower edge of the soil domain was fixed and lateral boundary was represented by springs as explained in section 4.3.5. To provide the friction force effected between the soil and root during the analysis, Finite Element is considered on effecting soil domain gravity forces (otherwise the friction between the soil and root is not affected in the analysis). For simplicity, the soil water pressure was not computed.

The length of the branches was also different to approximate their role in anchorage. Stress distribution within the soil body was discovered during the pulling out process. The results are discussed with regards to the consequences of slope stability, the role of root geometry in pulling out resistance, stress and strain distribution.

a) **Effect of root pattern**

As to the change in the root pattern, three types of formal root systems of H (with the horizontal branches), A (branches with the 45° angle to the horizon) and M (mixed

horizontal and angular branches) with different branch lengths were considered (Figure. 3.15). Each root system consisting of three pairs of roots in different directions, i.e. B1, B2, B3 and B4, B5, B6, linked to the vertical rigid stem RS, and taproot located just below the B3 root, was named as TR. The length of the taproot was 40 cm and each shallow lateral, B1 and B4 were 0.5 m, B2 and B5 were 0.35 m and B3 and B6 were 0.26 m. All the root elements were 10 mm in diameter (Figure. 4.9). To calculate the comparative effect of taproot element on the anchorage effectiveness, the taproot distal extremity TR was removed separately for each root type. Simulations were performed by the application of the displacement and the concentrated force at the rigid stem reference point.
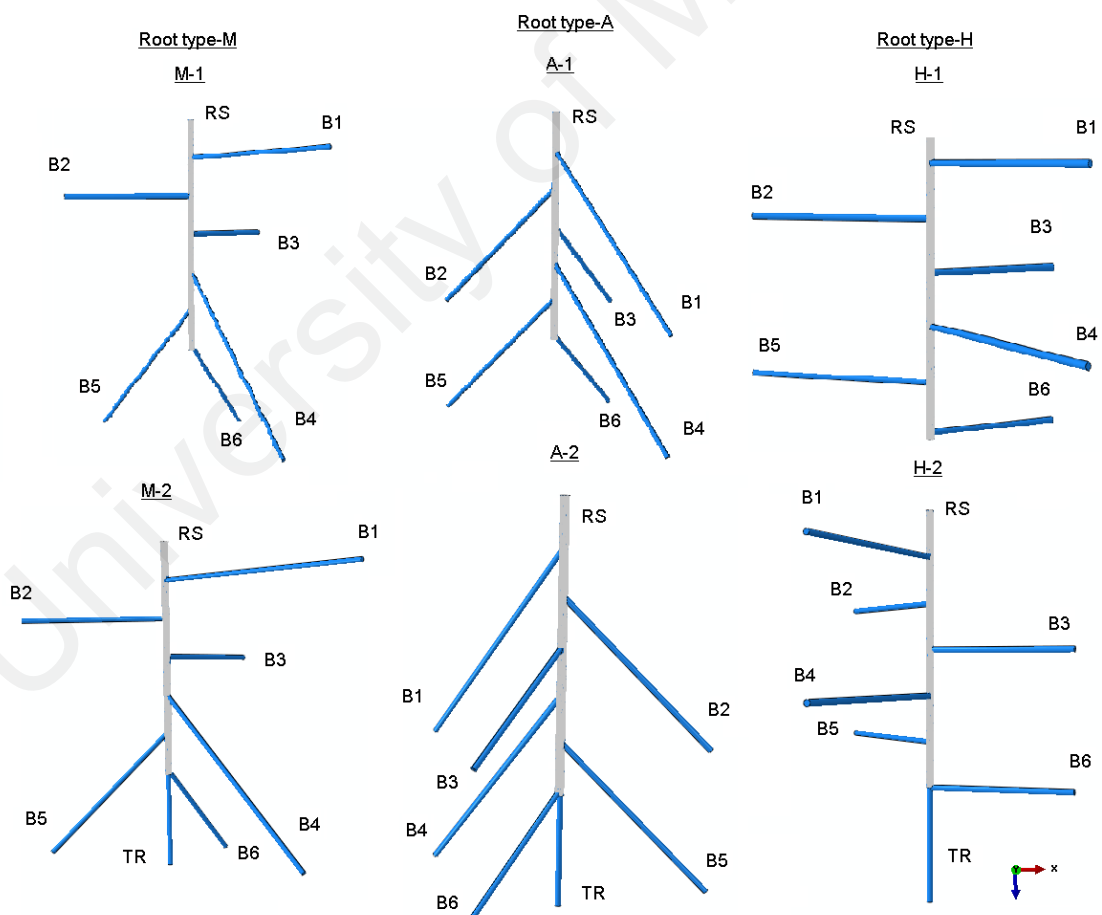
Figure 4.9: Geometrical description of the 6 root patterns with different branch lengths, angle to horizon, and with or without taproot element

b) Effect of root angle

For the effect of root inclination angle, a range of root inclination angle model including 15°, 30°, 45°, 50°, 52°, 53°, 54°, 55°, 60° and 75°. (Figure 4.9) were used. Each root system consisted of three pairs of roots in different directions, i.e. B1, B2 and B3 (which emphasizes the 3 geometrical perpendicular directions) linked to the vertical rigid stem RS. The length of each shallow lateral, B1 was 0.5 m, B2 0.35 m and B3 0.26 m. All the root elements were 10 mm in diameter (Figure 4.10). Simulations were performed by application of the displacement at the rigid stem reference point.
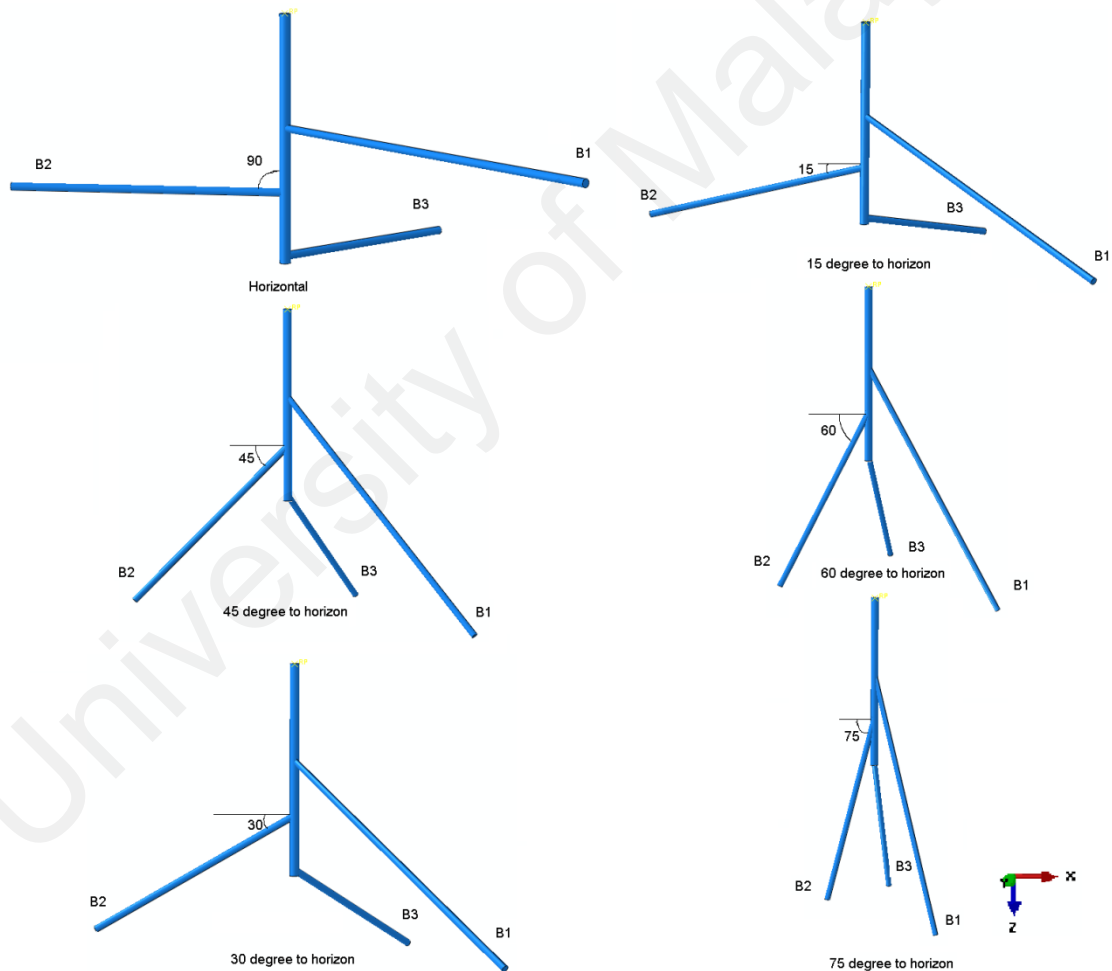
Figure 4.10: Geometrical descriptions of the 6 root patterns with different branch angle to horizon

4.6.3 The effect of soil cohesion and angle of internal friction on pulling out

The main factor in the root-soil matrix which is affecting the root anchorage is the friction between the root and soil. In the model used for 3.5.1 and 3.5.2, the first order roots were announced as the solid cylinder elements (C3D10) which are interacting with soil by friction behaviour but the second order root branches were modelled as beam element embedded in the soil; therefore, any movement between the soil and this element was not allowed until rapture. In this part of the study we can ignore the second order root branches and employ different root models as connoted by Figure 4.11.
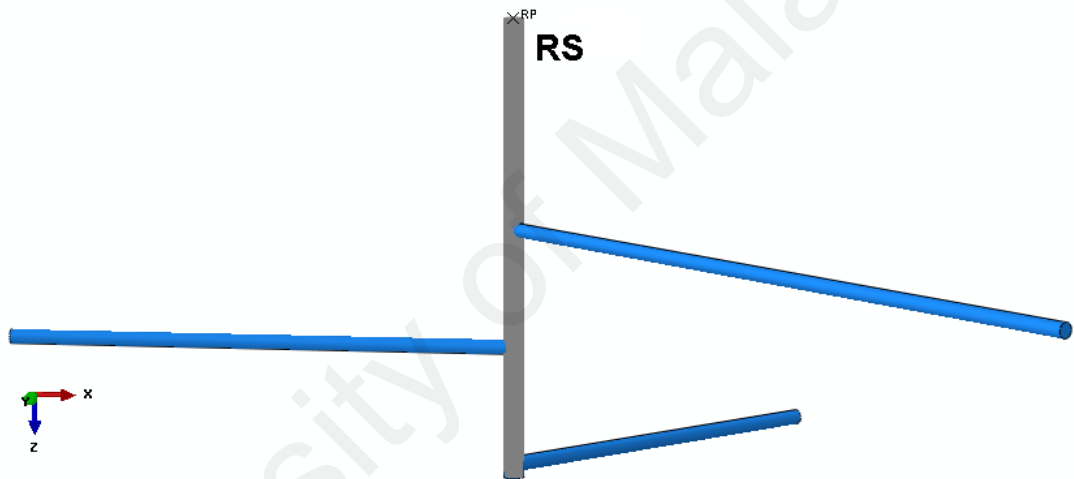
Figure 4.11: Geometrical employed root model for determination c and Φ effect on root anchorage

In this model, the first order branches were employed and 0.4 for friction coefficient from the previous work was used (second order branches were ignored due to their minor effect on this respect). The applied displacement on top of the rigid stem was converted to pulling out force.

The value of friction angle is almost fixed during the time and almost only influenced by the water content as well, but the cohesion value which depends highly on the matric suction in the unsaturated soil.

However, as discussed before the total cohesion intercept (c) have a direct relationship with the matric suction on the failure plane at failure $((u_a-u_w)_f)$ formula and indicated the angle for the rate of increase in the shear strength related to soil matric suction.

In this part, the magnitude of soil mechanical properties (such as c and ϕ) will be changed in one of the predefined models in 4.5.3 (model with horizontal branches as shown in Figure 4.9), to study the effect of the above-mentioned properties on stress distribution and also on the maximum and minimum values of the stress during the pulling out process.

a) Cohesion, c

As mentioned before in Figure 2.7, change in matric suction mainly affects the apparent cohesion value. In this part of the study, different cohesion values were used for the different soil types based upon the Lindeburg, Civil Engineering Reference Manual for the PE Exam (as shown in Table 4.1).

Based upon the Ferdlund et al., 1978;

$c_1=c'+(u_a-u_w)_1 tg\Phi^b$

$c_2=c'+(u_a-u_w)_2 tg\Phi^b$

$tg\Phi^b=(c_1-c_2)/((u_a-u_w)_1-(u_a-u_w)_2)$ (4.3)

Where: c_1 and c_2, Total cohesion intercept

u_a-u_w , matric suction

Φ_b , angle for the rate of increase in shear strength

Total cohesion and matric suction were measured in certain place at different time. Using above mentioned field output for matric suction and corresponding soil cohesion

value in Equation 4.3, 0.306572 was used as the average value for tgɸb during this study.

Table 4.1: Cohesion value for the different soil type (Lindeburg, 2001)

USCS Soil Group	c, as compacted (kPa.)	c, saturated (kPa.)
GW , GP	0	0
SM	50,24	20,1
SM-SC	50,24	14.35
SC	74,16	11
ML	67	9,1
ML-CL	64,6	22
CL	86,12	12,92
MH	71,77	20,1
CH	102.87	11

Kamal (2010) found that the magnitude of the matric suction can reach up to 100 kPa during the dry season in Kuala Lumpur. This amount is considered as the maximum amount of matric suction and 10 kPa is determined as the minimum amount (it was measured from the soil sample used for soil physical characteristics during this study). Based upon the extracted value of tgΦb from equation 41 (using the maximum and minimum value of matric suction in Kuala Lumpur stated by Kamal and cohesion value based on Table 4.1) and the cohesion value (c) belonging to saturated soil samples, correlations between the cohesion value (c) and matric suction for different soil categories were determined as shown in Figure 4.12. In this estimation the saturated soil condition was considered as the primary condition and cohesion value was shown to increase with the rising in matric suction value. Based on similarities in cohesion values observed in different soil classes in a saturated condition (Table 4.1), the modelled soils

were drived into three categories. The first category is known as highly cohesive soil (20-22 kPa) and includes sandy silt(SM), high plastic silt (MH) and low plastic silt to low plastic clay (ML-CL). Low plastic clay (CL) and sandy silt to sandy clay (SM-SC) are categorised as soils with normal cohesion value (12-14 kPa) while sandy clay (SC), low plastic silt (ML) and high plastic clay (CH) are classified as low cohesive soil (9-11 kPa).
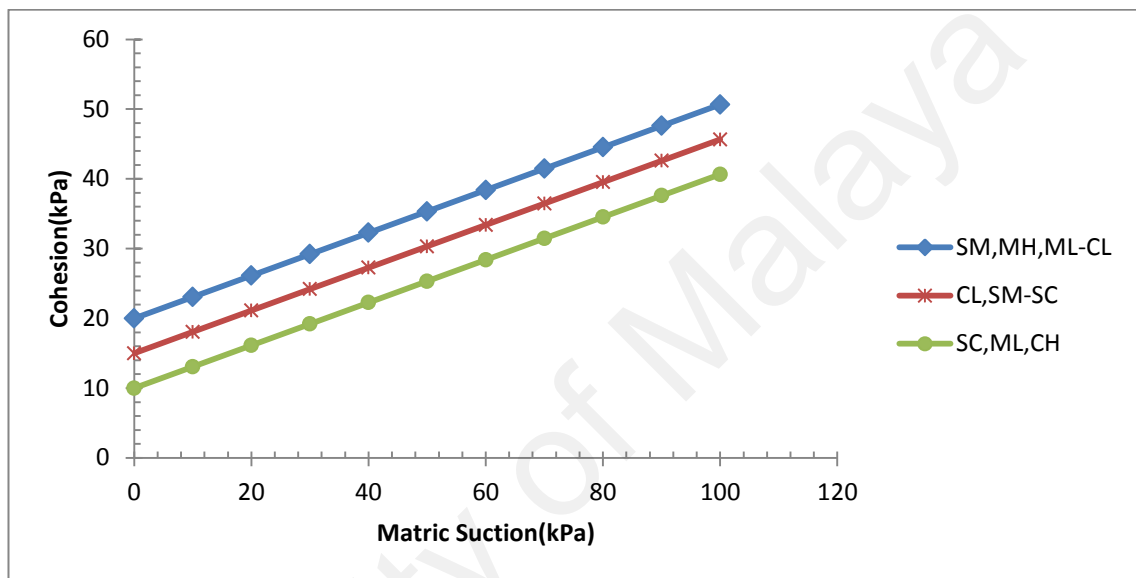
Figure 4.12: Relationship between total cohesion intercept (c) and matric suction

b) Angle of Internal Friction, ϕ

In this section of the study, different values of angle of internal friction were used for different soil types based on the Standard Penetration Test defined by Bowels at 1996 (Table 4.2)

SPT value shows a direct relationship with the soil plastic characteristics. As the SPT value rises, the soil is changing from loose to hard in sandy soil (sand, sandy silt and sandy clay). In this research changing in friction values are to demonstrate the various soil densities (25 ° to 30 ° for loose soil to 38 ° to 43 ° for dense soil). As described in section 2.7, the soil friction angle also directly affects soil bearing capacity.

Table 4.2: Angle of the internal friction (Bowles 1996)

SPT Penetration, N-Value (blows/ foot)	ϕ (degrees)
0	25 - 30
4	27 - 32
10	30 - 35
30	35 - 40
50	38 - 43

CHAPTER 5:

TEST RESULTS

5.1 General

In spite of the tricky and challenging nature of roots undergoing pull out, a significant improvement in the understanding of interactive properties between soil and root surface makes vegetation an attractive alternative for soil slope stability. Finite element simulation is helping to better understand the parameter involved and making this process predictable. Primary field pull out test and laboratory test were used to identify the trustable input data for finite element simulation. This chapter presents the results of the laboratory tests and pull out tests conducted in order to acquire the input data for numerical simulation.

5.2 Laboratory test result

This part of study presents the mechanical properties of soil and root where the pulling out process was performed. As described in section 3.2, laboratories tests were performed for soil located in the experimental area and for pulled out roots following the field pull out test.

5.2.1   Soil properties test result

As discussed in section 3.2.1, to predict the classification for the soil located in the pull out area, particle size distribution test was performed. To verify the soil mechanical properties, triaxial test was performed following the particle size distribution test. Finally, for an indication of the soil shear characteristics, direct shear test was also performed to complete the necessary input data for numerical simulation of the root anchorage during the pull out.

a) Particle size distribution result

The particle size distribution sheet is illustrated below in Figure 5.1
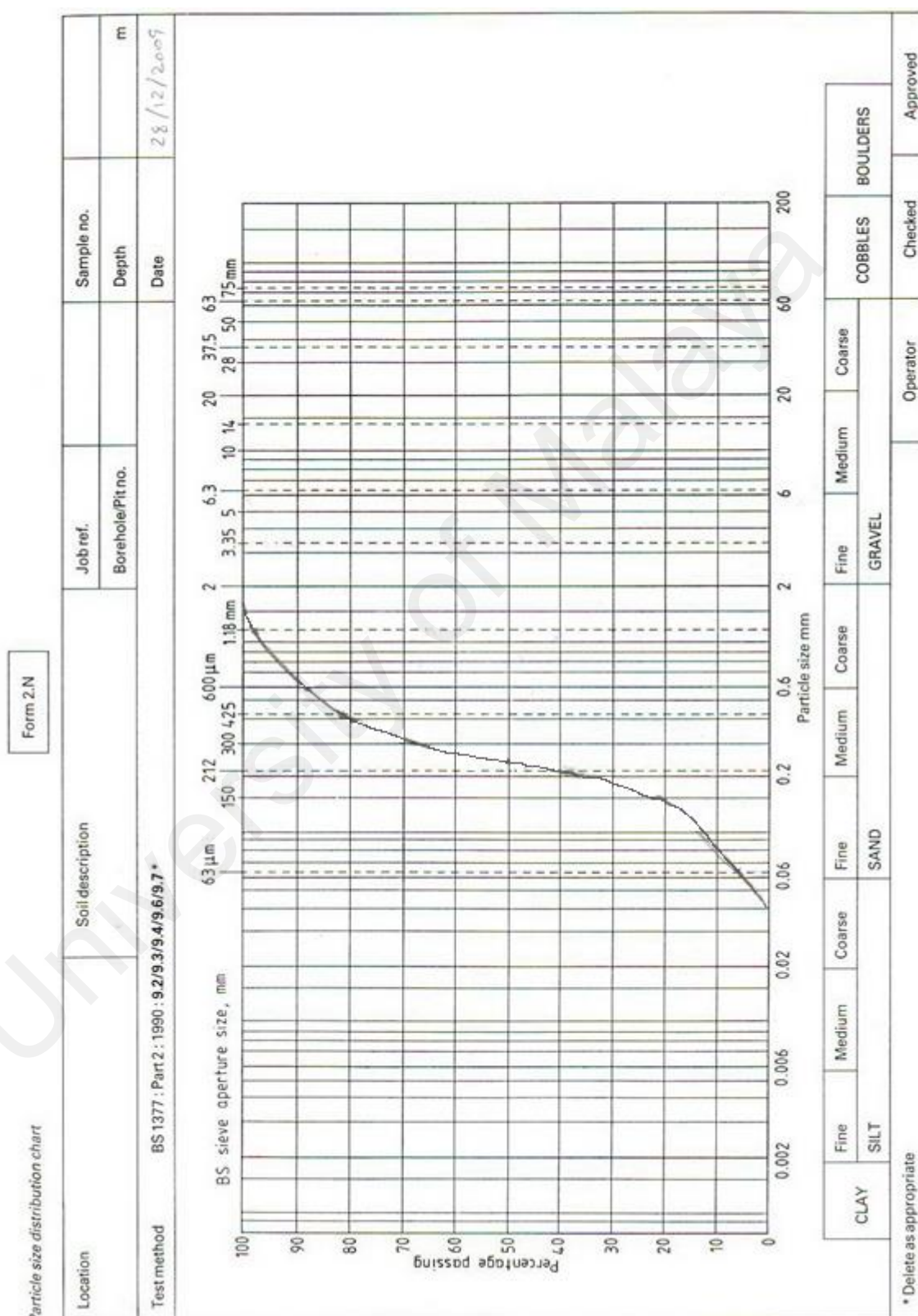
Figure 5.1: Particle size distribution chart for the soil sample

Based on the laboratory tests performed in accordance with section 3.2.1(a), the soil sample is classified as sandy silt, which contains 2% coarse sand, 60% medium sand, 32% fine sand and 6% silt. As mentioned in section 4.6.3(a) sandy silt soil is classified as a high cohesive soil (it is also proven further by the high cohesion value obtained from the direct shear test).

b) Triaxial tests

Three test specimens with diameters of 38 mm were used for this test. Samples were taken from 1 m depth therefor the cell pressure used for each sample were 0.01 MPa, 0.02 Mpa and 0.04 Mpa respectively. The rate of strain was chosen as 2% per minimum according to British Standard recommendations, and the test duration was 10 mm. The results of the test are plotted as curves of principal stress difference against strain as illustrated in Figure 5.2.
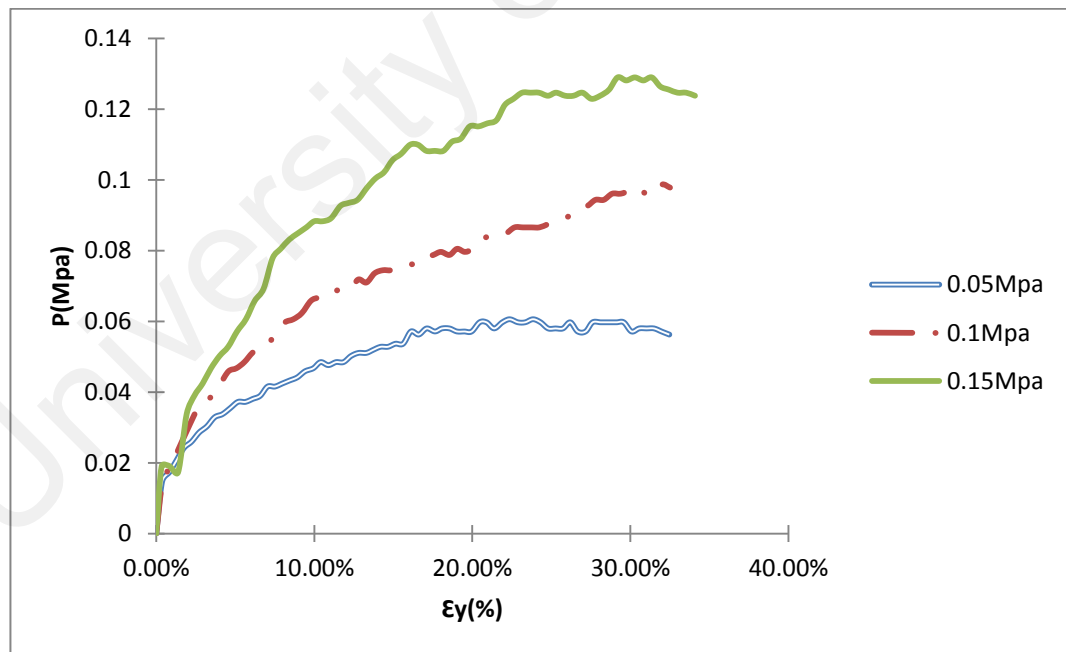

Figure 5.2: Triaxial tests for the soil sample

After application of the correlation for the restraining effect of the membrane (BS 1377:1990) the value of young modulus 'E' was determined to be 24 Mpa with the

poison ratio 'ν' was calculated as 0.34. Finally the average density of soil specimens was determined to be ρ=2.03 kg/dm3.

c) Direct Shear test(shear box test)

The Direct shear test (shear box) is carried out on an annular specimen of remoulded sample 5mm thick, with internal and external diameters of 70 mm and 100mm respectively. The main advantage of the direct shear apparatus is that it is relatively simple but still allows an infinite relative displacement without the necessity of reversing the direction of relative motion along the shear plane developed in the soil sample. The test was carried out at a rate of 0.048% per minimum to ensure that no excess pore water pressure exists on the failure plane by the time shear strength measurements are to be made.

Based on the laboratory test performed (in accordance with section 3.2.1(c)) the soil classified as being in between loose and dense to loose soil. The results of the test are plotted as curves of principal stress difference against strain as illustrated in Figure 5.3.
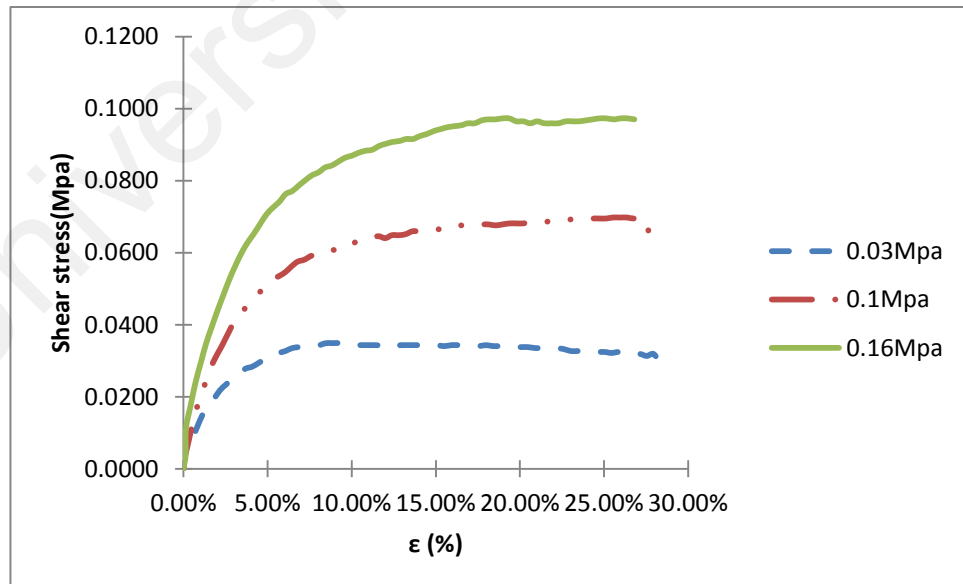

Figure 5.3: Direct shear test for the soil sample

The values of cohesion coefficient(c), friction angle (Φ) and dilation angle (ψ) were found to be; c=0.02Mpa, ϕ Maximum. =29˚ and ϕ Minimum. =27˚ and Ψ was calculated plane strain where: Ψ Maximum. =5˚ and Ψ Minimum. =0˚ rate of strain = 0%-30%

5.2.2 Roots mechanical properties test result

As described in section 3.2.2 ten series of specimen were examined during this test. Each series contains five specimens which were collected for certain diameters. The results where the specimen which failed at the wrong place (not in the middle) were ignored (due to small diameter of root, certain specimens were crushed and failed nearby test machine clamp). The results of the test are plotted as an x, y scatter of Young modulus against root diameter as illustrated in Figure 5.4.
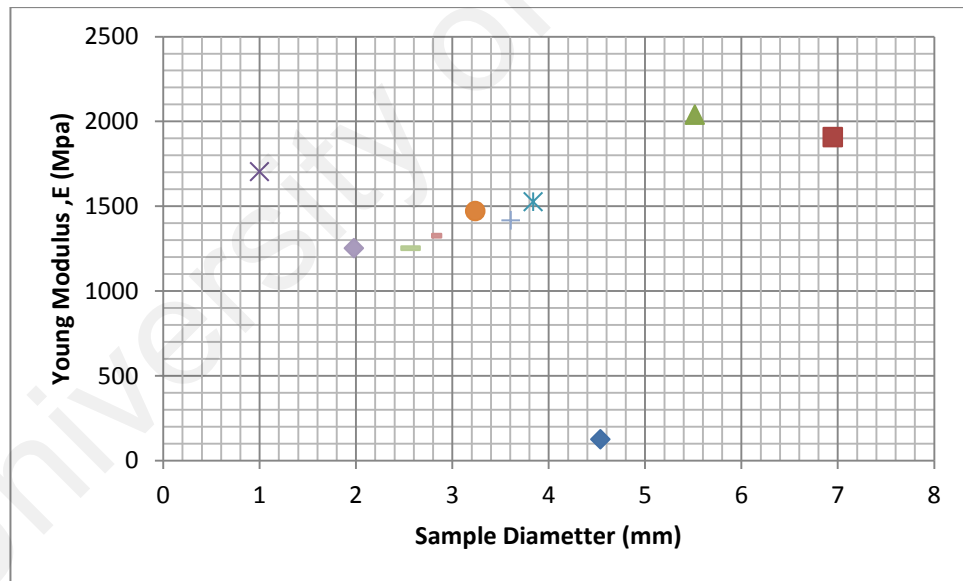
Figure 5.4: Tensile test result for the root sample

The value of young modulus E, poison ratio and yield stress was found out as below; E=1500 Mpa, ν=0.3 and yield stress=14 MPa. Finally the average density of root material specimens was also measured as ρ=0.54 kg/dm3.

5.3 Contribution of roots to the pull out strength

The findings of this study and effects of the root-matrix on the pull out strength are elaborated in this section. Recommendations made in this section include on how these effects can be incorporated into the slope stability analysis.

5.3.1   Field test and monitoring result

In this part of study, the maximum stem displacement during the pull out process was carried out using an LVDT and utilized as input data in the numerical simulation. The normal load recorded by the load cell at the top of stem was fixed as the maximum pulling out resistance and compared with the reaction force obtained from numerical simulation.
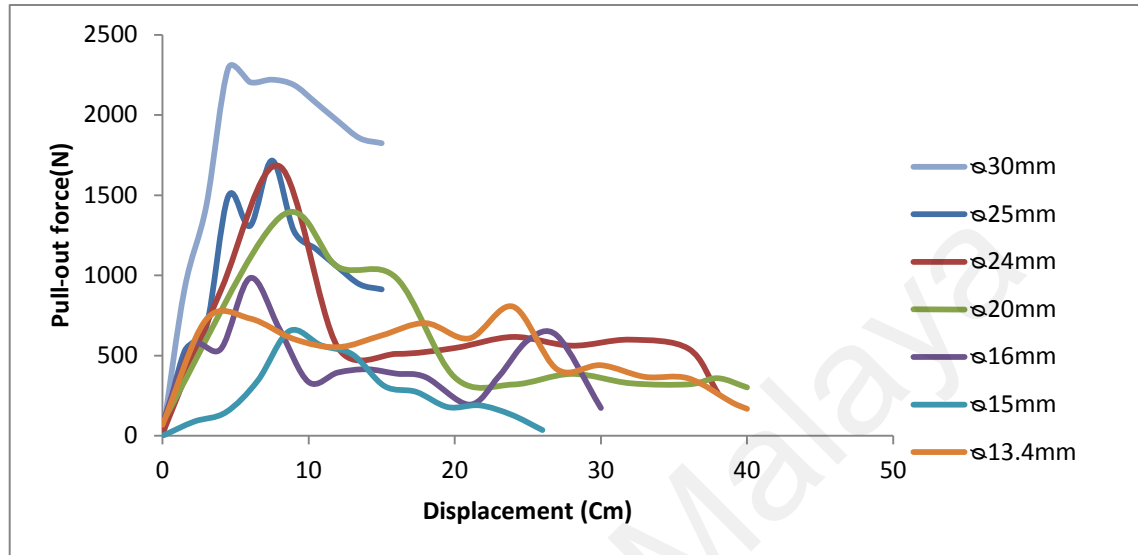
a) Pulling out force and displacement

It is discovered that the pulling out force changes during the pulling out process as shown in Figure 4.1. The average reading from the pulling out results is illustrated in Table 5.1

Table 5.1: The average reading of pulling out result for *Melastoma malabathricum*

	Range	Mean
Maximum.pulling out resistance(kN)	0.98-2.404	1.64
Stem Diameter (mm)	13.4-25	18.9
Maximum displacement(cm)	15-40	30
Displacement at failure (mm)	40-86.8	75.3

As illustrated in the Figure below, the pulling out force increases with the increase in the stem diameter and at the same time the failure displacement decreases. On the

other hand this experiment proves that the *Melastoma malabathricum* with a bigger stem diameter need a higher force for the pulling out as well as demonstrating a lower failure displacement (deformation).
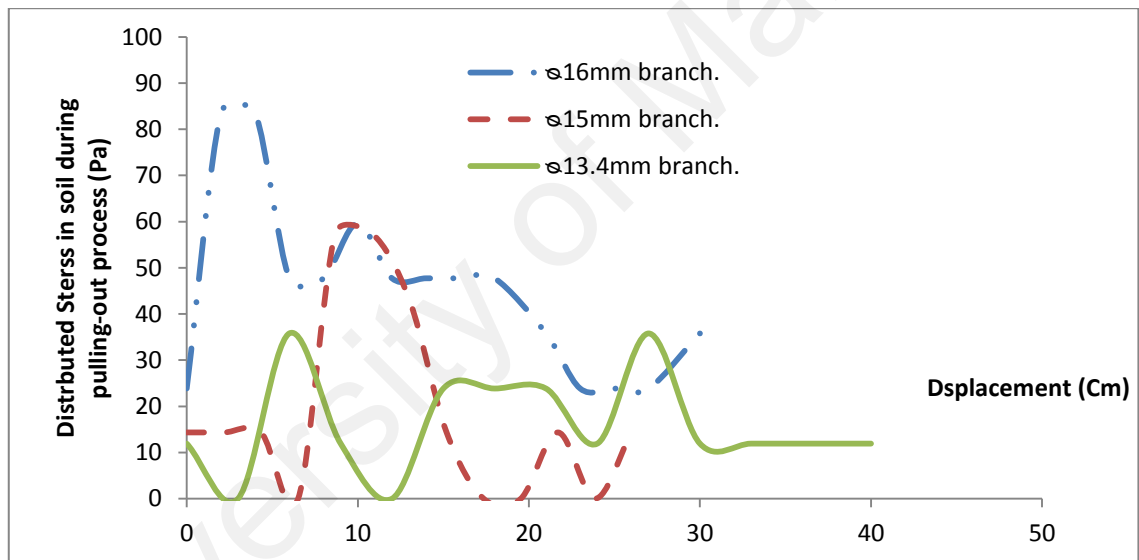

Figure 5.5: The pulling out force (N) vs displacement during the pulling out process

During the pulling out process all branches work together but the pulling out force is partially carried out by one or a group of branches and when failure occurred in this branch or group of branches it will cause a decrease in the pull out force. Consequently the force transferred to another branch or group of branches causes another rise in the pull out force and it keeps repeating until the failure. During this process the larger branches have failed at the higher force but smaller branches denoted more reformative characteristics during the pulling out process.

As reflected in the Figure 5.5, the trend line has a rising character until the failure point caused by increasing the diameter of the branch which carries the force during the process. In other words, smaller branches or a group of branches begin to distribute force and after their break, it became bigger until the general failure.

b) Stress distribution in the soil body

During the pull out test it was found out that the maximum dispersion for the examined root belonged to specimens with root diameters of less than 20 mm. Therefore diameters of 16 mm, 15 mm and 13.4 mm were chosen as indicators to plot the stress distribution curve against displacement. Distributed stress in the soil body was recorded for the specimen with stem diameter of 13.4 mm, 15 mm and 16 mm during the pull out using the pressure transducer in pre-determined point as illustrated in Figure 5.6. As illustrated in the above diagram, maximum stress occurs at the same place as the failure (0-10mm).

Figure 5.6: The stress distribution vs displacement during the pulling out process in the certain points

CHAPTER 6:

NUMERICAL SIMULATION RESULTS, ANALYSIS AND DISCUSSION

6.1 Introduction

Despite the complexity and problematic nature of root anchorage, a numerical simulation will help to understand and predict the anchorage behaviour such as pulling out force in different types of soil and with different root architectures. Preliminary field investigation to identify the soil and root mechanical properties coupled with computer scanning from roots which are pulled-out during the site pulling out test provide the numerical model to simulate the pulling out process.

Following the completion of the model, simulation of root pull out from previous experiments and subsequent energy balance analysis will be discussed in this chapter. The accuracy of this simulation will be controlled by comparing the simulation results with the results from the pull out experiment discussed in chapter 5. Moreover the accuracy of the simulation method will be controlled by comparing the simulation results with the results of well controlled laboratory test previously done (Siti Sara et al, 2010). Finally, the root anchorage is simulated in different soil and with different root architecture to clarify the effects of root architecture and soil characteristics on the root pulling out resistance.
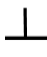
6.2 Verification of Numerical Simulation

To ensure the simulation accuracy, the experiment done by Siti Sara et al, 2010 was modelled and the simulation results were compared with the experimental ones. Siti Sara et al. (2010) reported a series of pull out test carried out by purposes of gaining greater insight into plant root–soil mechanical interactions. This study greatly simplified this complex problem by controlling root and soil properties by subjected the artificial

root models to the vertical uprooting forces. The model of the root systems varied from the aspect of root branching patterns and morphology which lead to the dissimilarity of the strengthening effect. Hence the used of the artificial roots have the advantages of possessing known, repeatable mechanical properties and also can be cast to a selected shape, due to lack of information about root material properties used in this work, values being considered from the literatures were use as input data for numerical simulation. In this research root-analogue architecture allows the effects of isolated morphology changes to be investigated experimentally. Research showed there were few factors which recognized to influence pullout resistance, there are the angle of lateral roots possesses by root systems as well as how deep the roots were embedded in soil medium. There were six simplified root models developed in total as shown in Table 6.1.

Table 6.1 Various types of artificial root models

| Structure Type	Diagram	Structure Type	Diagram
Dichotomous Type I (D1)	人	Herringbone Type II (H2)	＋
Dichotomous Type II (D2)	⊥	Combination Type I (C1)	朩
Herringbone Type I (H1)	个	Combination Type II (C2)	╪

For this comparison, the numerical result trend line was compared with the experimental result in each case as shown in Figure 6.12. As stated in the above mentioned paper, the root material used in this study was aluminium rod where branches were welded to connect to each other using aluminium welding. This issue can also affect the Young modulus for root model. Additionally, as the physical/mechanical properties of aluminium alloy are different depending on the alloying element, therefore average range was applied in this simulation. The effect of some of those characteristics is quite significant in the anchorage process such as density of the aluminium rod which is directly involved as the most influential factor in root anchorage (friction). On the other hand, due to the type of soil selected for performing this experiment (pure sand), the effect of dilatancy is significant in the anchorage development. As the angle of dilatancy (ψ) not mentioned in the above mentioned paper, this value was extracted from empirical formula for simulation. Due to lack of input data during this simulation, the friction coefficient is extracted from the empirical formula as below:

$$\mu = tg(2/3\ \Phi) \tag{6.1}$$

It seems this estimation does not accurately represent the friction coefficient for the interaction between aluminium rod and soil. This inaccuracy in estimation of root material properties, soil dilatancy and the friction coefficient between aluminium and soil can give rise to non-concurrence between the experimental and numerical results. However, shown in Figures 6.1 to 6.6, the numerical trend lines more or less match the experimental result in all cases.
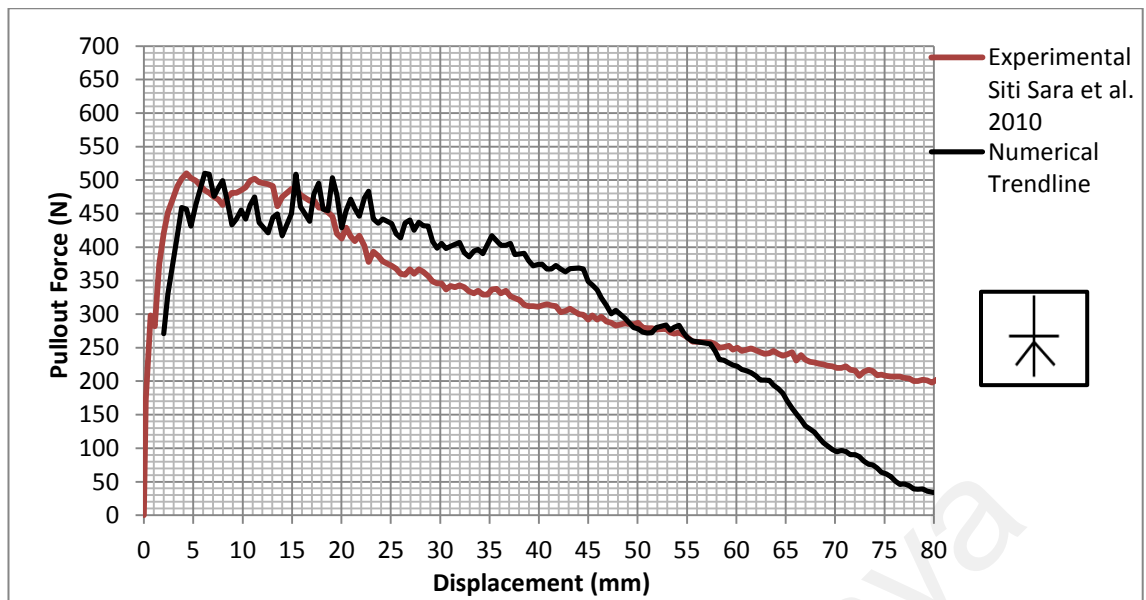
Figure 6.1: Pulling out force vs displacement for C1 model (Siti Sara et al. 2010)
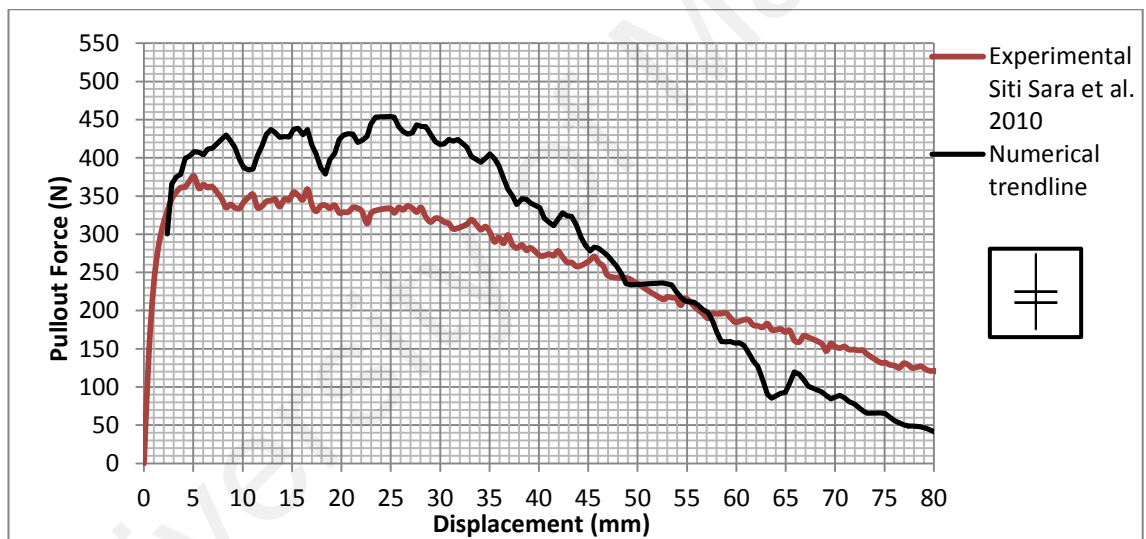
Figure 6.2: Pulling out force vs displacement for C2 model (Siti Sara et al. 2010)
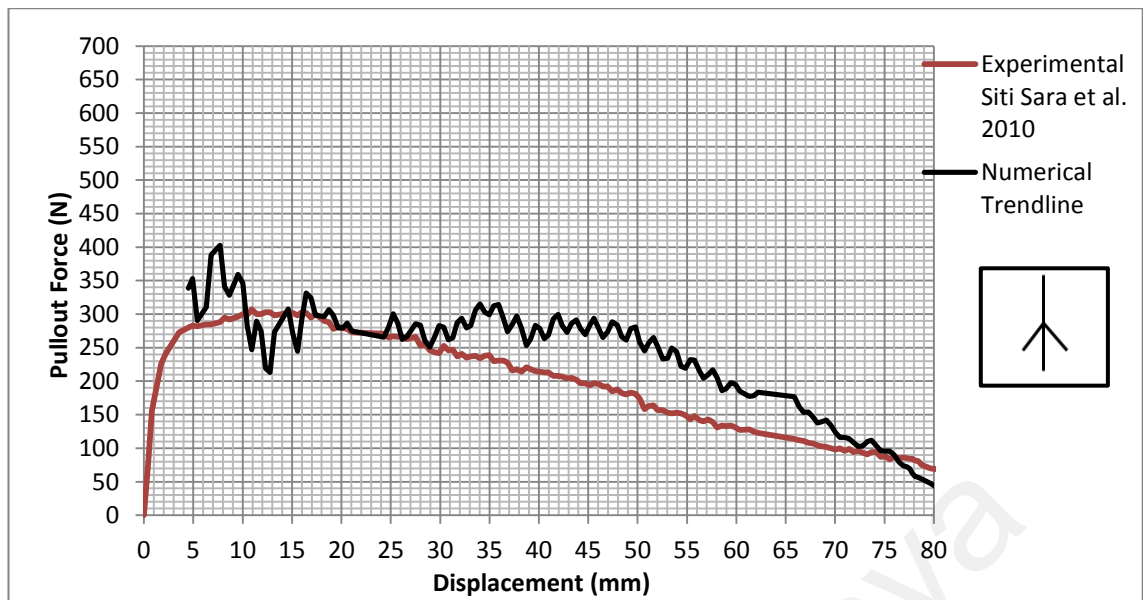
Figure 6.3: Pulling out force vs displacement for H1 model (Siti Sara et al. 2010)
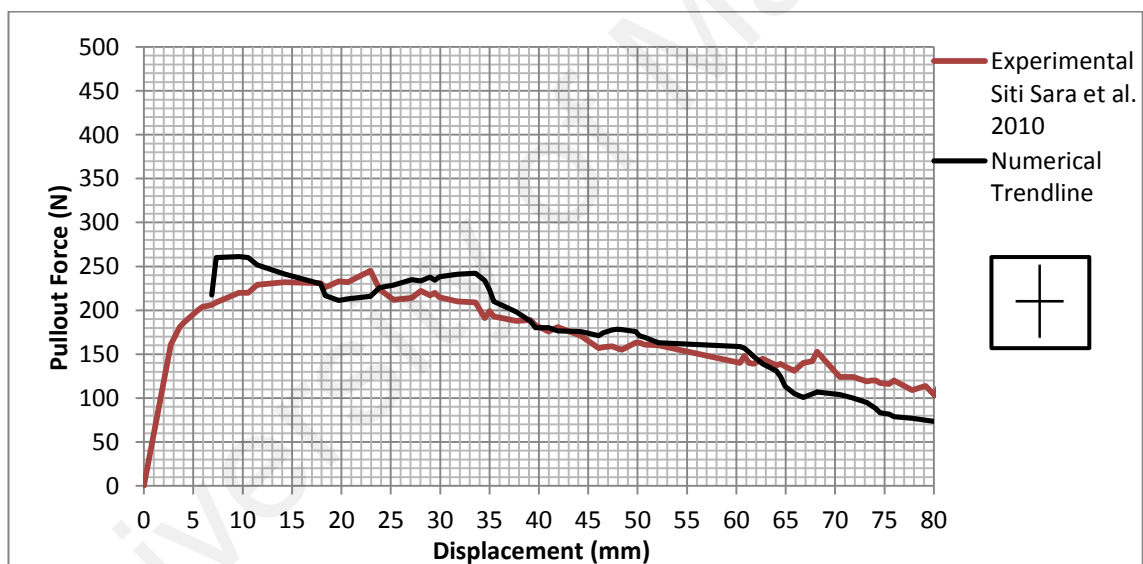
Figure 6.4: Pulling out force vs displacement for H2 model (Siti Sara et al. 2010)
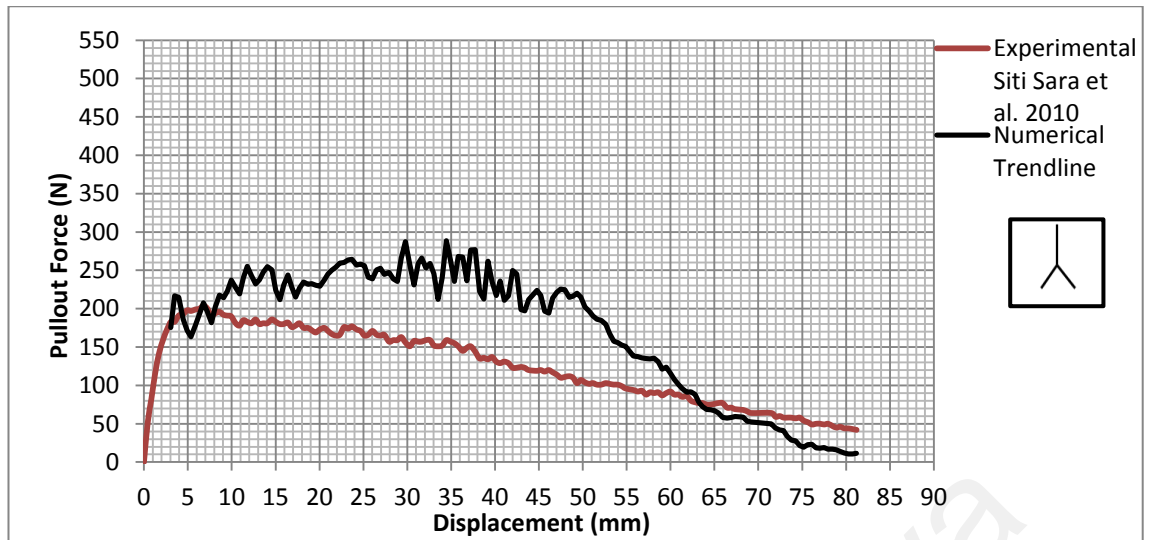
Figure 6.5: Pulling out force vs displacement for D1 model (Siti Sara et al. 2010)
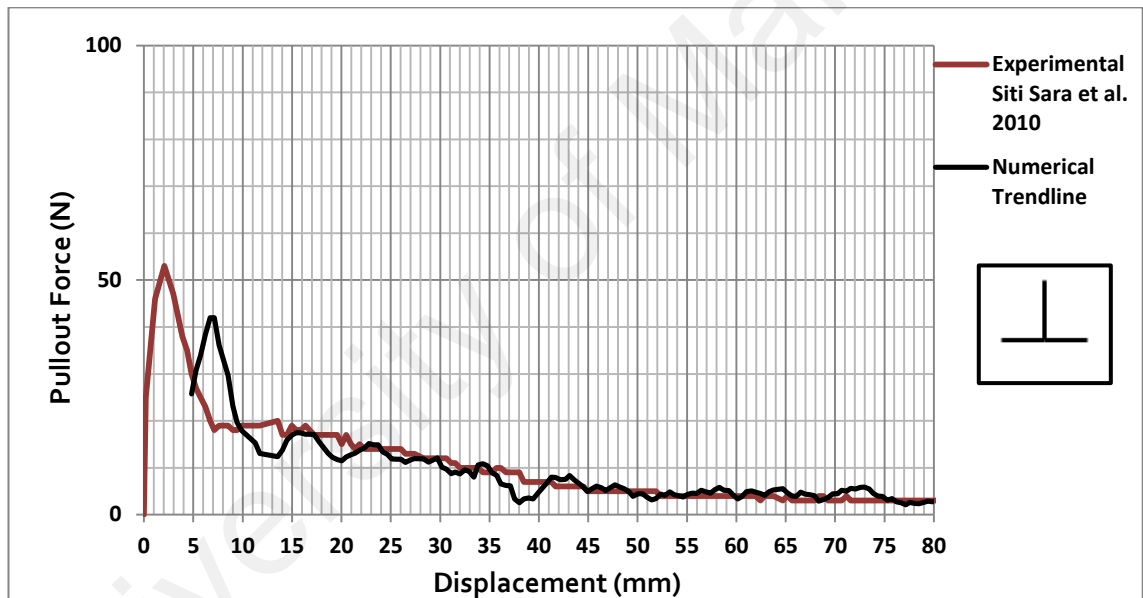
Figure 6.6: Pulling out force vs displacement for D2 model (Siti Sara et al. 2010)

From Figures above, most of the deviation between the numerical trend line and experimental result can be attributed to the inaccuracy of cohesion coefficient for vertical taproot cases. It is generally known that the most influential factor in root anchorage is friction. Friction force is affected by vertical load from the soil column weight above root surface and the friction coefficient between soil and root. In the case of vertical taproot, the resultant vertical load due to the soil column weight above root

surface is negligible. Therefore, the friction force is controlled by friction coefficient and at rest earth pressure on the root surface as depicted in Figure 6.7.
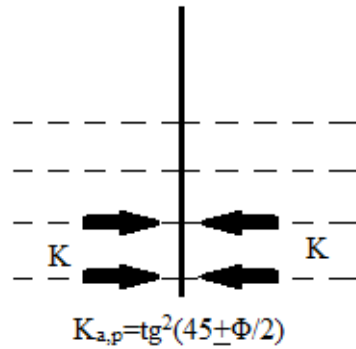
Figure 6.7: At rest pressure affected on vertical root

The value of at rest earth pressure is not huge therefore the control value for friction force during pull out in cases with horizontal taproot, is the friction coefficient. Due to the inaccuracy of the friction coefficient between aluminium and soil, comparison of the numerical and experimental response curve illustrates the worst case when the long vertical taproot is examined alone. By examining the comparison between the curves, it was found that the most accurate result belongs to the root model with more horizontal roots. It is also affirmed that soil mechanical properties is more influential than root mechanical characteristics.

6.3 Simulation of field pull out test

According to real root pulling out experiment described in chapter 5, different roots show different reaction against the force. The main roots or first order branches mostly do not rupture and only slide in the soil during the pulling out process while the hair roots or second order branches mostly resist against the pull out force until their rupture.

To achieve more realistic simulation results (despite the restrictions stated in 4.3.1), the main roots were modelled as 3D cylinder element (due to their dominating form). Interaction in between the main root and soil was considered to be tangentional frictional behaviour to simulate the sliding in soil during pulling out.

The effecting stress on hair roots is mainly axial tension due to the pulling force and they normally do not resist against any effecting moment or other kinds of stress. Due to this fact and also the hair roots frangibility, the hair root is simulated as beam element in this simulation work. The hair root is considered to be embedded in the soil body because during the experimental work, it was proven that hair roots almost do not slide in soil during the pulling out until their rupture.

Since it was proven that the stem role in pulling out only connects the main roots and transfers the force to the roots, in this simulation the stem was modelled as rigid element. Applied displacement at the top of the rigid stem (rigid stem reference point) converts into the pulling out force in the root – soil system.

Due to the very small root diameter even for main roots, the serve element distortion often occurs. To escape this, critical elements (smallest and most distorted element) were scaled during this study. Controlling the stable time increment for model can be done without significantly affecting the results. The nodes associated with these elements often have very little mass and, hence, contribute very little kinetic energy to the model. To prevent aliasing data, the anti-aliasing filter built in the ABAQUS software was employed in this analysis.

6.3.1   Comparison between the experimental and numerical results

When comparing the pulling out force applied during the experiment for three different roots which are scanned and modelled, the simulation results highlighted adaptation between the RF-D curves which is shown in Figures 6.8, 6.9 and 6.10.

In these Figures, first of all, the natural root is illustrated. After that, the root model is built in the ABAQUS 6.10.ef, and at the end, the diagram for the pull out force against displacement based on both the numerical and experimental result is compared.

As demonstrated in the Figures.6.8 to 6.10, comparison between the pulling out force applied during the experiment and model simulation illustrated acceptable similarity which emphasizes on the accuracy of the finite element analysis.

As signified in the diagrams, the experimental curve is smoother than the numerical ones. Three reasons can cause this effect; first of all, the output from the data logger is already interoperated in a diagram form, meaning that some of the small picks are automatically smoothened in the diagram. Second reason is the hypothesis which is used to build the model, where it is assumed that all second order roots will be ruptured and during the experiment it is observed that some of the second order roots may be pulled out during the process. Final reason for the occurred dent in the Figure is the aliasing effect which occurred when a signal is simplified at a series of discrete point at time. However, there are not enough data points collected in order to correctly describe the signal.

Root Sample(1)
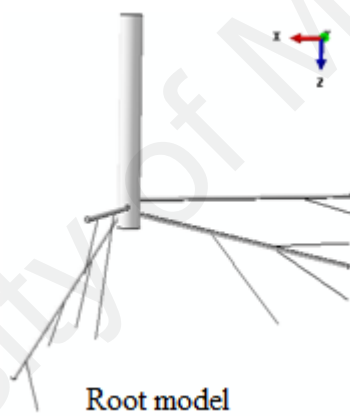
Root model

Figure 6.8: Comparison between numerical and experimental result for root sample (1)

Root sample (2)

Root model

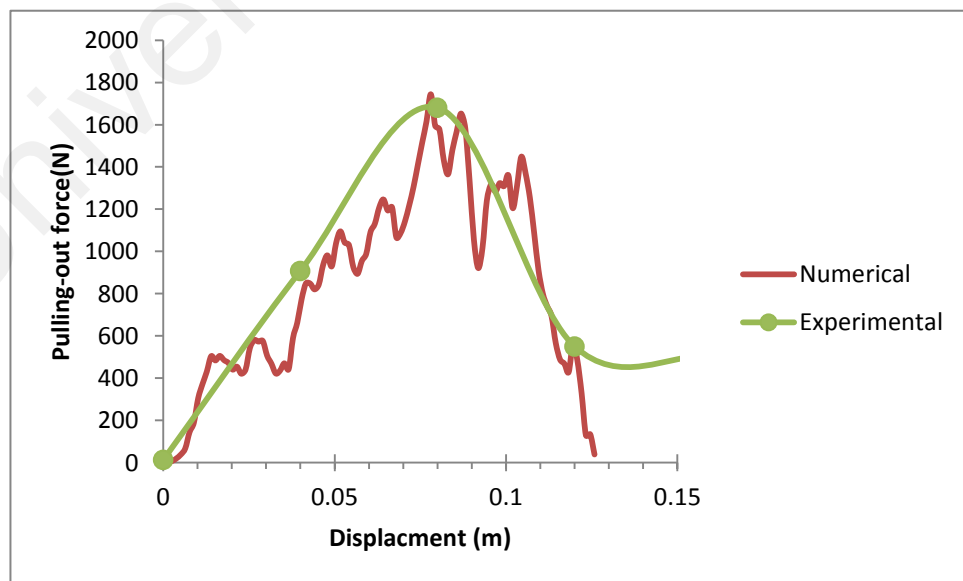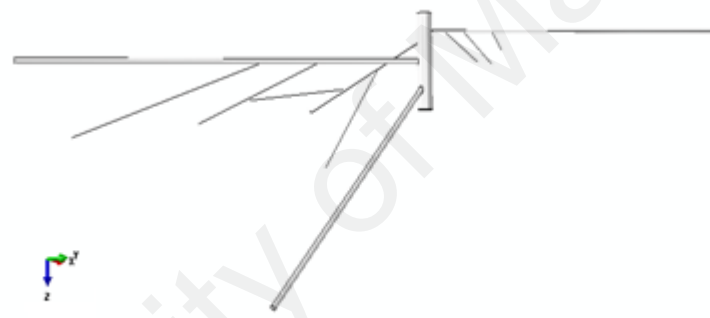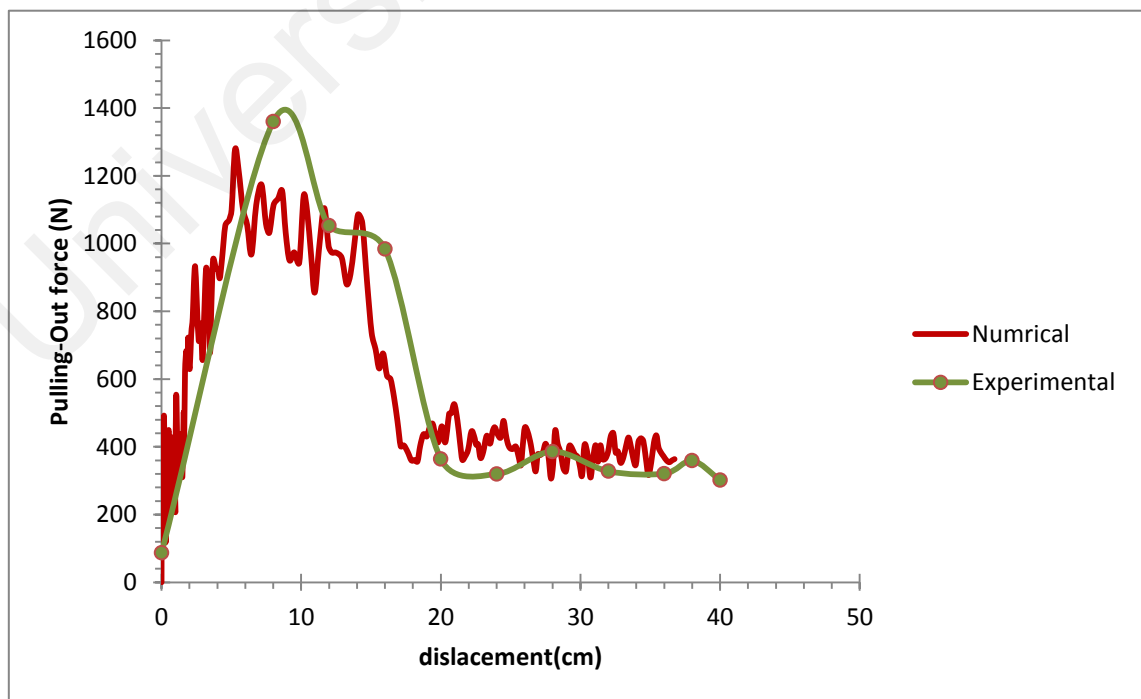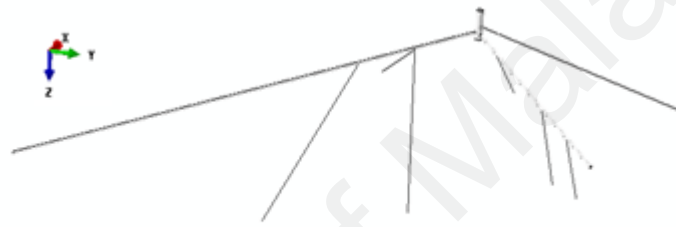**Figure 6.9:** Comparison between numerical and experimental result for root sample (2)

Root sample (3)

Root model
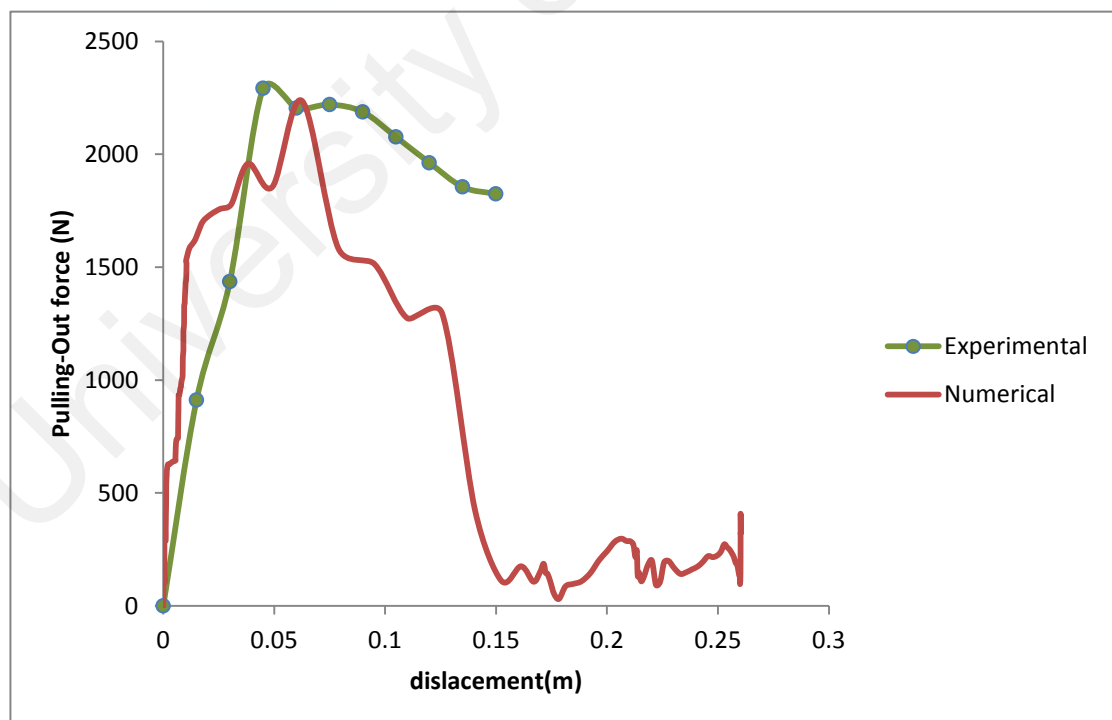
Figure 6.10: Comparison between numerical and experimental result for root sample (3)

6.3.2 Energy balance analysis

An energy balance equation can be performed to estimate whether a simulation is making an appropriate quasi-static response. Consider the pulling out test applied to root-soil system, the work applied by the external forces in stretching the root equals the internal energy in the root-soil system.

The energy history for the performed quasi-static simulation would appear as shown in the Figure 6.11. Based on the energy history plot the next conclusion can be obtained;

• Inertia forces are negligible.

• The velocity of material in the test specimen is very small.

• Kinetic energy is negligible.

And as the speed of test increases the response of the root-soil system becomes less static and more dynamic. At the same time material velocities and therefore, kinetic energy become more significant. The kinetic energy of the root-soil system not exceeds a small fraction (1-5%) of its internal energy throughout this quasi-static analysis. Therefore results from explicit simulation, reflects a quasi-static solution.

The energy balance (ETOTAL) during all time periods remains nearly constant at zero. A constant energy balance is an indication that the solution is stable. Approximately until the 25th second, the whole model energy remains nearly constant at zero; after that the External work (ALLWK) starts to rise up until the maximum amount and later on the internal (ALLIE) and then on the kinetic energy (ALLKE).
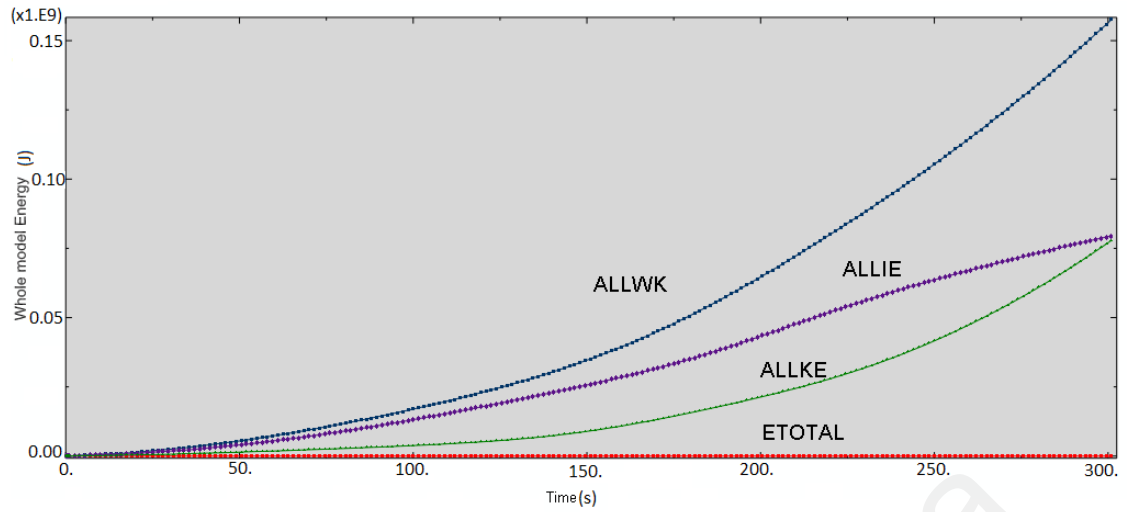
Figure 6.11: Diagram of whole model energy in pulling out process.

6.3.3 Von- Mises stress and Logarithmic strain distribution contour

The Von-Mises stress and logarithmic strain distribution during the simulated pulling out process is illustrated in Figures 6.12 to 6.17. As it is shown in Figures 6.16 and 6.17, for thinner roots, the Mises stress and Logarithmic strain are concentrated at the beginning of the root (place that roots are joined into the stem). With the increase in root diameter, stress and consequently strain concentration point move towards the middle of the root.
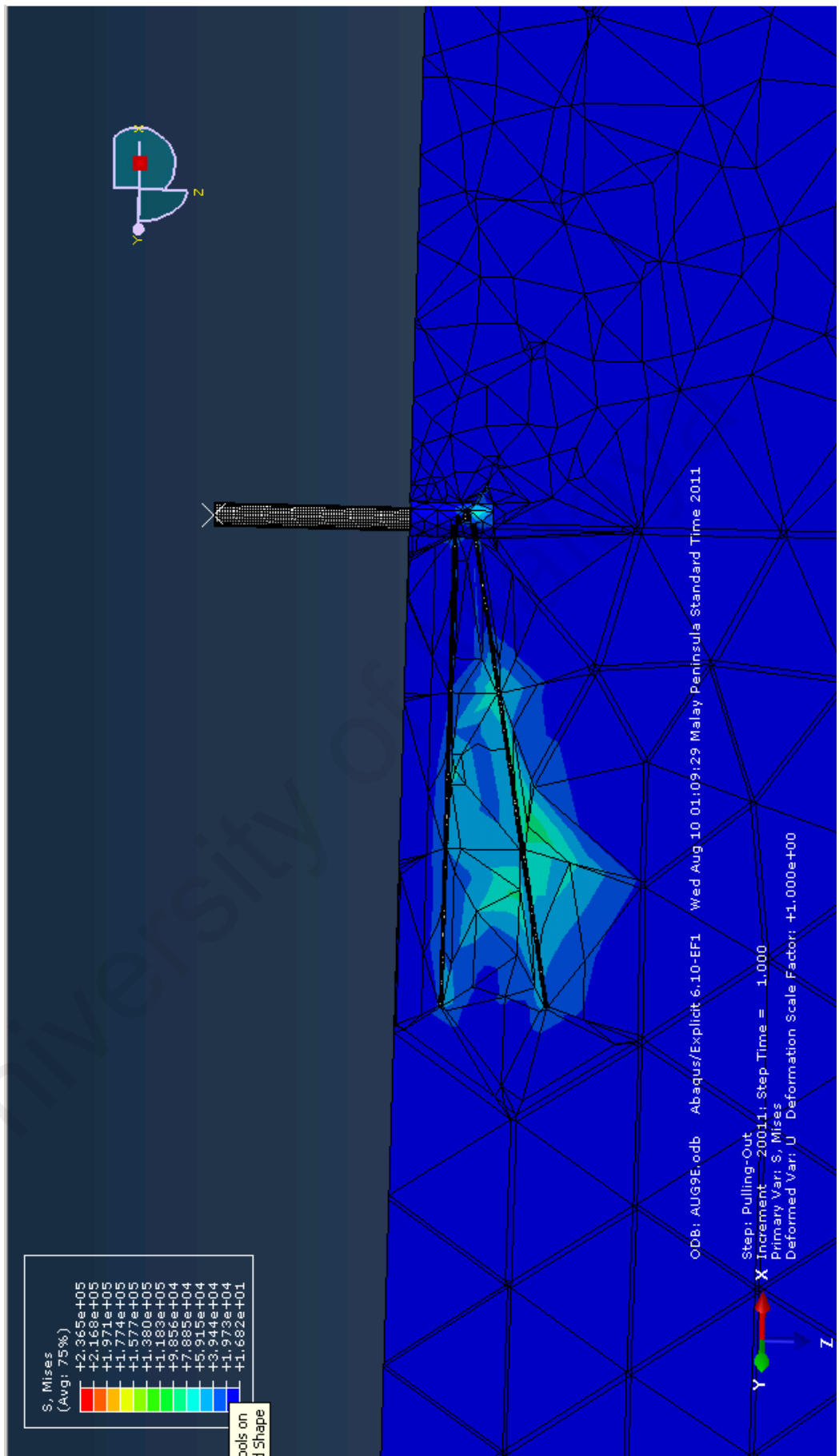
Figure 6.12: Von-Mises stress distribution contour for Root sample (1)
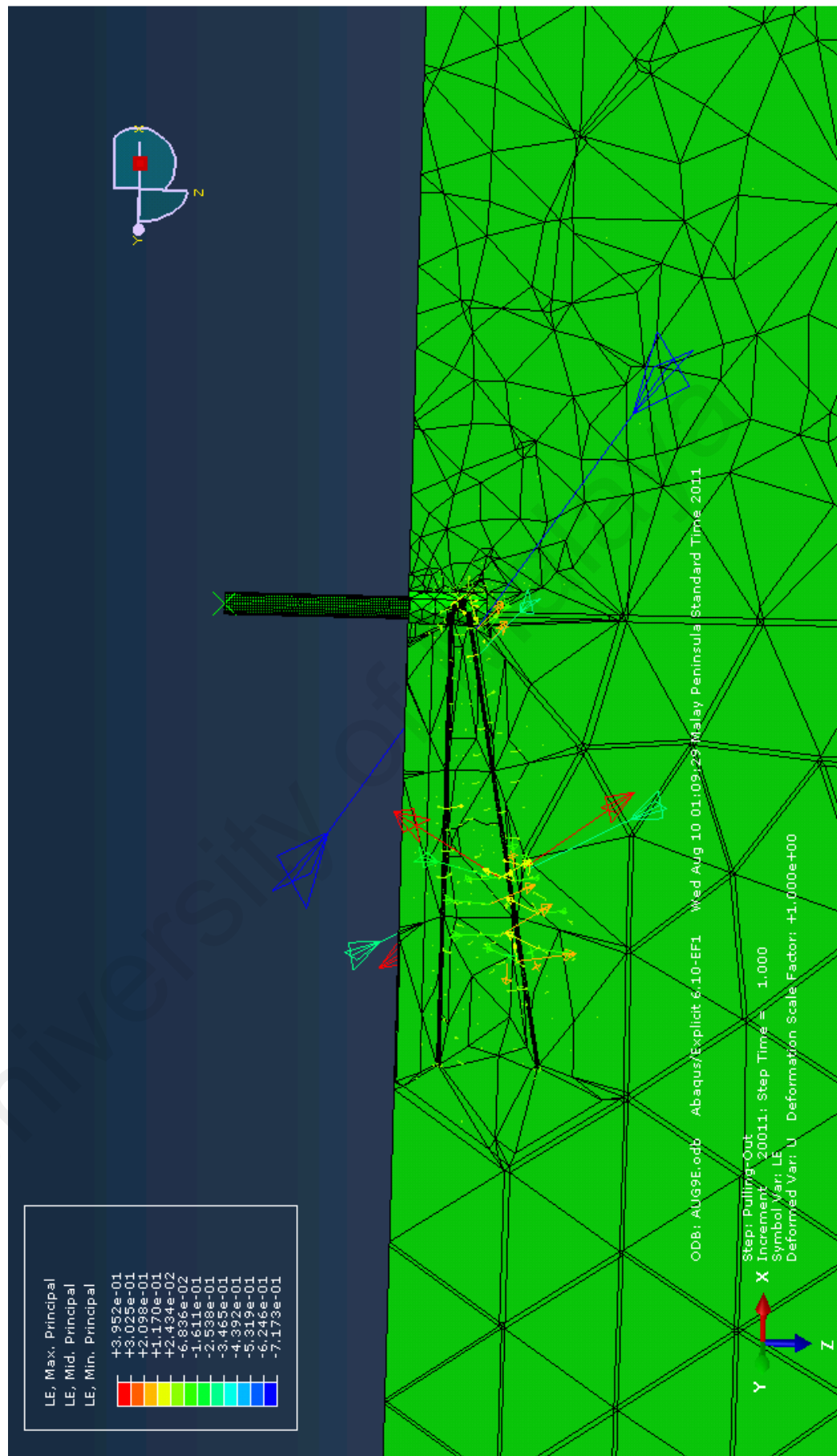
Figure 6.13: Logarithmic strain distribution contour for Root sample (1)
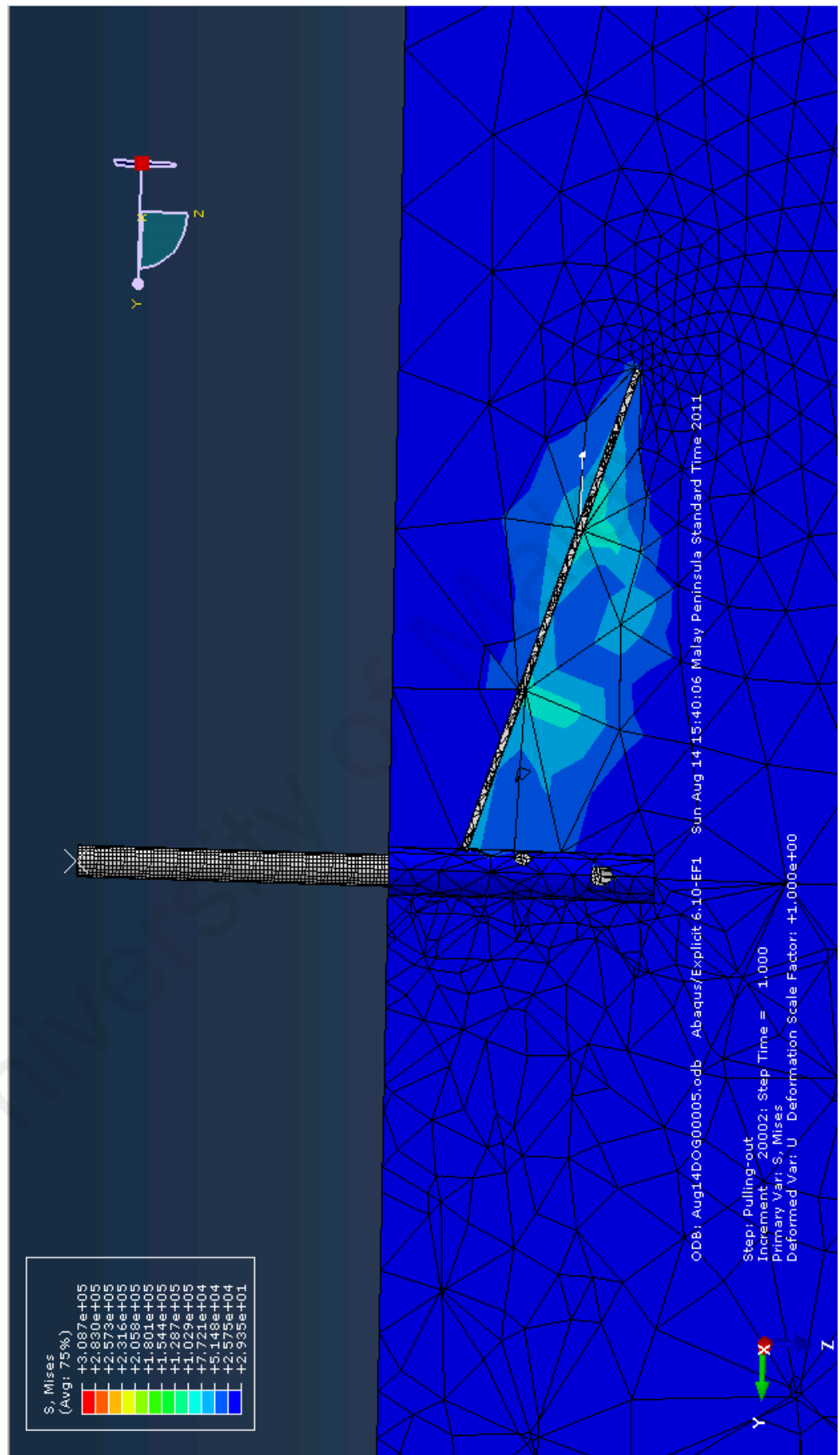
Figure 6.14: Von-Mises stress distribution contour for Root sample (2)
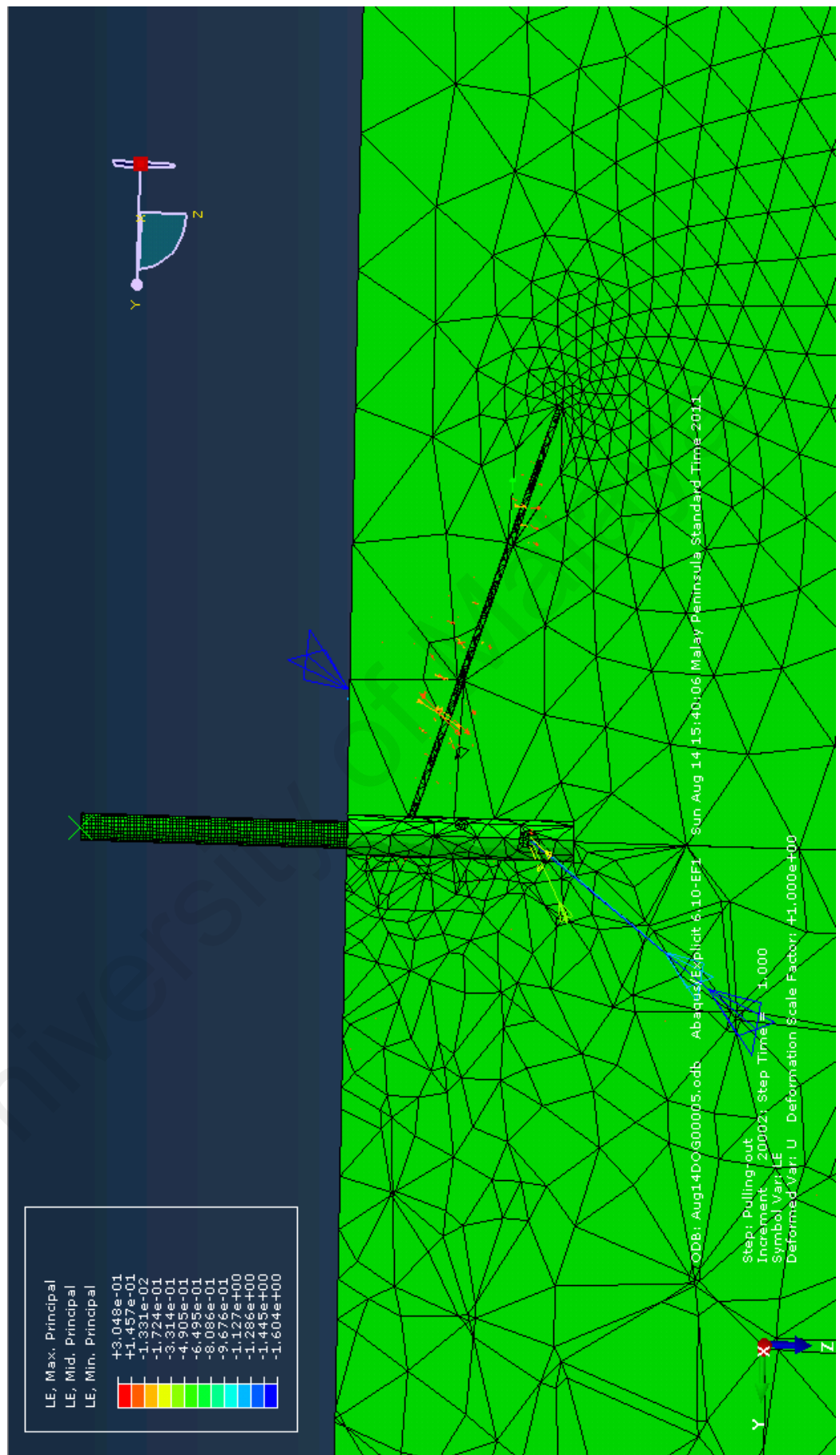
Figure 6.15: Logarithmic strain distribution contour for Root sample (2)
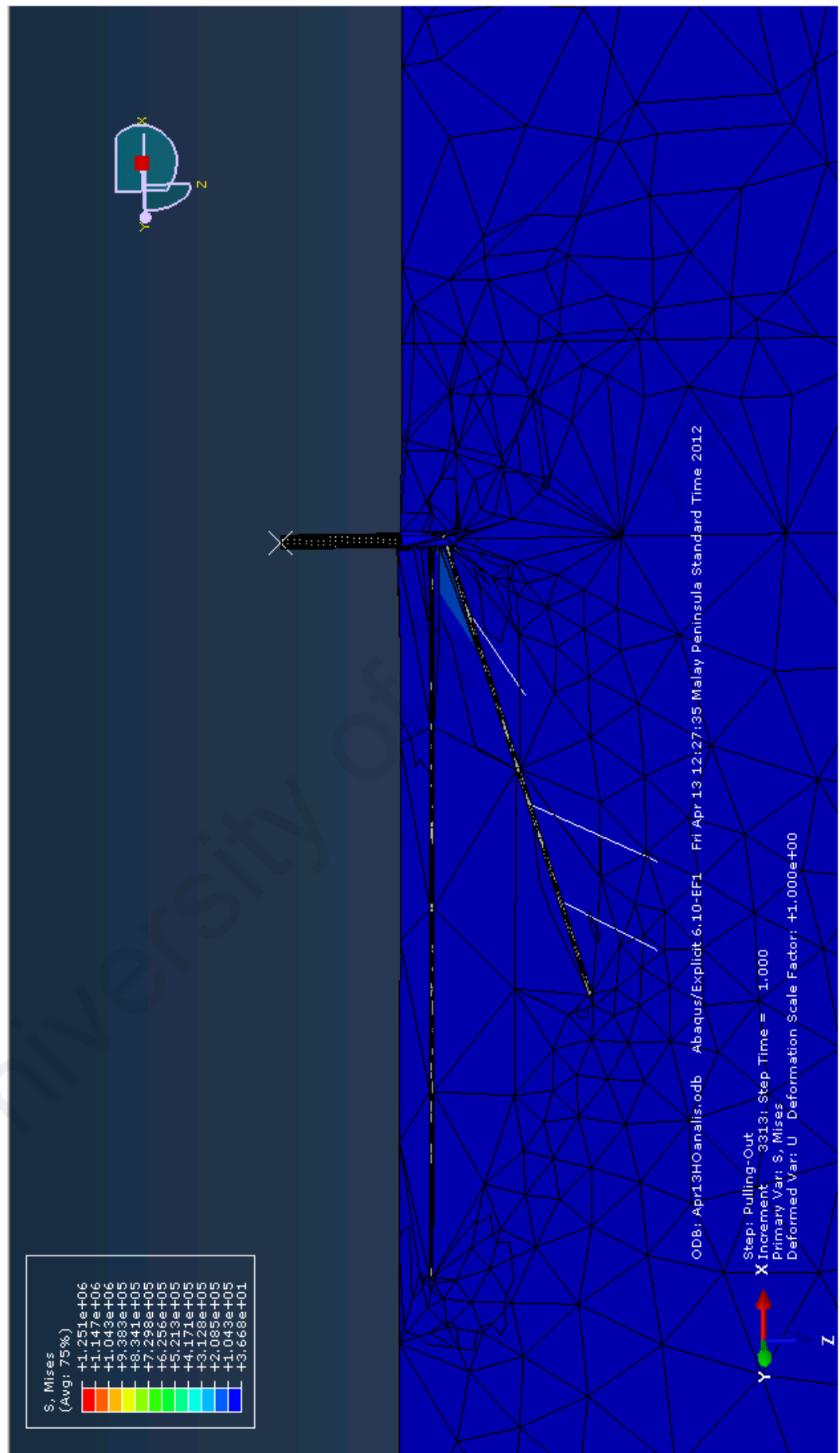
Figure 6.16: Von-Mises stress distribution contour for Root sample (3)
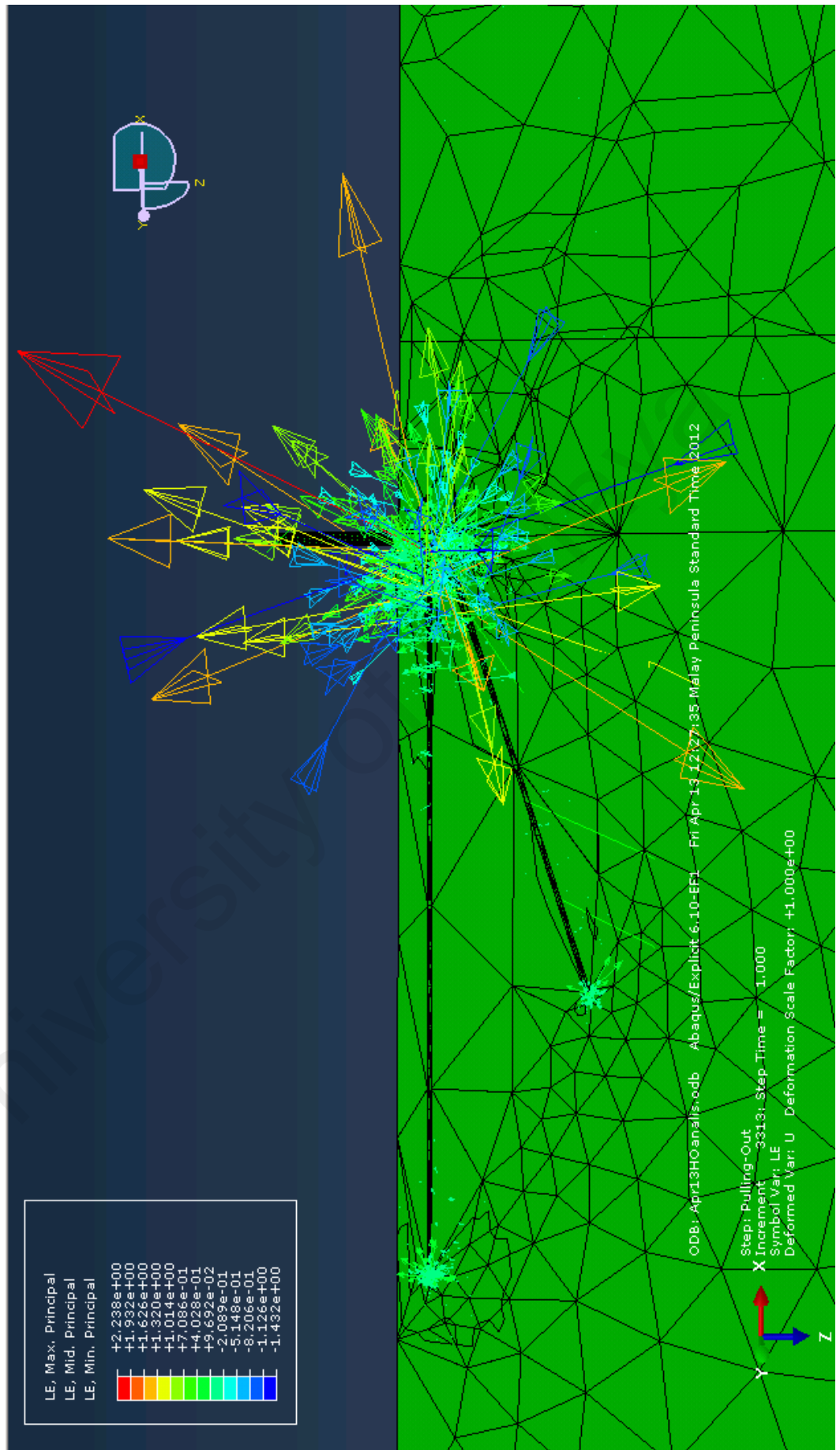
Figure 6.17: Logarithmic strain distribution contour for Root sample (3)

During the pulling out, force is transferred from stem into the roots until failure. Whatever failure that happens later, the concentration point is placed nearer to the end of the root. Thus, in roots with smaller diameter, failure happens fast, so that the whole root length is not activated during this process. Therefore stress and stain concentrate only at the root start and only cause longer displacement due to the root length.

However, as it is shown in Figures 6.12 and 6.14 for thicker roots, failure is happening later, so there is enough time to transfer stress and consequently strain concentration point to the inside of the root length. As it is visible in Figures 6.13 and 6.15, the stress and strain concentration point in most of the cases are located at almost the middle of the root.

In the other hand, as illustrated in Figure 6.12 and will be further discussed later, the stress distribution concentrates more in angular roots than the horizontal ones.

6.3.4   Comparison between the three simulated roots

Three simulated root systems (as per 6.3) were chosen from three different root samples with different number and diameter of the first order lateral roots borne on the central taproot and root geometry.

When comparing the simulation results for those different roots which are scanned and modelled, it is discovered that stress and strain distribution contour are more effected by the root length compared to the root diameter hence the pulling out force is under the influence of root diameter. The species with longer roots distribute the stress and consequently strain in a wider range of soil, but the pulling out force is less compared in thicker roots. However, species with longer roots did not show any serious effects on the maximum pulling out force. The pulling out force as denoted by Figure 6.18 is only different by the main root diameter. It was discovered by the simulation

result and also proved by the experimental outcome, in which in roots with bigger diameter, the pulling out force is larger than in roots with smaller diameter.

Because the stiffness of a root is a function of its diameter to the fourth power, numerous small roots will not only decrease the anchorage rigidity but also increase the resistance in tension. Pulling out resistance is higher in samples with larger roots. This increase in anchorage efficiency can be explained by the high root volume and number of large lateral roots.

Numerous thin lateral roots, even if they are not large, will augment the pulling out resistance. However, our model does not include the anisotropic material properties of root wood and such properties are a priority for future modelling studies.
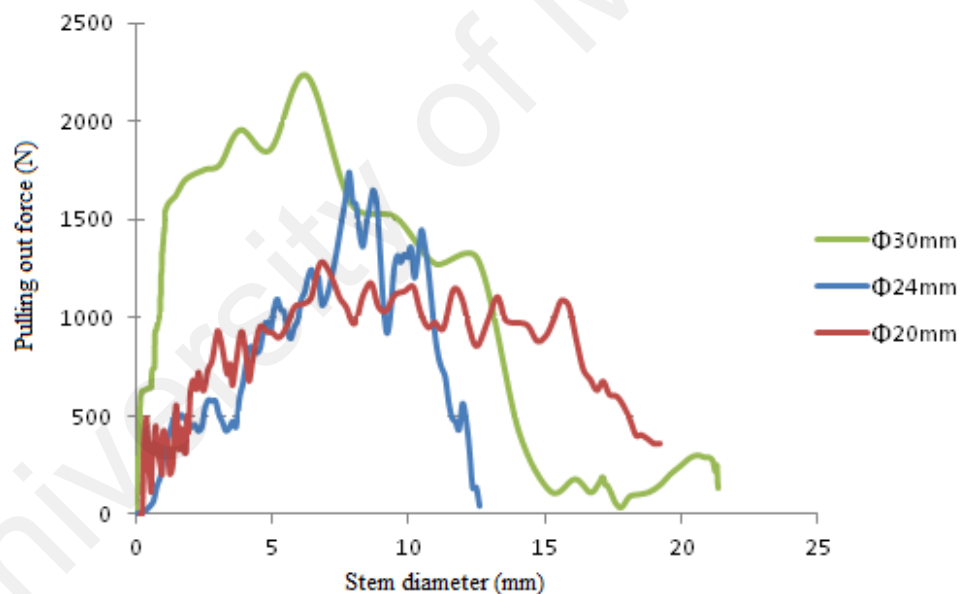
Figure 6.18: The pulling out force (N) vs displacement diagram during the pulling out process resulting from simulation

During the pulling out simulation, plastic strain around the stem is limited almost in the same stress distribution pattern but the logarithmic strain is distributed in a wide range. Although this phenomenon occurs in real situations species' pulling out, it has not been explained comprehensively before. It has been proven that soil mobilization is

subjected to low or negative isostatic pressure when lifted by the roots. Therefore, failure occurred and uplifting is induced. The geometrical structure of the root systems also affected the soil behaviour during uplifting in those simulations.

In this model, the soil failure is predominant, where the roots and soil are held in tension during the pulling out. Changing the root strength had little effects on the pulling out resistance of the model.

6.4 Effect of root architecture on pulling out

This part is divided into three segments; first of all the effect of a long taproot to the pulling – out process will be discussed, after this the effect of root architecture as per as section 4.6.2 a, and later on section 4.6.2 b will be discussed. (Root pattern and root inclination angle)

The response curve which is representative of the behavior of the whole mechanical system is defined as f-d, i.e. force against calculated displacement at the top end of the rigid stem (as reference point). In this approach, as simulation is motivated by a compulsory displacement (simulation input), the resulting force is defined as the 'reaction force' RF (simulation output) calculated at the reference point. At any point of the movement, the stiffness of the system is distinct by the slope of the tangent at the recent point of the f-d curve. The Anchorage strength corresponds theoretically to the maximum force reached before failure. In the current analyses, strength is defined as the maximum reaction force considered in a certain displacement range, as it is assumed that severe plasticization of the system had already occurred at this period. In each root type, the relative differences in the pulling out force between different roots patterns are defined to compare the relative effects of removing the taproot.

The Mises stresse and Logarithmic strains _ as defined in the ABAQUS list of variable -are visualized in soil elements using the ABAQUS CAE visualization module

104

to characterize the total stress and deformation effecting root - soil system during the pull - out process. This information is suitable to explain the difference in the pulling out force and displacement in each root model. The location of high positive LE11 and LE22 values indicated the zones where the opening modes of failure are in progress.

In this part of study, the hair roots are removed from the model because it was supposed that the hair root effect is constant for all cases. Moreover, root architecture affected by the main roots and hair roots should not play a reasonable role in this issue. Therefore, the role of hair roots is negligible in root architecture.

6.4.1　Effect of long taproot

As illustrated in Figure 4.7, the root sample 2 has a branch which is located relatively deeper and has a steeper inclination angle. The Von-Mises stress distribution contour and Logarithmic strain distribution contour occurred by the pulling out process are illustrated in Figure 6.19 (Von-Mises stress) and Figure 6.20 (Logarithmic strain) respectively. As it is specified from the above mentioned Figures, the Mises stress almost do not concentrate in the soil surrounding the deep located root in comparison to the more shallow ones. When pulling out occurred, the stress is distributed into the soil while the failure occurred. Stress distribution affects the soil surrounding the root starting from shallower roots until the deeper ones. Most of the time before the deeper roots got their share in stress distribution, the failure has occurred. In such a case, the logarithmic strain concentrates at the end of the root as it is shown in Figure 6.15. Since stress concentration points in the soil are the places that roots branches are locked, when stress decreased logarithmic strain increased.

Therefore in deeper and thinner roots, the logarithmic strain is more than in the shallower and thicker roots. This phenomena justifies the longer displacement for thinner roots than thicker ones as shown in Figure 6.18
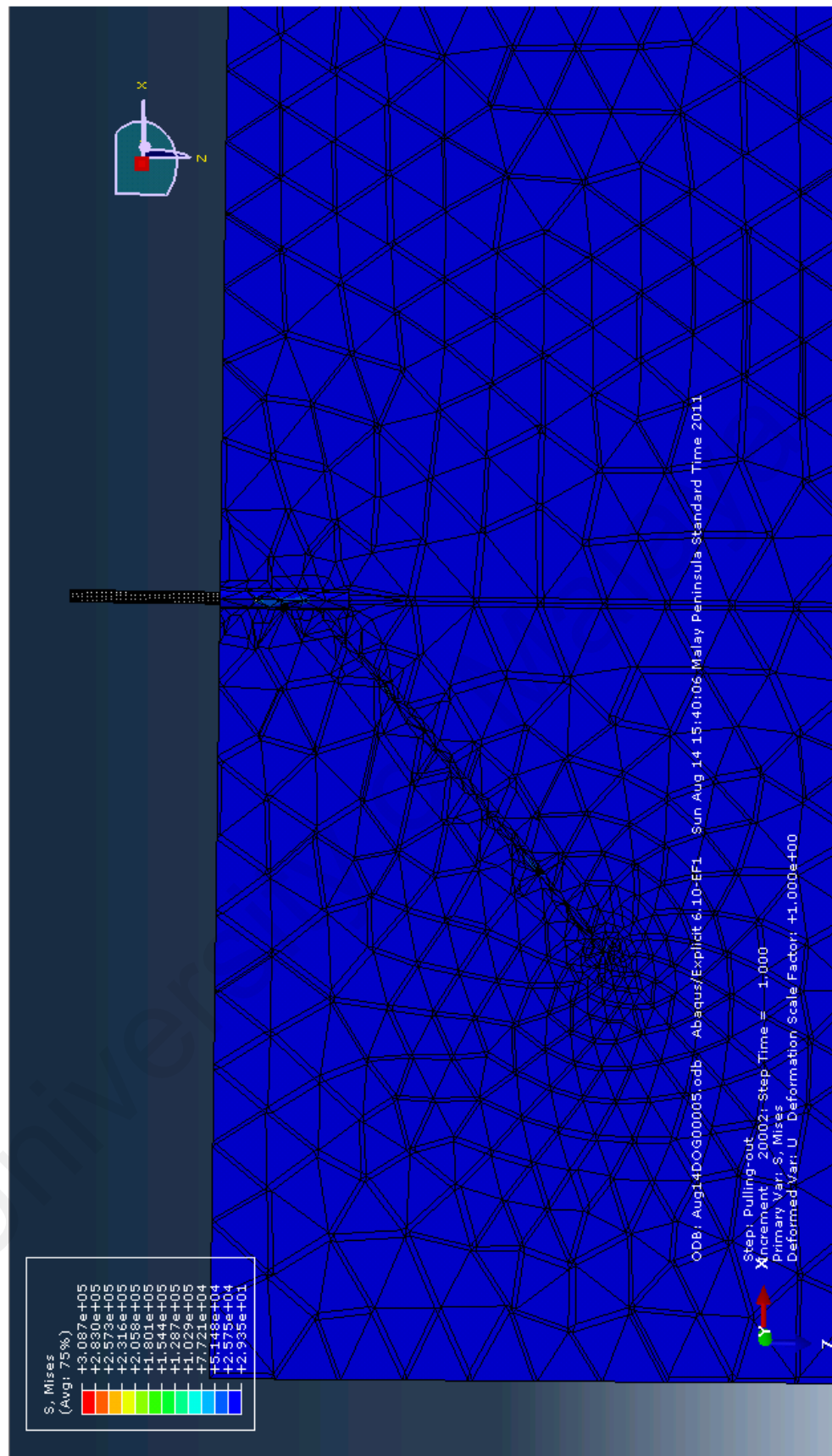
Figure 6.19: Vone-Mises stress distribution for the deeper root on Root sample (2)

Figure 6.20: Logarithmic strain distribution for the deeper root on Root sample (2)

As presented in Figure 6.21, both models showed almost identical stress distribution pattern, because as discussed earlier, the stress concentration rarely occurs in deep roots. Only the pulling out reaction force and Mises were different, (in the model with long taproot the value is more than the original model).

a) Root Sample 2 modelled as per as section 4.6.1

b)Modified Root Sample 2 modelled as per as section 4.6.1
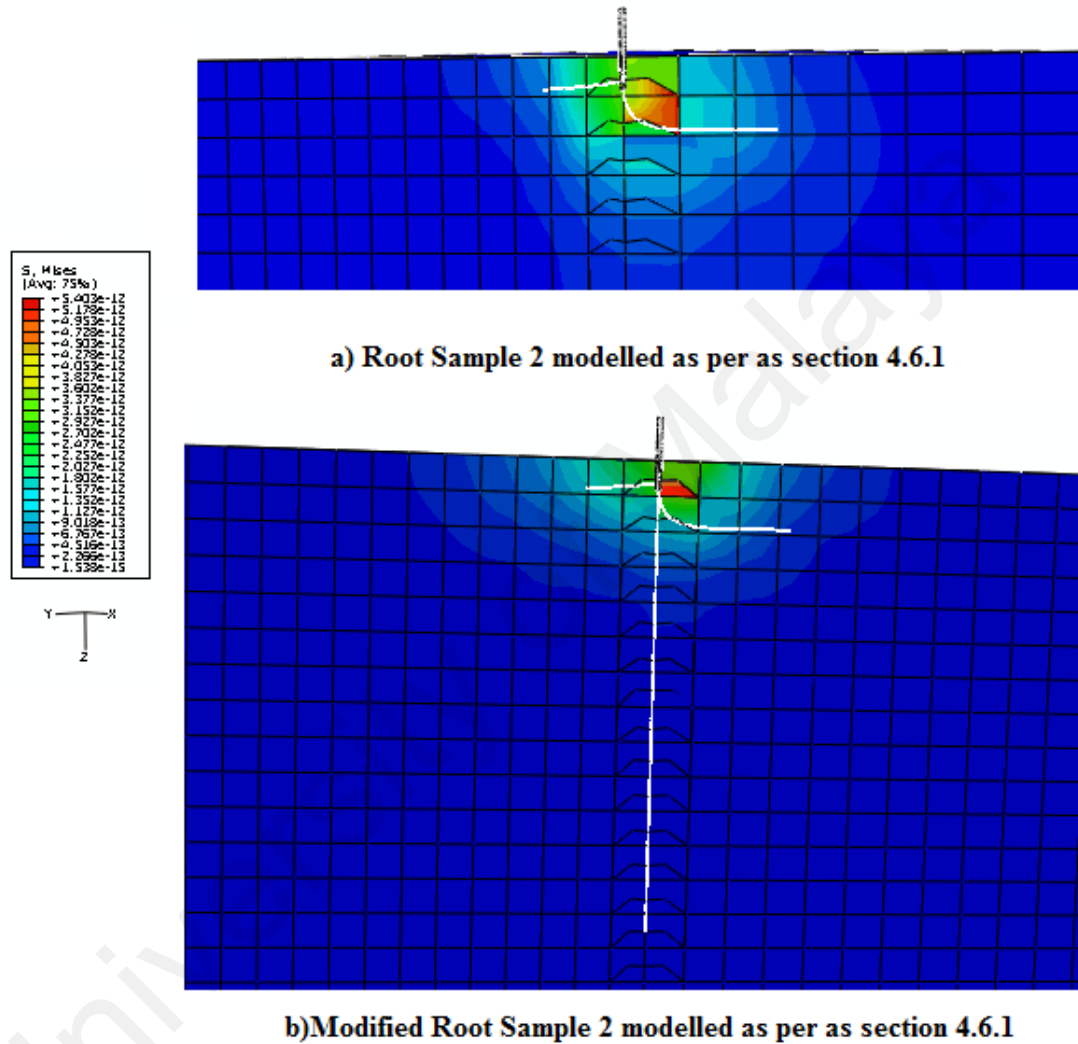
Figure 6.21: Stress distributions in the (a) Root sample 2 and (b) modified Root sample 2

In other words, in plants with longer taproots, due to the increase in root length, the friction force rises despite the negligible weight of soil column located above the root. Due to this effect, the bonding in the root-soil matrix fails later and the rate of the pulling out force shows an increase. Consequently, elastic characteristics of root will

have more time to have an effect. Due to this effect, the root anchorage characteristics are improving, which causes larger range of displacement in root soil matrix during the pull out and improving in root anchorage characteristics.

6.4.2 Effect of root pattern

In this part the different root pattern was simulated and results were compared to estimate the effect of various patterns on the root anchorage capacity. The response curves, i.e. the force-displacement (f-d) curves, for soil–root systems are derived from the FEM simulations of the pulling out force (Figure. 6.22).

Reaction forces are computed in the stem at the point where a horizontal displacement is imposed. The maximum displacement considered in the simulations is illustrated in Figure 6.23.

Based on the f-d curves, the stiffness of the root–soil systems is calculated at the maximum amount of the RF belonging to each root model. Stiffness at any given displacement corresponding to the maximum RF in each root model is defined as the tangent to the f-d curve at the related point.
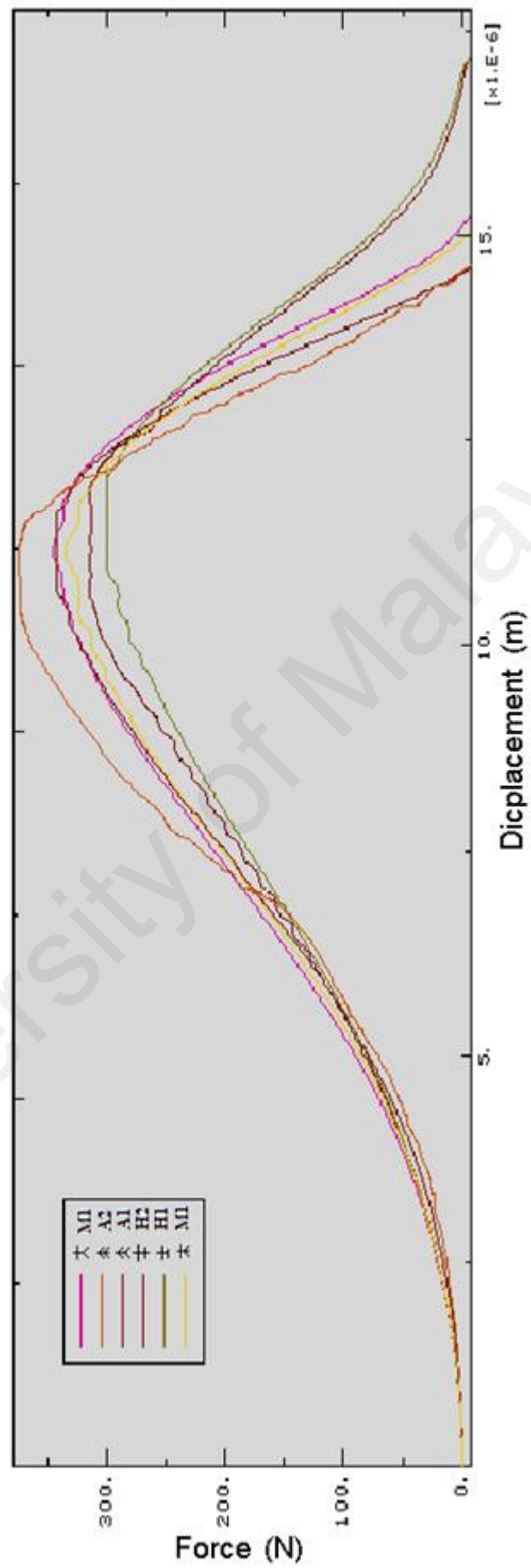
Figure 6.22: Reaction forces versus displacement curves resulting from the simulations
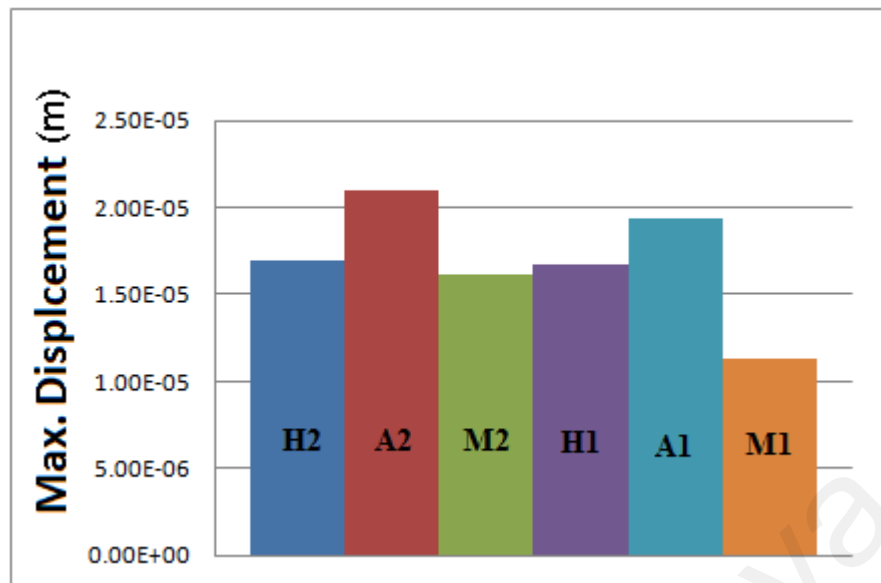
Figure 6.23: Maximum displacement during the pulling out process relevant to each root pattern.

In cases where the taproot is removed, the f-d curves followed different trajectories. Thus analysis of the taproots contribution to the pulling out force showed that the taproot effect on the root anchorage strength is sensible. The pulling out force is loss due to the removal of taproot which is approximately 5%. The maximum taproot effect on the pulling out force belonged to root type A (7.92%) and the minimum belonged to root type M (2.98%). In the cases of root pattern, the analysis of the root pattern contribution to the pulling out force reflected that the root pattern has a significant role in the pulling out force and consequently the anchorage strength. The maximum strength projected in the root pattern A and root patterns H and M showed respectively 15.55% and 10.01% less in the pulling out force respectively. During the pulling out test, it was also proven that, effects of the root pattern and taproots are more significant than the effects of stem displacement.

The displacement loss is due to the removal of taproot which is nearly 13%. The maximum taproot effect on displacement belonged to root type M (30.51%) and the minimum belonged to root type A (1.76%). In the cases of root pattern, the maximum

displacement during the pulling out process is shown in the root pattern A and root patterns H and M which displayed respectively 19.09% and 22.88% less in displacement respectively.

In root pattern A (Figure 6.24), the local opening modes of failure are initiated in zones with more values of LE11 and LE22 in comparison with the patterns M (Figure 6.25) and H (Figure. 6.26).
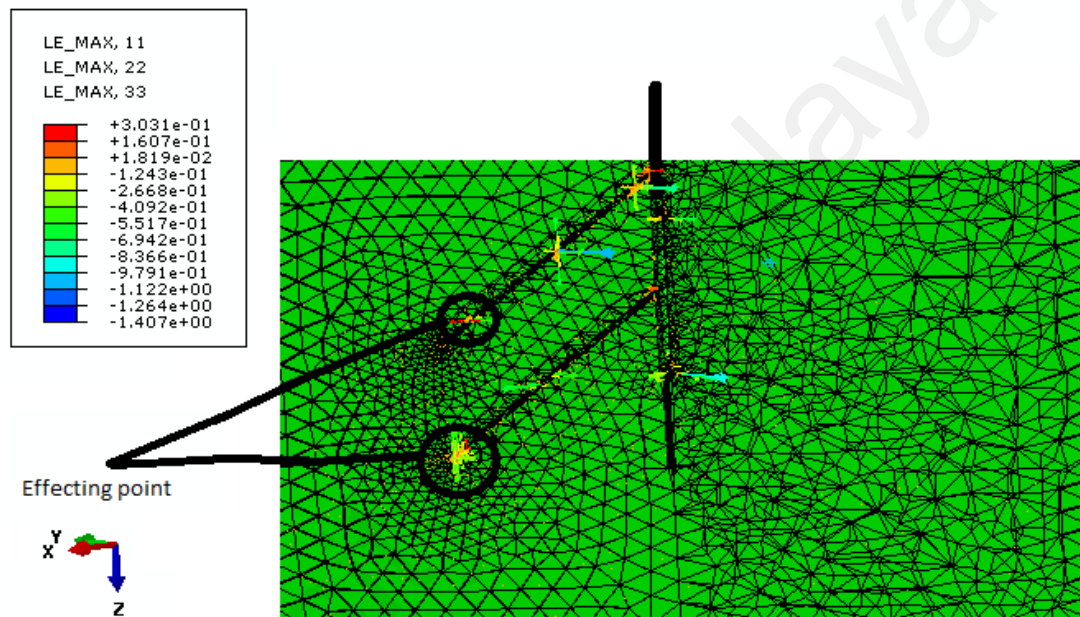
Figure 6.24: Maximum logarithmic strain concentrations points for pattern A.
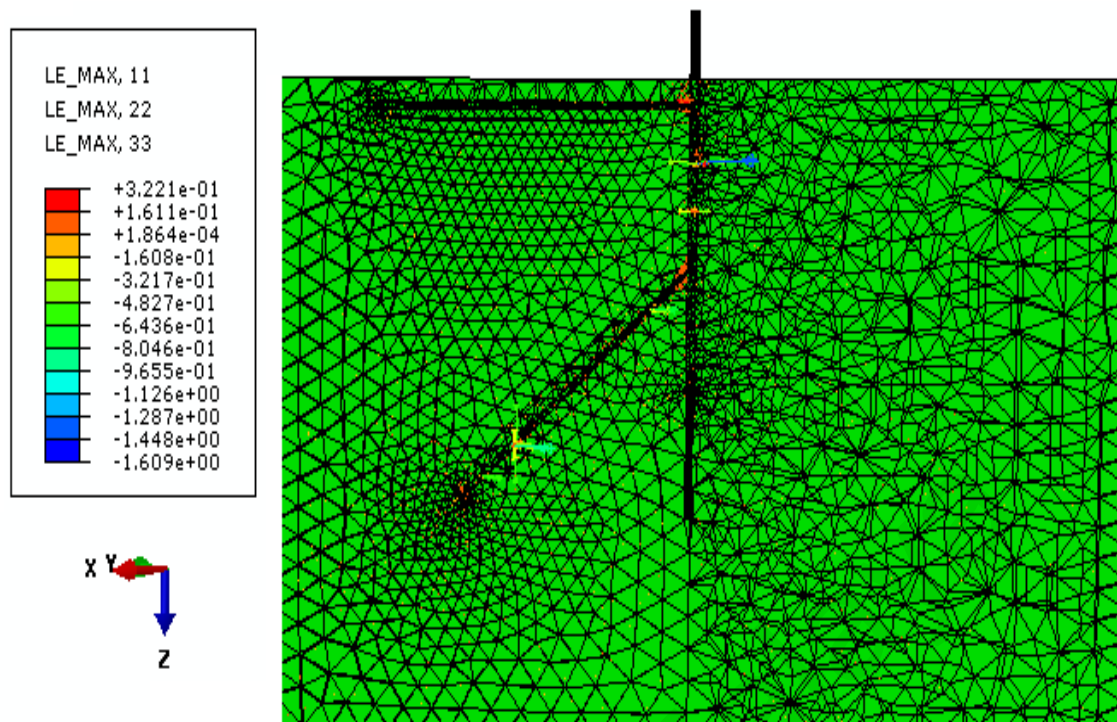
Figure 6.25: Maximum logarithmic strain concentrations points for pattern M.
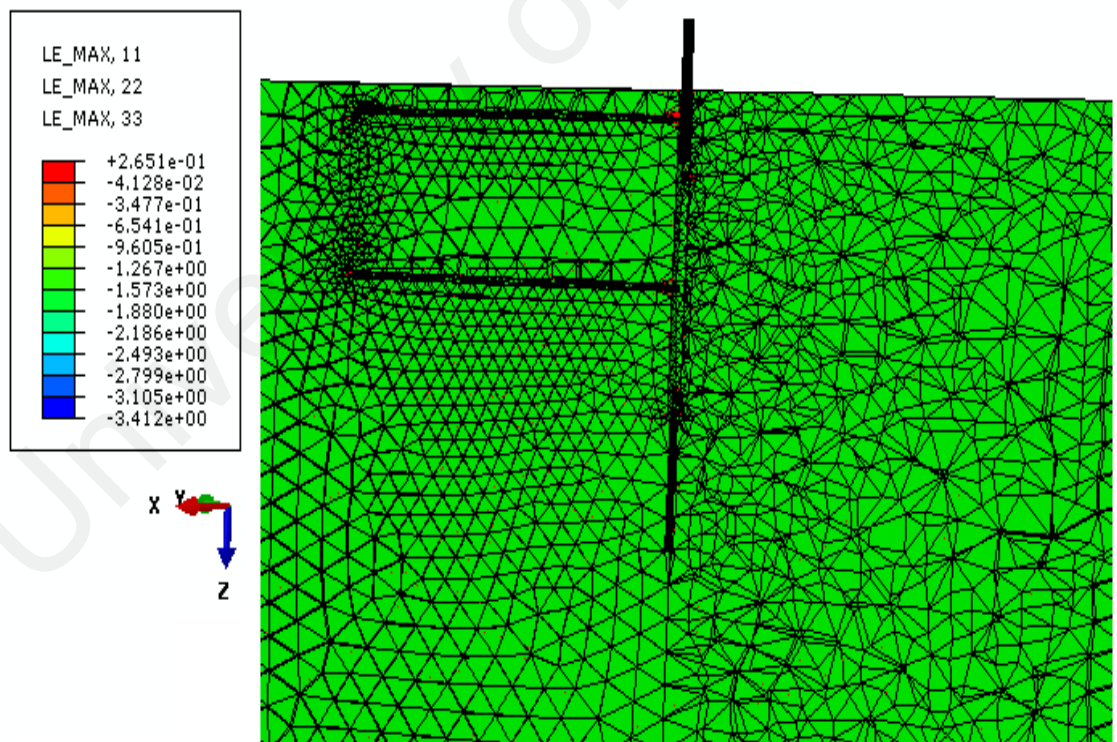
Figure 6.26: Maximum logarithmic strain concentrations points for pattern H.

Related stress and logarithmic strain are also demonstrated for all root patterns, which revealed the priority in the value of maximum stress for root pattern A(Figure 6.27) in comparison with H and M (Figure. 6.28).
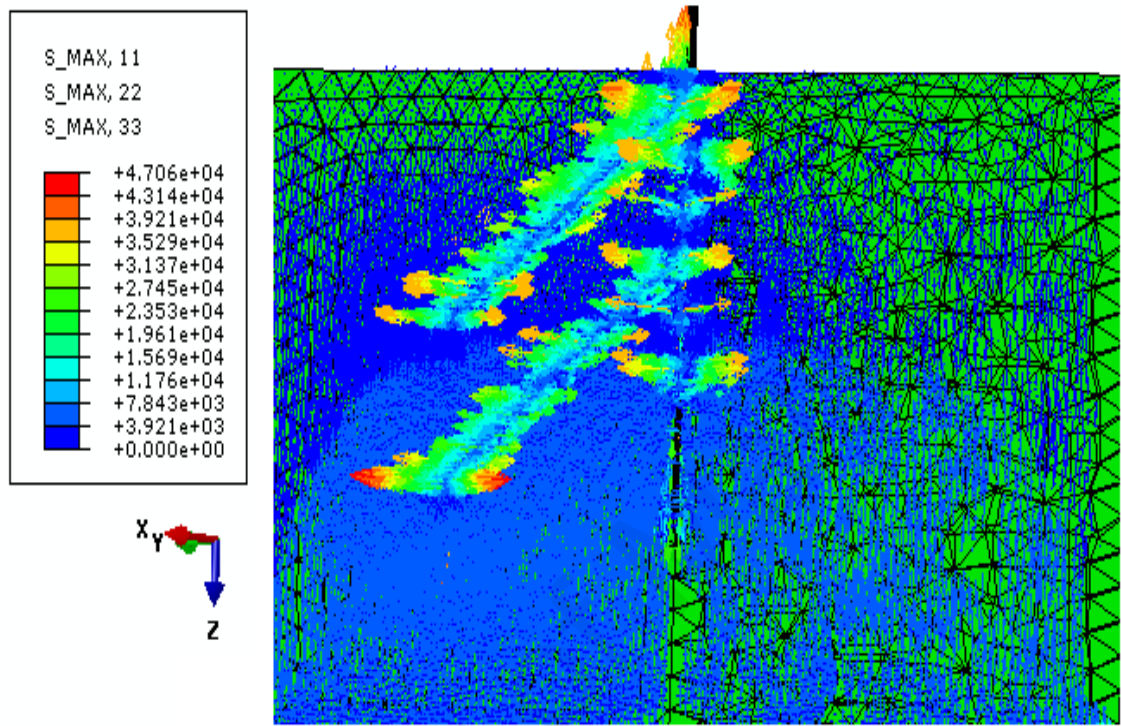
Figure 6.27: Maximum stress concentrations points for pattern A.
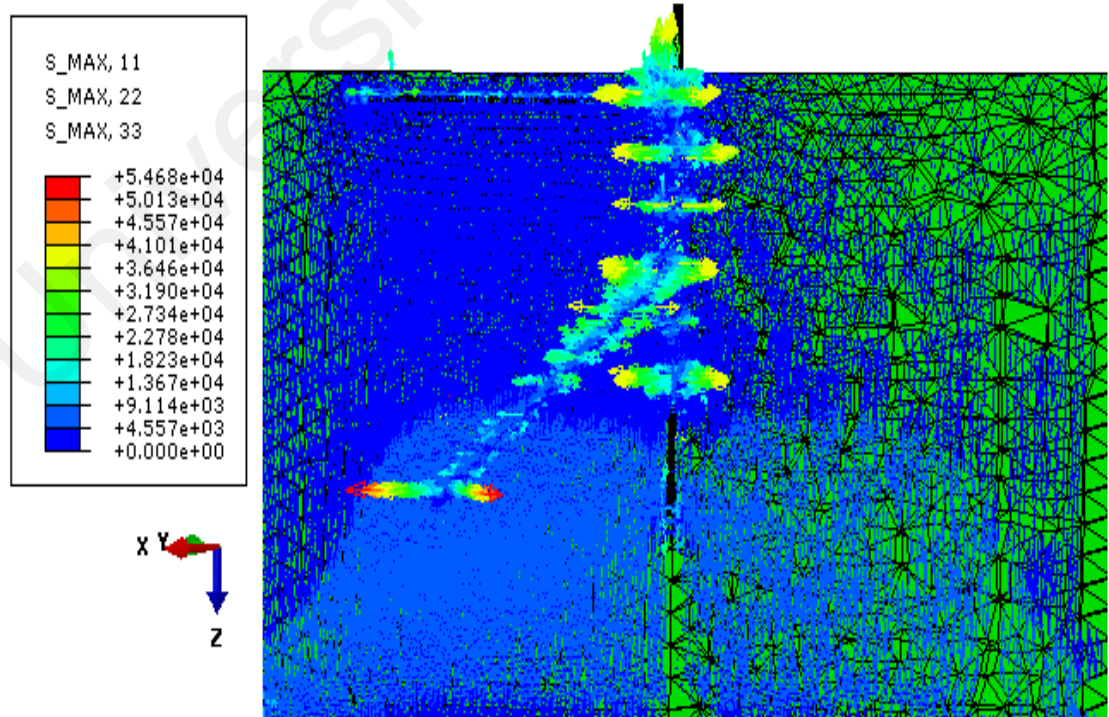
Figure 6.28: Maximum stress concentrations points for pattern M.

As denoted above, the stress and logarithmic strain are distributed mainly in the soil region mobilized with angular branches, for instance in root pattern M where almost all horizontal branches are not switched to the distribution process. In summary, it is found from this part of simulation that the maximum distribution occurred in root pattern A and the minimum in root pattern H.

During the analyses it is revealed that, the angular branches play a more effective role in root anchorage whereas the horizontal branches display a slight role in this issue. This effect is due to the negligible soil column weight at the top of the branch surface and consequently the low friction force. As specified, one of the major factors involving the root anchorage process is friction in between the root skin and surrounding soil. It is well known that the friction is affected by friction coefficient and vertical impressive force. Friction coefficient has almost constant values in root anchorage, but vertical impressive force is caused by soil column weight in top of the root which is changing depending on the case. It is clearly demonstrated in Figure 6.29, (W1>>W2). As a result, the friction force consequently the anchorage force is sufficiently higher for angular branches in comparison with the horizontal ones.

The soil weight is a component which contributes to the friction force counter balancing the pulling out forces on root anchorage. The importance of root–soil weight on root anchorage is quantified by Coutts as 13–45% that of the total anchorage system.
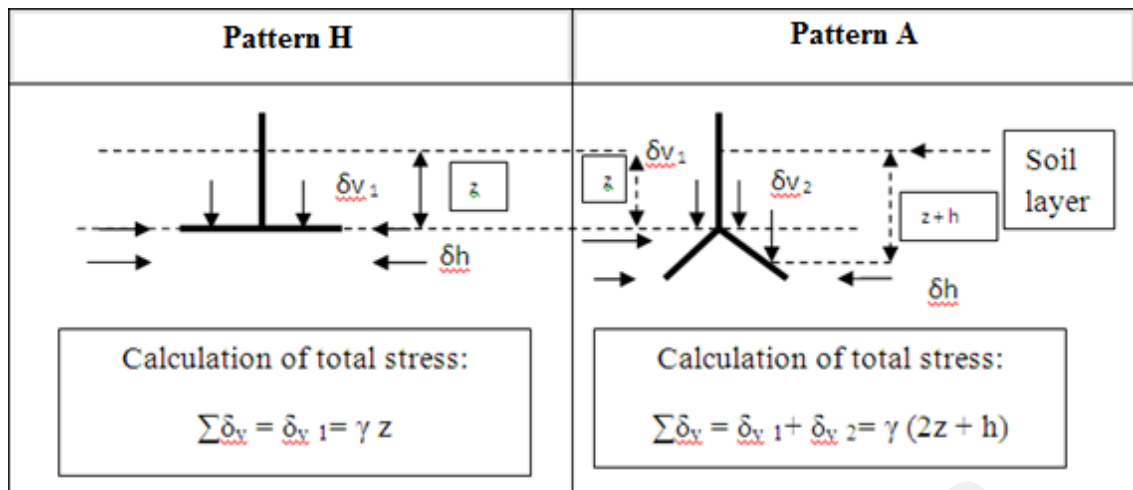
Figure 6.29: Comparison of soil column weight for horizontal branches with angular branches

This effect therefore indicates why the pulling out resistance is more in root pattern A in comparison with the root pattern H. During the analyses it is also found that, because of the limited soil surface which surrounds the taproot causes less friction effect, the effect of the taproot is too short in comparison with the angular ones.

6.4.3   Effect of root inclination angle

The response curve is representative of the behaviour of the whole mechanical system and is defined as f-d, i.e. force against displacement, calculated at the top end of the rigid stem (as reference point). In this approach, as the simulation is motivated by a compulsory displacement (simulation input), the resulting force is defined as the 'reaction force' RF (simulation output) calculated at the reference point. At any point of the movement, the stiffness of the system is distinct by the slope of the tangent at the recent point of the f-d curve. Anchorage strength corresponds theoretically to the maximum force reached before failure. In the current analyses, strength is defined as the maximum reaction force considered in certain displacement ranges, as it is supposed that severe plasticization of the system had already occurred at this period. In each root type, the relative differences in the pulling out force between root patterns and different

branch angle – starting from the horizons and various angles (15 °, 30 °, 45 °, 50 °, 52 °, 53 °, 54 °, 55 °, 60 ° and 75 °) are defined.

The response curves, i.e. the force-displacement (f-d) curves, of the soil–root systems are derived from the FEM pulling out simulations (Figure 6. 30 and 6.31).
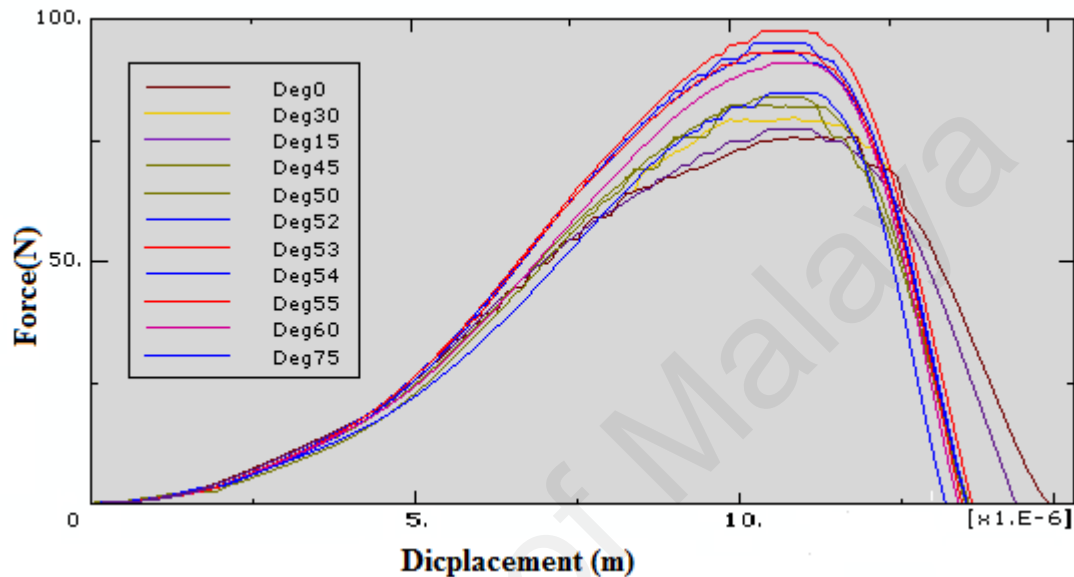
Figure 6.30: Reaction forces versus displacement curves resulting from the simulations

Reaction forces are computed in the stem at the point where a horizontal displacement is imposed. Based on the f-d curves, the stiffness of the root–soil systems is calculated for each root model as the tangent to the f-d curve at the related point.

The analysis of the roots branches angle contribution to the pulling out force and the anchorage strength illustrated that the roots branch angle has a significant role in the pulling out force and consequently the anchorage strength. Maximum strength is demonstrated in the root pattern with the 53 ° deviation angle to the horizon and for the more deviated root, the pulling out resistance starts to decrease. Root patterns with 0 °, 15 °, 30 ° , 45 ° until 52 ° deviation angle to the horizon denoted 22.23%, 20.52%, 18.13%, 15.72%, 13.82% and 2.48% less in the pulling out force respectively. For steeper angles (more than 53º) the pulling out resistance and consequently the

117

anchorage strength start to decrease from 4.39% for an angle of 54 ° to 13.05% for an angle of 75 ° (subsequently 4.64% for 55 ° and 6.69% for 60 °). The effects of the root patterns are considerable to stem displacement during the pulling out test. During the analysis it is found that the maximum stiffness also belongs to the root pattern with the deviation angle of 53 °.
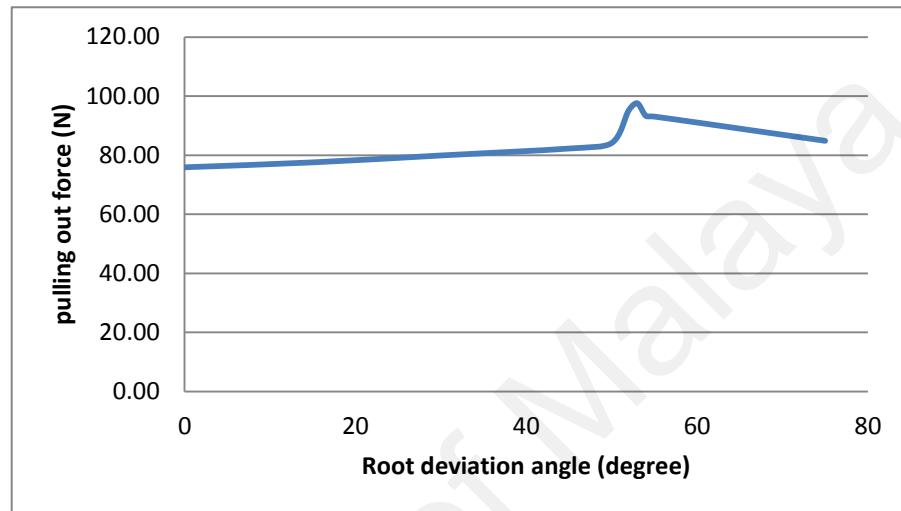
Figure 6.31: Effect of root angle on pulling out force

This issue can be explained by the effect of soil column weight on the top of the roots. By increasing the inclination angle, the height of the soil column at the top of the roots increases and at the same time, the length of the root horizontal projection also decreases. This change in root inclination angle is caused by the increase in soil area at the top of the root until some critical values of root inclination angle are reached, after that the soil area at the top of the root starts to decrease.

The root inclination angle which caused the maximum area to be reached by the soil at the top of the root should be defined to reach the maximum pulling out reaction force in root-soil system. This maximum area and inclination can also be calculated as below (Figure 6.32).

L_V=root length vertical projection

L_H=root length horizontal projection

A= Effecting area

L= root length

α = root inclination angle
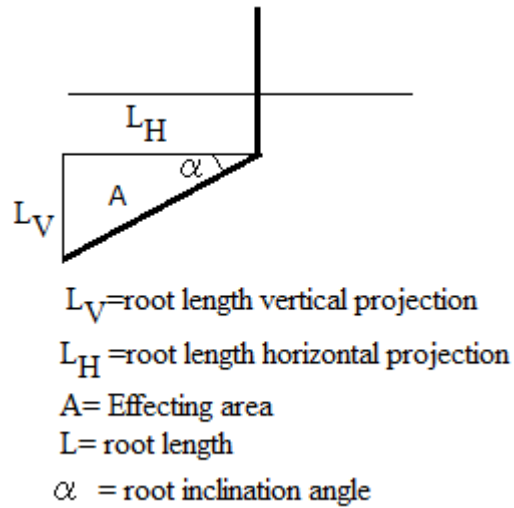
Figure 6.32: Mathematical solutions for optimum root inclination angle due to pulling out process

$$A= (1/2)\ L_H\ L_V \tag{6.2}$$

Where: L_V=root length vertical projection and L_H =root length horizontal projection

$L_V = L\ cos\alpha$

$L_H = L sin\ \alpha$

$A= (½)\ L sin\ \alpha\ L\ cos\alpha$

$A= (½)\ L^2 sin\ \alpha\ cos\alpha$

$A= (1/2)L^2\ (sin2\alpha)/2$

$A'(\alpha) = (1/4)\ L^2*2cos2\alpha$

$A'(\alpha) = (1/2)\ L^2\ cos2\alpha$

To get A maximum, $A'(\alpha)$ should become zero

$A'(\alpha) = 0$

$cos2\alpha = 0$

$2\alpha = 90\ °$

$\alpha = 45\ °$

As it is clear from the above, the maximum pulling out reaction force should reach below 45 degree of root inclination angle while the maximum pulling out reaction occurs below 54 degree which is 8.4% higher.

Thus, the increase proves that soil shear resistance which is resisting pulling out is controlled not only by the direct friction between soil mass and root surface but also by the grain interlocking resistance. This effect can be explained as; when grains are packing densely, they tend to spread apart from each other. The expansion of the particle matrix due to the shear stress is called dilatancy. Due to the extra force required for the particles to dilate against the confining pressure, the dilatant soil should have a greater reaction force against pulling out. Based upon the simulation results, the dilatancy effect on pulling out is evaluated as 8.4%. %. As illustrated in Figure 6.31, this effect manifests as a peak in the illustrated curve for 45 ° to 54 ° root inclination angle.

Based upon the Von Mises stress distribution diagram illustrated in fig 6.33, 6.34 and 6.35 the stresses are distributed mostly in the upside of the root branches and in regards to the increase in branch angle, the stress also increases until the deviation angle equals to 60 ° (Von Mises stress curve was only built for horizontal roots, and inclination angles equal to 15 degree, 30 degree, 45 degree, 60 degree and 75 degree therefore the maximum value is shown on 60 degree instead of 53 degree which is the exact amount) . In all cases, the stress is concentrated on the connection point between the stem and branches which is also followed by the logarithmic (LE). (Figure 6.36, 6.37 and 6.38)

It can be explained by the diameter of the chosen root model as described in 6.3.2 where the root chosen was relatively thin to show the effects of inclination angle.
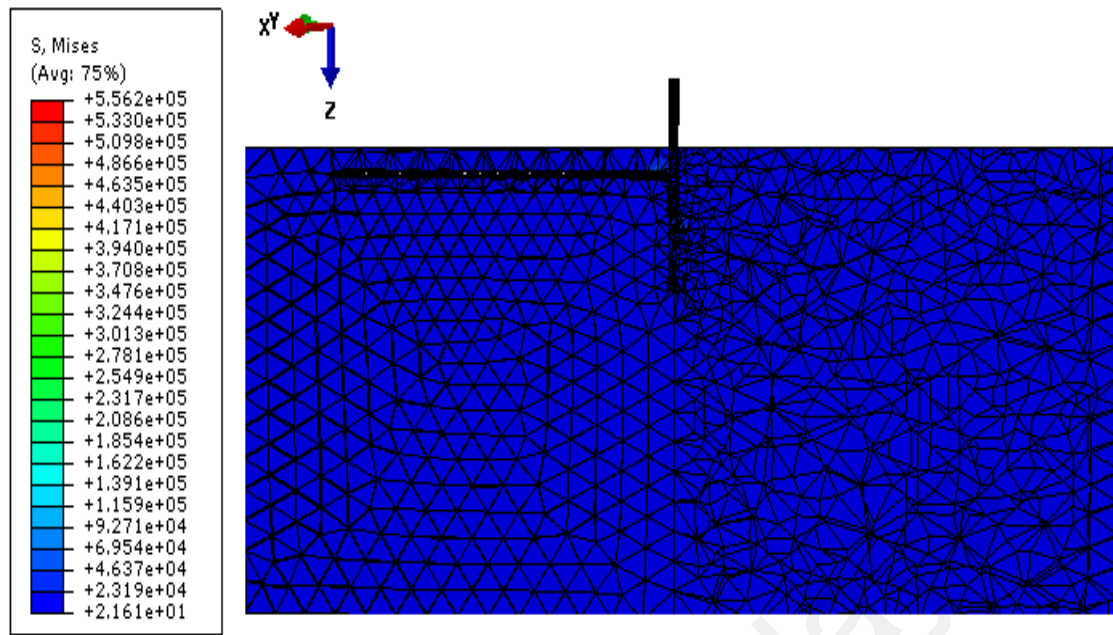
Figure 6.33: Von Mises stress distribution components for horizontal root patterns.
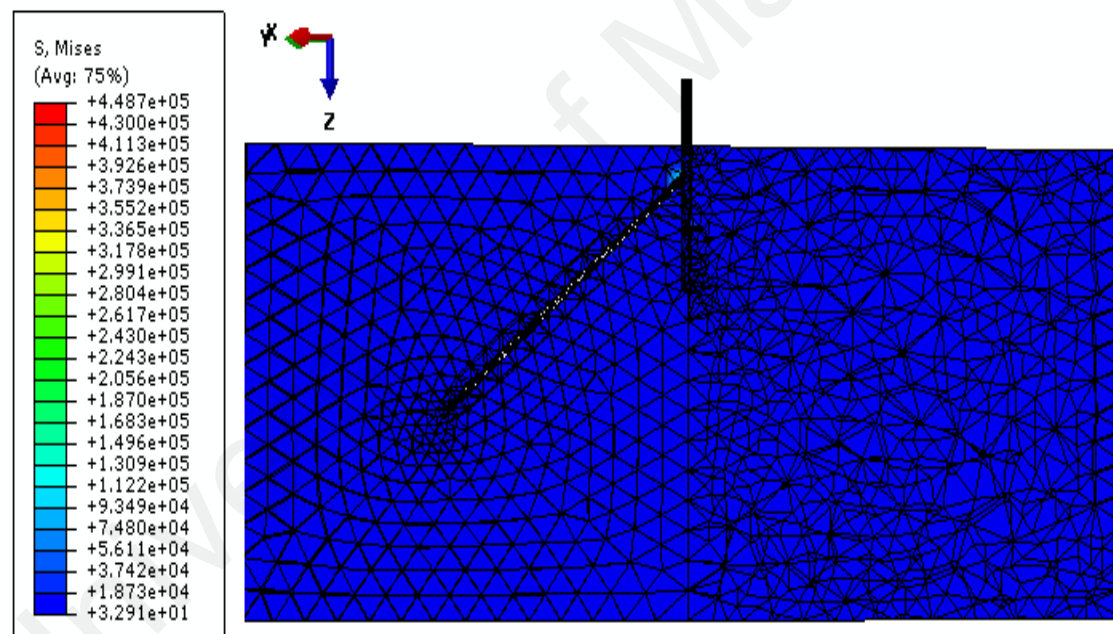
Figure 6.34: Von Mises stress distribution components for root patterns with 45°
inclination.
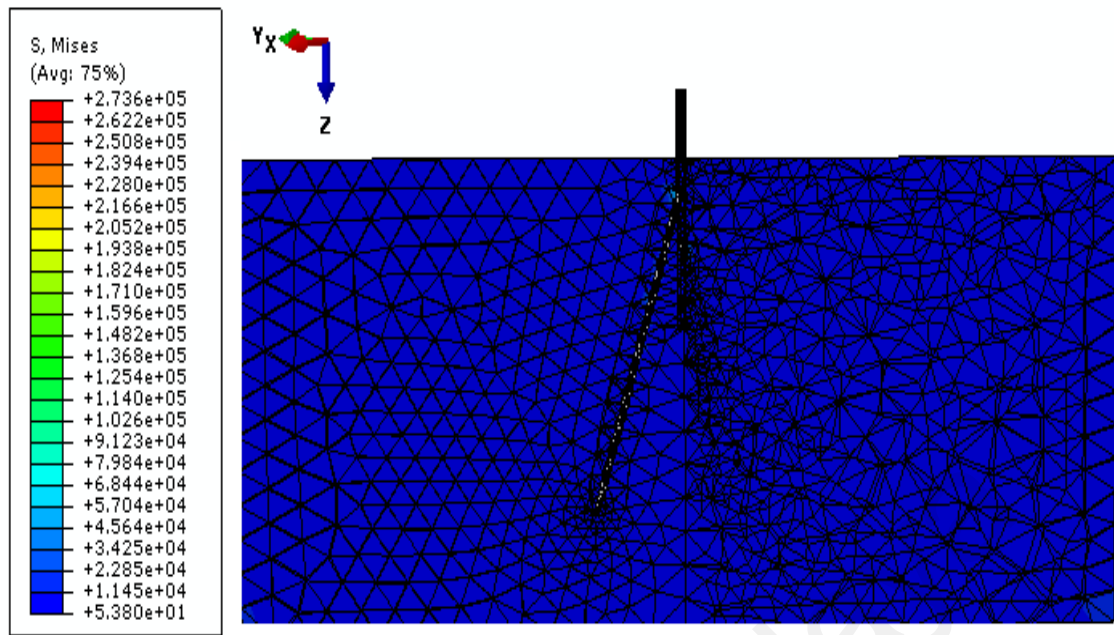
Figure 6.35: Von Mises stress distribution components for root patterns with 75° inclination.
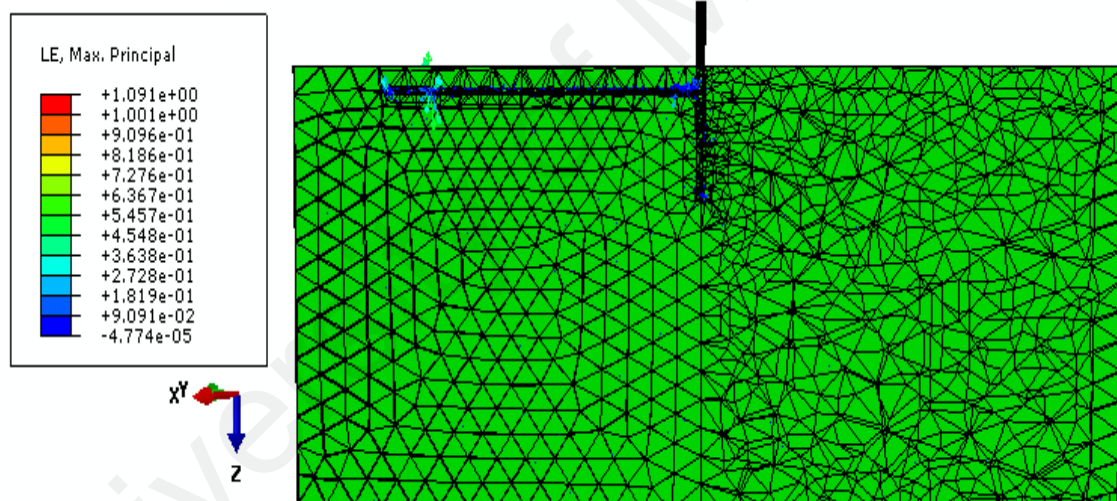
Figure 6.36: Logarithmic strain distribution components for horizontal root patterns.
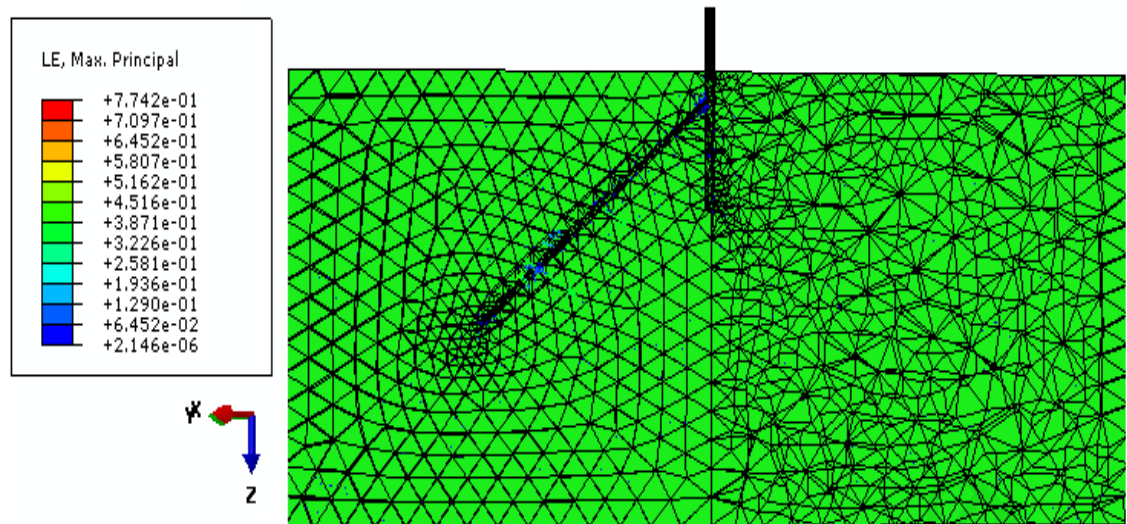
Figure 6.37: Logarithmic strain distribution components for root patterns with 45 °
inclination.
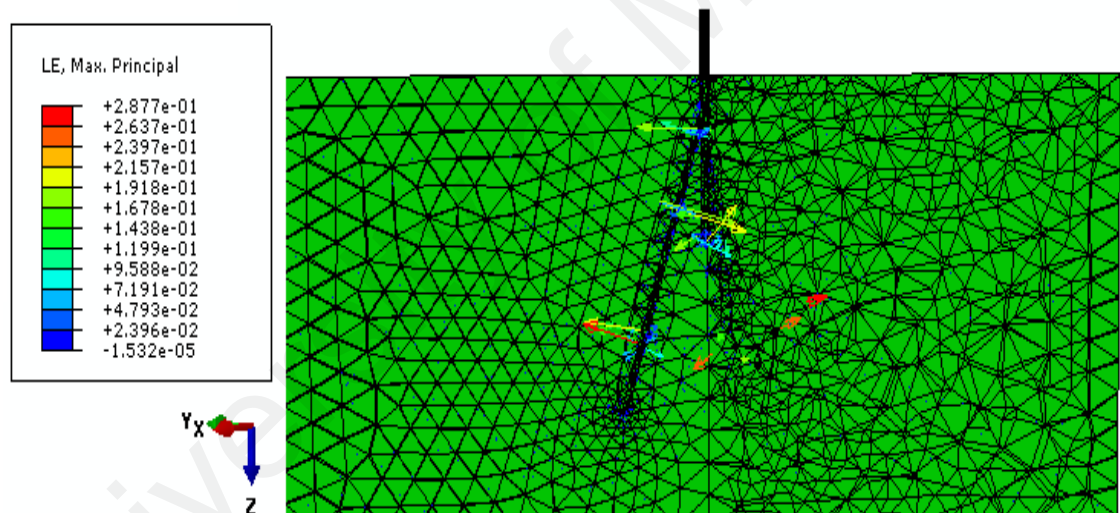
Figure 6.38: Logarithmic strain distribution components for root patterns with 75 °
inclination.

6.5 Effect of soil characteristics (c and Φ) on pulling out

It is clear from the theory that during the pulling out process the weight of the
system alone is not sufficient to produce enough isostatic pressure to prevent soil failure
according to the Mohr–Coulomb theory. Additionally, the soil that is lifted during
pulling out is subject to the low or negative isostatic pressure, thereby increasing the

sensitivity to variations in soil shear strength, which is triggered by the soil cohesion c. The soil friction angle also influences the pulling out resistance. To prove this effect in this part, the pulling out process was simulated for the unique root model but with different cohesion (c) and friction angle (Φ). The f-d response curve, Vone-Mises stress and Logarithmic strain distribution couture were compared in the different cases.

6.5.1   Effect of Soil Cohesion

Simulation in eight models with difference in only the c value helped to define the influences of matric suction on the pulling out force and slope stability respectively.

a)   Impact of Soil cohesion on Pulling out

As proven by the experimental results, the required force during the pulling out process increases due to the increase of the matric suction and consequently the cohesion coefficient, as displayed in Figure 6.39.
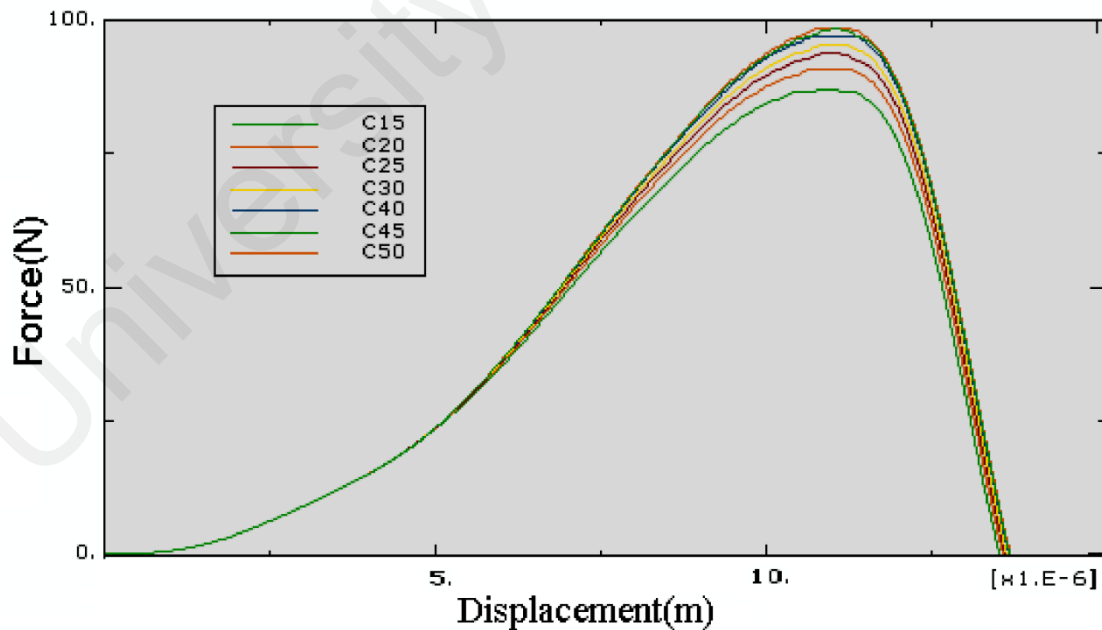
Figure 6.39: The pulling out force for different soil cohesion coefficient value

In both cases (inclination angles of 15 ̊ and 60 ̊) the pulling out force increases with the improvement of matric suction and consequently rises in the cohesion coefficient.

Moreover, the coefficient of determination (R2) is obtained from both the linear regressions where the value of R2 belongs to the roots with steep deviation angle (15 °) being more than the roots with a sharp angle (60˚). Therefore, the result for root with 15˚ deviation angle was considered in this study.

For soil types SC, ML and CH when the matric suction rises from zero (saturated situation) to 10 kPa (during rainy season), the pulling out force is improved by 11.11%. At the same rise of matric suction, the pulling out force increases at 10.41% with the soil types CL and SM-SC and 3.07% for soil types SM, MH and ML-CL.

When a matric suction scaling up from 10 kPa (during rainy season) to 100 kPa (during dry season) the required value of the pulling out force shows growth of 20.14% for the soil types SC, ML, CH, 13.53% for the soil types CL, SM-SC and 12.05% for the soil types SM, MH and ML-CL.

The linear regressions for the maximum pulling out force in simulated unsaturated soil for different matric suctions (via different c) are drawn (Figure 6.40) and appropriate equation is determined as shown in Figure 6.40.

As specified from the simulation result, the maximum effect of soil cohesion and consequently matric suction on the pulling out reaction force belongs to the soil with higher plasticity or soil with more clayey content. On the other hand, with the decrease of sand in soil, the effect of cohesion is increased.

Generally, the simulation results showed that increase on cohesion were caused by the rise in required pulling out reaction force because cohesion is intensifying the interlocking force. This effect is causing rise in soil shear strength and consequently the pulling out reaction force. Therefore, the soil with smaller particular size and larger plasticity are more prepared to be affected by the interlocking force due to higher interparticular friction present in such soil.
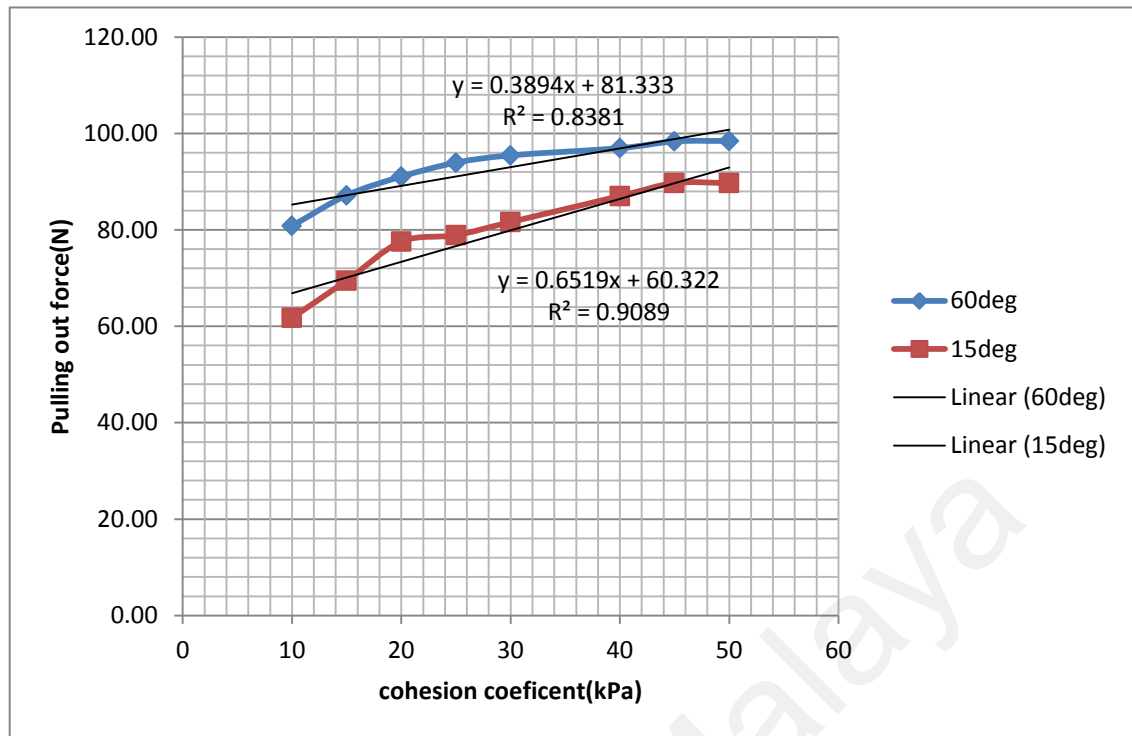
Figure 6.40: Linear regressions between "c" and maximum pulling out force.

b) Impact of Soil cohesion on soil stress and strain distribution contour

As it was discussed before, up to 45% of factors involved in root anchorage are about friction between the root and soil and another 10% is about the interlocking force in between soil grains which is mainly related to the cohesion strength.

As displayed in Figure 6.40, the comparison of the stress and consequently strain distribution contour revealed that with increases of the soil cohesion, stress and strain are influential in a more limited area (just near the root). The Maximum Misses stress is rising while improving the soil cohesion strength until 20 kPa in a linear order. When soil cohesion strength value reaches 20 kPa, the pulling out reaction force steel rises only with a more moderate rate. It is also visible in Figures 6.41 to 45.
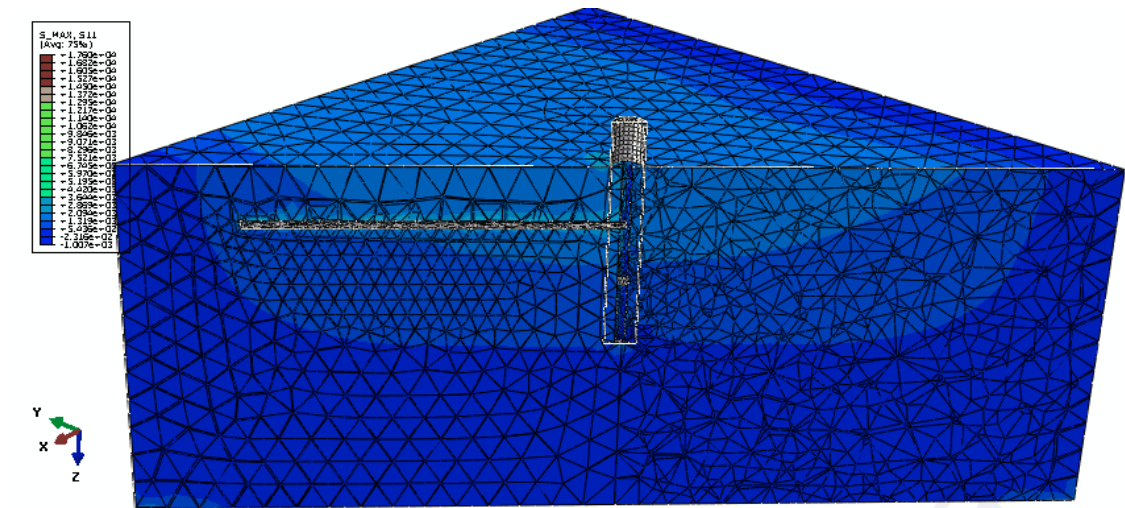
Figure 6.41: Stress distribution contour for c=5kPa

Figure 6.42: Stress distribution contour c=10kPa
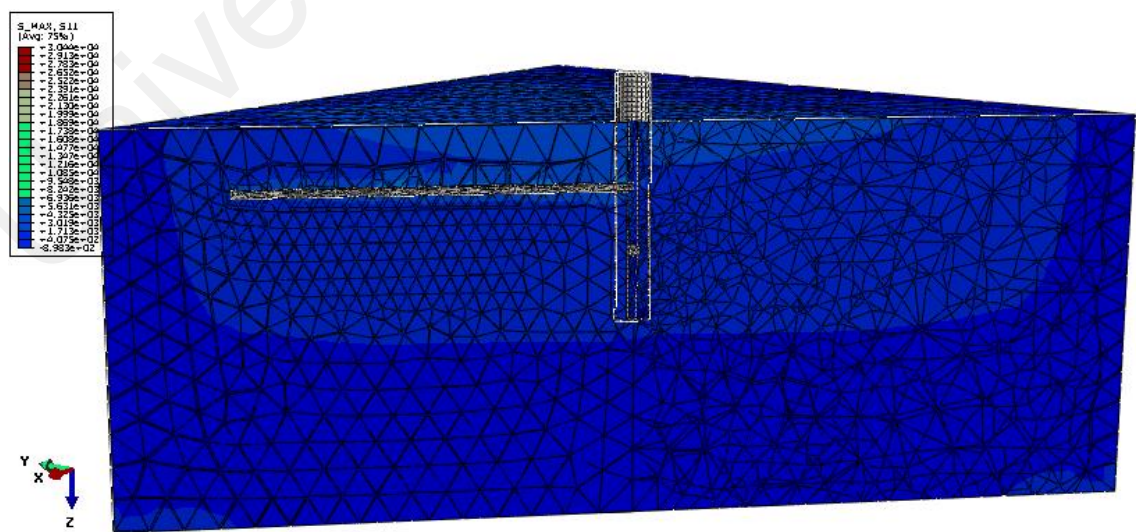
Figure 6.43: Stress distribution contour for c=20kPa
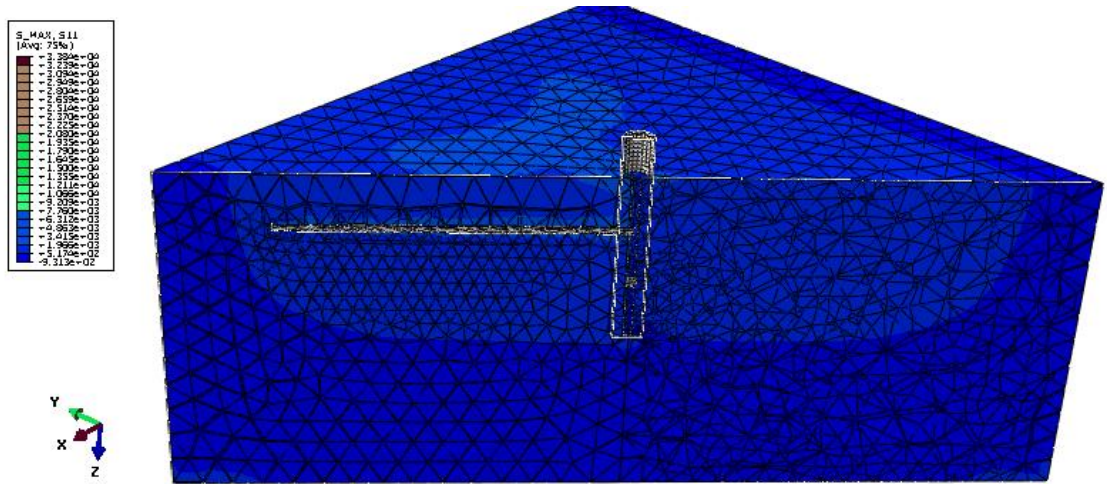
Figure 6.44: Stress distribution contour for c=30kPa
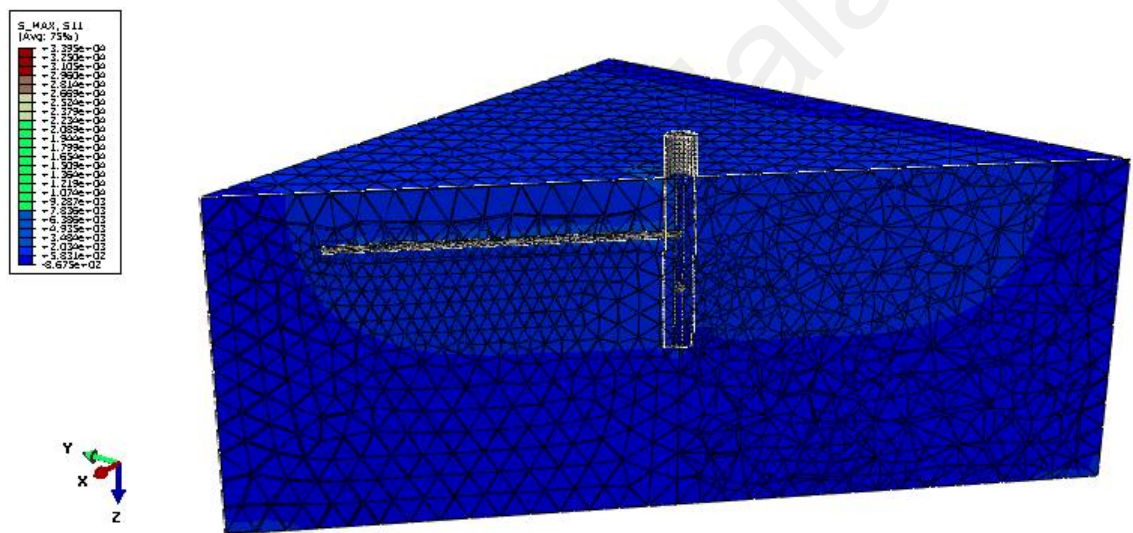
Figure 6.45: Stress distribution contour for c=40kPa

6.5.2 Effect of Friction angle Φ

Simulation in six models with different Φ was done to define the friction angle effect on pulling out. Simulation results denote that the change in friction angle (Φ) does not play any significant role (in the pulling out force in the root model) except when the inclination angle is near to being horizontal.

This can be explained by the effect of the soil bearing capacity. As explained, the soil bearing capacity is related to the friction angle. As evident in Figure 6.46, the soil

bearing capacity and consequently the friction angle is mostly affected by horizontal roots because angular root slid in soil is easier than horizontal ones during the pulling out, therefore the soil bearing capacity effect is more on horizontal or roots with inclination angle which is nearly horizontal than roots with higher inclination angles. On the other hand root is not rigid material and during the pulling out, the root horizontal projection decreases with time (depending on root material stiffness). Therefore, the equation used in Figure 6.46 changes as below:

$$F_{\text{pulling out}} = \int_{L_2}^{L_1} q_f L_x . d_x$$

(6.3)
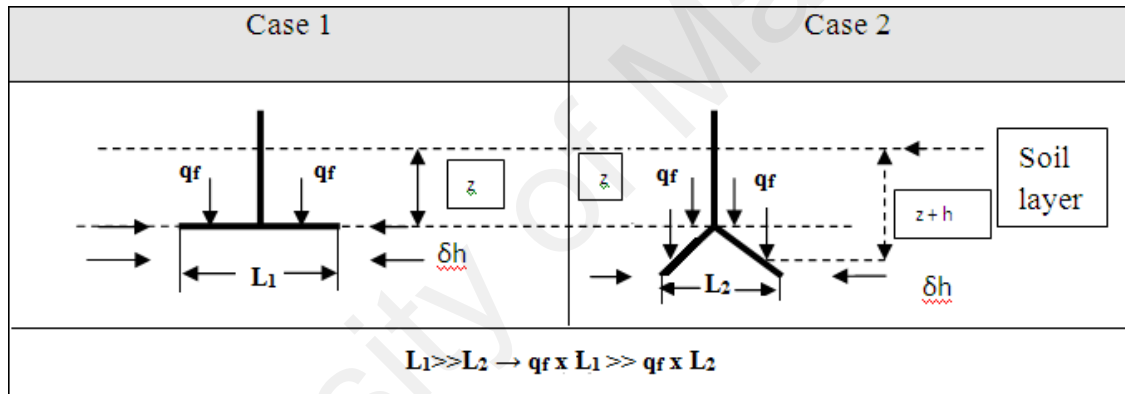
Figure 6.46: Comparison between Bearing capacity effect and friction effect in horizontal and angular branches.

Due to this effect, to analyse the effect of friction angle we should use the roots with the horizontal or at least steep deviation angle (bearing capacity is affected usually more in horizontal root or root with a steep deviation angle). On the contrary, the friction effect is habitually affecting roots with higher deviation angle. Therefore to obtain better results, analysis is done for roots with 15° deviation angle.

Required force during the pulling out process increases due to the increase of friction angle and consequently improvement in the soil structure (as shown in Figure 6.47).
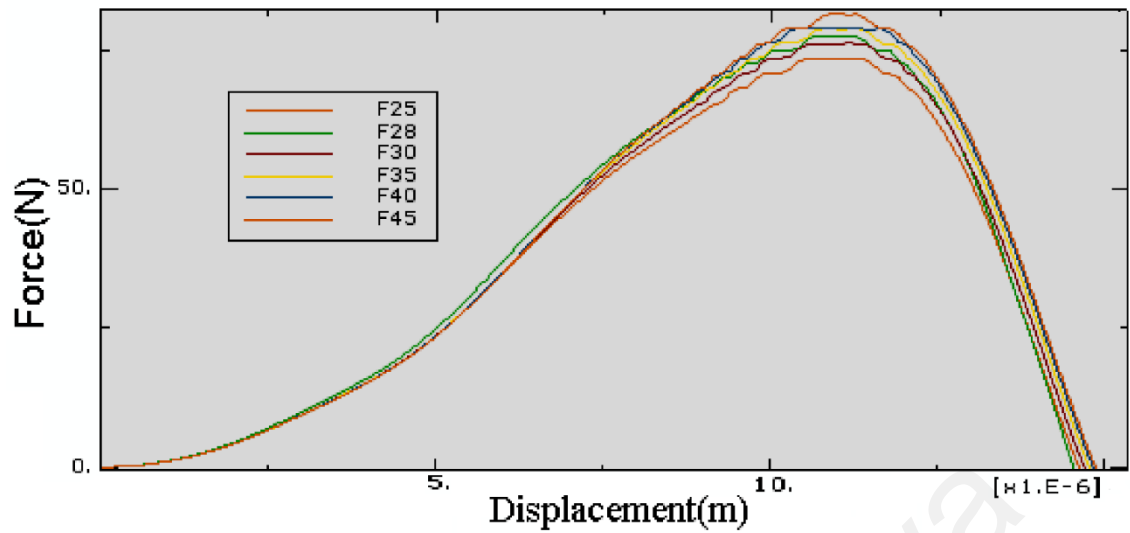
Figure 6.47: The required force on soil during pulling out process for different friction angle

When the friction angle increases from $25°$ to $45°$, the pulling out force improves by an average of 5.46%. This change is simulated for $25°$, $28°$, $30°$, $35°$, $40°$ and finally $45°$. It is found that increase in the pulling out is maximum between Φ equal $25°$ and $28°$ and minimum between $40°$ and $45°$ of the friction angle. The linear regression for the maximum pulling out force in simulated unsaturated soil for different soil friction angles is drawn in Figure 6.48 and the appropriate equation is as follows:
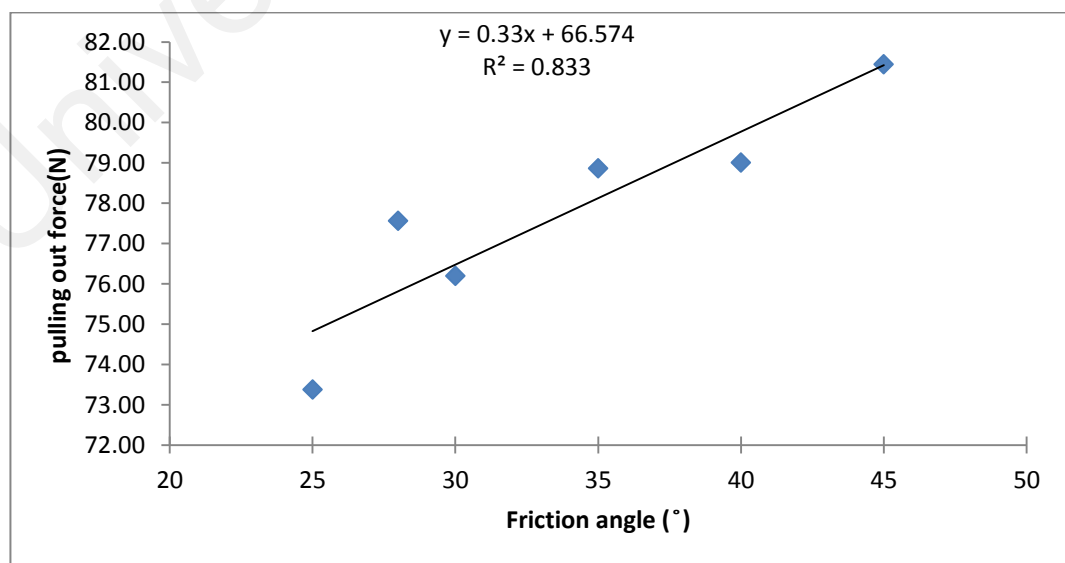
Figure 6.48: Linear regressions between Φ and maximum pulling out force.

From all the stated above, it can be concluded that, vegetation has a silence role in soil improvement by effect on soil matric suction and at the same time by upgrading the soil bearing capacity on the pulling out process. It was also proven that the internal friction angle has a minor effect on root anchorage resistance. It can be explained by Mohr coulomb failures envelop. As illustrated in this envelope, the cohesion coefficient is a value which represented soil adhesion from the beginning but friction angle only starts when failure started in soil (representing the failure development in soil).

<div align="center">

CHAPTER 7:

CONCLUSION AND RECOMMENDATION FOR FUTURE WORK

</div>

7.1 Conclusion

7.1.1   Influence of root-soil matrix effect on pulling out resistance for *Melastoma malabathricum*.

Based on the results obtained from the field pulling out test, the following conclusions can be made:

During the pull out process, all the branches are involved but the pulling out force is mainly supported by one branch or a group of branches and when failure occurs in this branch or group of branches, the force is transferred to another branch or group of branches and this repeats until the final failure. This pattern reveals a slight rise and fall in the force-time curve.

The required force was changed during the pull out process. Almost in all experimental cases the maximum pulling out force was obtained in 0-10 cm displacement and after that, long deformation range in roots was observed until 40 cm. This characteristics (long deformation before rapture in roots) is one of the major factors in root soil matrix which affect the root anchorage.

It was also observed that, the pull out force increases with the increase on stem diameter but at the same time the failure displacement shows a decrease. It can be explained as more ductile characteristics in roots with larger diameter. In other word, as the stem and consequently root diameter increases, the pull out force is also rising and at the same time the root became more ductile which is caused decreasing in failure displacement.

Maximum stress distribution in soil was also occurred at the same time as the pull out force reached maximum value and after that, the stress distribution decrease in the soil. It means that in almost 25% percent of final displacement, failure happened in soil block, and after that, the root anchorage is only a result of constraint between root branches and soil which seems to be a major factor in root anchorage. This fact proven by the root anchorage simulation subsequently.

7.1.2   3D numerical simulation of root anchorage

Based on the numerical simulations of the *Melastoma malabathricum's* soil–root matrix, the following conclusions are generated:

According to the field surveys of root architecture, a 3-D numerical model of the soil–root system is developed and successfully applied on the simulation of the in-situ pulling out behaviour. The model simply consists of the first order roots and second order root branches with modified interaction between soil and roots as specified in chapter 6.

Comparison between the RF-D diagram for experiment and numerical simulation denotes an acceptable similarity which proves the accuracy of the built model.

The numerical results indicate that the pulling out loading is mainly carried out by the first order root (taproot), whereas the hair roots (second order root branches) only play a minor role in providing the pulling out resistance.

The main factors that influence the Mises stress and logarithmic strain distribution are the root length and root architecture. Hence, the root diameter only influences the pulling out force value.

The stress distribution contour which elaborates on the maximum of soil bearing capacity during the pull out process, follow the pull out force. It shows that the stress distribution is more concentrated on root in comparison with the soil.

This fact is that, the soil effect in root anchorage during the pull out process is limited to almost 25% of the final displacement and after that, the failure happens in soil block. After the failure of the soil block, the remaining factor in effect for the root anchorage is only adhesion in between the unruptured root and soil.

The soil block failure point is matching with the maximum of Mises stress and consequently, the maximum of logarithmic strain.

7.1.3 The effect of root architecture on the root anchorage

Root architecture is the most affecting factor in root anchorage in comparison with the soil mechanical characteristics.

The significance of this part of study is to highlight the role of root architecture which can be also used for artificial root design as solution for shallow slope stability problem.

a) Effect of long taproot

Models with a long taproot demonstrated almost the same stress distribution; only the required pulling out force, concentrations and amount of stresses are different. In other words, the long taproot does not influence the stress distribution. The effect of root length is more apparent in comparison with the root diameter on stress distribution in the soil body. That is, longer roots distribute the stress and consequently strain in the wider range of soil.

b) The effect of root pattern

Removing the taproot can decrease the pulling out reaction force between 7.92% and 2.98%., and the maximum effect of taproots belongs to the angular pattern of roots and the minimum belongs to the mixed pattern.

The displacement loss due to the removal of taproot is nearly 13%. The maximum taproot effect on displacement belonged to the mixed pattern and the minimum belonged to the angular pattern of roots.

The maximum root anchorage is illustrated in the angular root pattern with 15.55% in compared with the horizontal root pattern due to the effect of friction on the root anchorage process.

c) The effect of root angle of inclination

Roots located deeper inside the soil contribute more anchorage strength because of the effects of the soil column weight in the upward part of the root.

Root deviation angle from $0°$ to $53°$ can increase the pulling out reaction force until 22.23% and after this, the pulling out reaction force begins to decrease.

Maximum root anchorage is illustrated in root pattern with deviation angle of $53°$ and the minimum occurred in the horizontal root pattern due to the effect of friction.

Combination of the outcome from this chapter shows that the most effective pattern for root anchorage is the angular pattern with taproot and angle of inclination that equals to $53°$.

7.1.4 The effect of soil matric suction and friction angle on root anchorage

Based on the numerical simulations of the soil–root system, the following conclusions are made:

The root anchorage capacity has a direct relationship with the soil cohesion and accordingly, the matric suction.

The relationship curve between the soil cohesion and maximum root anchorage in the soil indicates that when matric suction value increases, the soil cohesion rises causing the maximum pulling out force to also rise and consequently the root anchorage in the soil improves.

The soil cohesion value and accordingly matric suction announce a direct proportion to root anchorage. However, in soil with higher plasticity as CH (fat clay), the effect of soil cohesion on root anchorage is maximum. With the increasing silt content, when the plasticity is reduced, the matric suction effect decreases.

Root anchorage decreased with the increasing of the saturation which is resulted in increasing the matric suction and respectively soil cohesion (c). Therefore, anchorage minimum value reaches under the saturated condition.

In respect to the soil friction angle, root models with a deviation angle of $15°$ display more effects on increasing the pulling out force than root models with a deviation angle of $53°$ during increase on the matric suction value. In other word, the friction angle change does not illustrate any effect on the root anchorage in roots with larger angle of inclination ($53°$) due to the bearing capacity effect.

However, the maximum value of the pulling out force belongs to the root model with a deviation angle of $53°$.

Soil friction angle was affecting the root anchorage only in horizontal roots or roots with steep deviation angle due to the effect of soil friction angle on the bearing capacity and consequently, the root anchorage. This effect has a direct relationship with the maximum pulling out force and simultaneously the roots anchorage.

The cohesion coefficient change (matric suction) is more effective than the friction angle for improving the root anchorage

The anchorage in soil is affecting mostly until the soil become failure. Therefore, the effect of soil cohesion is more than the effect of friction angle.

7.2 Recommendation for further works

In general, more species need to be tested to validate our model and more elaborated pore-viscoplastic models can be developed to incorporate the effects of pore water in the mechanisms of uplifting. To also predict more accurate result, the determination of the correct mechanical properties for the root and soil is important.

Due to the assignment of root mechanical properties, the tensile machine Instron with a flat clamp is performed during this study. To get a more accurate result, the special clamp should be designed and use for root tensile test. With the normal flat clamp, it is difficult to test the root because either the root skin is delaminated from the root body or the root body was crushed, consequently the rapture occurs at the incorrect places. Therefore we need to conduct various tests to obtain statistically correct results for the roots mechanical characteristics.

On the other hand, as it will take years for the vegetation to grow, it is possible to use artificial anchors in simple forms, various materials as aluminium PVC to replace the natural root in anchorage process. The materials and forms can be examined to understand the best effect on the anchorage capacity.

Researches can also be done for other groups of plants, as plants with deeper or thicker roots to determining the ratio of the pulling out force increases in respect to the increase in the root diameter.

REFERENCES

Abe Kazutoki and Ziemer. Robert R. (1991). Effect of tree roots on a shear zone: modeling reinforced shear stress. Canadian Journal of Forest Research (21) , 1012-1019.

Achim A., Ruel J.C., Gardiner B.A. (2005). Evaluating the effect of precommercial experimentation, modelling, and development of simple indices. Canadian Journal of Forest Research 35 , 1844-1853.

Anderson M.G. and Lloyd D.M. (1991). Using a combined slope hydrology-stability model to develop cut slope design charts. Proceedings - Institution of Civil Engineers , 91 , 705-718.

Audi Munir, B. M. (2009). Site Investigation, Sampling and Slope Stability Analysis at kilometer 141 141 KL-Kuantan highway. Pahang: Faculty of Civil & Earth Resources Universiti Malaysia, Pahang.

Barnes, G. (2000). Soil Mechanics: Principles and Practice, Second Edition. Palgrave Macmillan.

Bathe K.J. and Wilson E. L. (1973). Solution methods for eigenvalue problems in structural mechanics. International Journal for Numerical Methods in Engineering, 6 , 213-226.

Bathe K.J. and Wilson E.L. (1976). Numerical methods in finite element analysis. Englewood cilffs: Prentice-Hall Inc.

Bishop A. W. and Morgenstern N. (1960). Stability Coefficients for Earth Slopes. Geotechnique Vol 10, No. 4 , 129-150.

Bishop, A. (1959). The principle of effective stress. Teknisk Ukeblad,106(39) , 859-863.

Bowles, J. E. (1996). Foundation Analysis and Design(5th.edition). New York: Mc-Graw Hill.

Brenner, R. (1973). A Hydrological model study of a forested and a cutover slope. Hydrological Sciences Journal, Vol.18, Issue 2 , 125-144.

Chia-Cheng Fan and Chih-Feng Su. (2008). Role of roots in the shear strength of root-reinforced soils with high moisture content. Ecological engineering 33 , 157-166.

Coduto, D. P. (1998). Geotechnical Engineering:Principles and Practices. New jeresy: Prentice Hall.

Coppin N.J.and Richards I.G. (1990). Use of vegetation in civil engineering. London: Butterworths.

Coutts, M. P. (1986). Components of tree stability in Sitka spruce on peaty gley soil. Forestry 59 , 173-197.

Coutts, M. P. (1983). Root architecture and tree stability. Plant and Soil 71 , 171-188.

Crook M. J. and Ennos A. R. (1996). The anchorage mechanics of deep rooted larch, Larix europea X L. japonica. Journal of Experimental Botany 47 , 1509-1517.

Danjon F., Fourcaud T., Bert D. (2005). Root architecture and windfirmness of mature Pinus pinaster Aı¨t. New Phytologist 168 , 261-269.

Der-Guey Lin, Bor-Shun Huang, Shin-Hwei Lin. (2010). 3-D numerical investigations into the shear strength of the soil–root system of Makino bamboo and its effect on slope stability. Ecological Engineering 36 , 992-1006.

Dupuy L., Fourcaud T., Lac P., Stokes A. (2007). A generic 3D finite element model of tree anchorage integrating soil mechanics and real root system architecture. American Journal of Botany 94 , 1506-1514.

Dupuy L., Fourcaud T., Stokes A. (2005a). A numerical investigation into factors affecting the anchorage of roots in tension. European Journal of Soil Sciences 56 , 319-327.

Dupuy L., Fourcaud T., Stokes A. (2005b). A numerical investigation into the influence of soil type and root architecture on tree anchorage. Plant and Soil 278 , 119-134.

Dupuy L., T. Fourcaud, A. Stokes. (2005). A numerical investigation into factors affecting the anchorage of roots in tension. European Journal of Soil Science 56: , 319-327.

Faisal Hj. Ali, Bujang B.K. Huat , R.S.K. Rajoo. (2006c). Stability Analysis and Stability Chart for Unsaturated Residual Soil Slope. American Journal of Environmental Sciences 2 (4) , 154-160.

Faisal Hj. Ali,Thamer Ahmed Mohamed Hashim , Bujang B.K. Huat. (2006a). Relationship Between Shear Strength and Soil Water Characteristic Curve of an Unsaturated Granitic Residual Soil. American Journal of Environmental Sciences 2 (4) , 142-145.

Faisal Hj.Ali, Bujang B. K. Huat , T. H. Low. (2006b). Water infiltration characteristics of unsaturated soil slope and its effect on suction and stability. Geotechnical and Geological Engineering ,24 , 1293-1306.

Faisal Hj.Ali, Saravanan M., Low Tian Hut. (1999). Influence of soil suction on shear strenght of residual soils. Kuala Lumpur: World Engineering congress.

Faisal Hj.Ali. and Normaniza O. (2009). Incorporation of the soil-root matrix reinforcement effect into the slope stability analysis. Kuala Lumpur, Technical report presented to Public Works Department Malaysia.

Fourcaud T., J.N. JI, Z.Q. Zhang, A. Stokes. (2008). Understanding the impact of root morphology on overturning mechanisms: a modelling approach. Annals of Botany,Volume101, Issue 8 , 1267-1280.

Fourcaud T., L. Dupuy, D. Sellier, P. Ancelin , P. Lac. (2003b). Application of plant architectural models to biomechanics. Proceedings of international symposium on plant growth modeling, simulation, visualization and their applications (pp. 462-479). Beijing, China: Tsinghua University press.

Fourcaud T., P. Lac, P. Caste´ra , P. De Reffye. (2003a). Numerical modelling of shape regulation and growth stresses in trees. II.Implementation in the AMAPpara software. Trees—Structure and Function 17 , 31-39.

Fredlund D. G. and Hardy R. M. (2000). The 1999 R.M. Hardy Lecture: the implementation of unsaturated soil mechanics into geotechnical engineering. Canadian Geotechnical Journal, vol. 37, no. 5, 963-986.

Fredlund D.G.and Morgenstern N.R. (1978). Stress state variables for unsaturated soils. geotechnical engineering Div. Am. Soc. Civ. Eng.

Gasmo J. M., Tahardjo H., Leong E. C. (2000). Infiltration effects on stability of a residual soil slope. Computer and Geotechnics, vol. 26, no. 2, 145-165.

Graf Frank, Frei Martin, Böll Albert. (2009). Effects of vegetation on the angle of internal friction of a moraine. Journal Forest Snow and Landscape Research. 82,1, 61-77.

Gray, D. H. (1973). Reinforcement and Stabilization of Soil by Vegetation. Geotechnical Engineering Vol.100 No.GT6, 695-699.

Gray D.H., A.T. Leiser, C.A.White. (1980). Combined Structural-Vegetative Slope Stabilization. Civil Engineering-ASCE, Vol.52, No.1, 82-85.

Gray, D.H. (1995). Influence of vegetation on the stability of slopes. In D. Barker, Vegetation and slope, Stability, Protection and Ecology, London: Thomas Telford. (pp. 2-12)

Gray D. H. and Harukazu Ohashi. (1983). Mechanics of Fiber Reinforcement in Sand. Journal of Geotechnical Engineering, Vol. 109, No. 3, 335-353.

Gray D. H., Robbin B. Sotir . (1996). Biotechnical and Soil Bioengineering Slope Stabilization: A Practical Guide for Erosion Control. New York: John Wiely & sons, ink.

Greenway, D. R. (1987). Vegetation and Slope Stability. In M. G. Richards, Slope Stability: Geotechnical Engineering and Geomorphology (pp. 187-230). New York: John Wiley and Sons.

Greenwood, J. R. (2004). "A Program for Routine Slope Stability Analysis to Include the Effects of Vegetation, Reinforcement and Hydrological Changes. Eco-and Ground Bio-Engineering: The Use of Vegetation to Improve Slope Stability"Proceedings of the First International Conference on Eco-Engineering 13–17 September 2004" (pp. 193-203). Dordrecht: Springer.

Greenwood John R., Joanne E. Norris, Jo Wint. (2004). Site Investigation for the Effects of Vegetation on Ground Stability. Eco-and Ground Bio-Engineering: The Use of Vegetation to Improve Slope Stability"Proceedings of the First International Conference on Eco-Engineering 13–17 September 2004" (pp. 203-213). Dordrecht: Springer.

Hansen J. Brinch (1961). A General formula for bearing capacity. Danish geotechnical institute Bulletin No.11, 38-46.

Haisler W. E., Stricklin J. A. , Key J. E. (1977). Displacement incrementation in non-linear structural analysis by the self-correcting method. International Journal for Numerical Methods in Engineering, 11, 3-10.

Hamza O., A.G. Bengough, M.F. Bransby, M.C.R. Davies, P.D. Hallett. (2007). Mechanics of root-pullout from soil: A novel image and stress analysis procedure. Eco-

and Ground Bio-Engineering: The Use of Vegetation to Improve Slope Stability"Proceedings of the First International Conference on Eco-Engineering 13–17 September 2004" (pp. 213-223). Dordrecht: Springer.

Jennings J.E. and Burland J.B. (1962). Limitation to the use of effective stress in partly saturated soils. Geotechnique Vol.12 , 125-144.

Johansson, J. (2000, January 27). Soil Improvement Techniques. Retrieved May 9, 2010, from Soil Lequifaction web site: http://www.ce.washington.edu/~liquefaction/html/how/soilimprovement.html

Kamal Hossein, (2010). Effect of Rainfall on Matric Suction and Stability of a Residual Granite Soil Slope. DUET Journal, 37-41.

Kachanov, L. M. (2004). Fundamentals of the theory of plasticity. New York: Dover Publications Inc.

Kazimi, S. M. (1982). Solid Mechanics. New Delhi: Tata McGraw-Hill.

Khuder H., Stokes A., Danjon F., Gouskou K., Lagane F. (2007). Is it possible to manipulate root anchorage in young trees? Plant and Soil 294 , 87-102.

Khalilnejad A, Faisal HJ Ali, Normaniza O. (2012). Contibution of the root to slope stability. Geotechnical and Geological Engineering Vol.30, No.2, 277-288.

Khalilnejad A, Faisal HJ Ali, Normaniza O. (2012). Finite element simulation for contribution of matric suction and friction angle to stress distribution during pulling-out process. International Journal of Geomechanics (ASCE), DOI: 10.1061/(ASCE)GM.1943-5622.0000243.

Kirsten L. and Fourie L. (1999). The strength of root reinforced soil. Proceeding Third Conference on Environmental Engineering (p. 10pp). Kwa Maritane.

Landsildes in Malaysia. (2012, April 3). Retrieved April 20, 2012, from Wikipedia: http://en.wikipedia.org/wiki/Landslides_in_Malaysia#Events

Li Jinyu, Yang Qing, Luan Maotian. (2010). Limit Equilibrium Analysis of the Influence of Matric Suction on Unsaturated Soil Slope Stability. Journal of Convergence Information Technology,Volume 5 , 167-175.

Li S.C., Sun H.L., Yang Z.R., Xiong W.L., Cui B.S. (2007). Root anchorage of Vitex negundo L. on rocky slopes under different weathering degrees. Ecol. Eng. 30 , 27-33.

Li A.G., Z.Q. Yue, L.G. Tham, C.F. Lee, K.T. Law. (2005). Field-monitored variations of soil moisture and matric suction in a saprolite slope. Canadian Geotechnical Journal Vol. 42 , 13-25.

Lindeburg, M. R. (2001). Civil Engineering Reference Manual for the PE Exam . CA: Professional Publications.

Mattheck Claus and Breloer Helge (1995). The Body Language of Trees: A handbook for failure analysis. London: HMSO.

Matyas E.L. and Radhakrishna H.S. (1968). Volume change characteristics of partially saturated soils. Geotechnique, Vol.18, Issue 4 , 432-448.

Mase George Thomas, Mase George E. (2002). Continuum mechanics for engineers. Boca Raton: CRC press LLC.

Michalowski R.L. and Cermak J. (2003). Triaxial compression of sand reinforced fibres. Journal of Geotechnical and Geoenvironmental Engineering. 129 , 125-136.

Michalowski, R. (1997). Limit stress for granular composites reinforced with continuous filaments. Journal of Engineering Mechanics , 852-859.

Mottershead J.E. and Stanway R. (1986). Identification of combined viscous and Coulomb friction - a numerical comparison of least-squares algorithms. Transactions of the Institute of Measurement and Control, vol. 8, no. 1 , 9-16.

Moaveni, S. (2008). Finite element analysis. New Jersy: Pearson Prentice Hall.

Moor, J. (2000). Effects of soil type of the root anchorage strength of Pinus radiata. Forest Ecology and Management 135 , 63-71.

Morgan, R. (2007). Vegetative-based technologies for erosion control. Eco-and Ground Bio-Engineering: The Use of Vegetation to Improve Slope Stability"Proceedings of the First International Conference on Eco-Engineering 13–17 September 2004" (pp. 265-273). Dordrecht: Springer.

Nicoll B. C. and D. Ray. (1996). Adaptive growth of tree root systems in response to wind action and site conditions. Tree Physiology , 891-898.

Nicoll B.C., Gardiner B.A., Rayner B., Pearce A.J. (2006). Anchorage of coniferous trees in relation to species, soil type, and rooting depth. Canadian Journal of Forest Research 36 , 1871–1883.

Ning Lu and Likos William J. (2006). Suction stress characteristics curve for unsaturated soil. Journal of geotechnical and geoenvironmental engineering , 131-142.

Nordin, A. (1995). Slope instability problems-the Malaysian experience. In D. Barker, Vegetation and slopes, Stabilization, Protection and Ecology (pp. 264-270). London: Thomas Telford.

Nordin, A, Normaniza, O. , and Faisal, H.A. (2011). Soil-root shear strength properties of some slope plants. Sains Malaysiana. 40 (10), 1065-1073.

Normaniza, O. (2005). The Contribution of Leucaena leucocephala (Lam.) de Wit to Slope Stability. (PhD Thesis). Kuala Lumpur: UM.

Normaniza O.and Barakbah S.S. (2006). Parameters to predict slope stability—soil water and root profiles. Ecol. Eng. 28 , 90-95.

Normaniza Osman, Mohamad, N.A. and Che Hassandi, A. (2011). Pull-out and tensile strength properties of two selected tropical plants. Sains Malaysiana. 40(6), 577-585.

Normaniza, O. and Barakbah, S.S. . (2011). The effect of natural succession on slope stability. Ecological Engineering 37, 139-147.

Oden J.T. and Ripperger E. A. (1981). Mechanics of elastics structures. New York: Mc-Graw Hill Inc.

Owen D.R.J. and Hinton E.. (1986). Finite element in plasticity. Swansea: Prineridge Press Limited.

Poulos H.G. and Davis E.H. (1974). Elastic Solutions for Soil and Rock Mechanics. New York: John Willey & Sons, Inc.

Rahmanian Saeed and Maleki Mohamad. (2007). ABAQUS Finite Element Software. Tehran: Simaye Danesh.

Rees, D. W. (2006). Basic engineering plasticity: an introduction with engineering and manufacturing applications. Oxford: Elsevier.

Ruel J.C., Larouche C., Achim A. (2003). Changes in root morphology after precommercial thinning in balsam fir stands. Canadian Journal of Forest Research 33 , 2452-2459.

Sasan Moafian, Bujang B.K. Huat, Vahed Ghiasi. (2009). Evaluation on Root Theories and Root Strength Properties in Slope Stability. European Journal of Scientific Research Vol.30 No.4 , 594-607.

Sellier D. , T. Fourcaud, P. Lac. (2006). A finite element model for investigating effects of aerial architecture on tree oscillations. Tree Physiology 26 , 799 – 806.

Schor Horst J. and Gray D. H. (1995). Landform grading and slope evolution. Journal of geotechnical engineering , 729-734.

Siti Sara Mustapa Kamal, Faisal Ali and Normaniza Osman. (2010). Model Study on Root Pullout Failure. GEOTROPIKA Kota Kinabalu, (p. 69). UTM.

Skempton A. W. and Hutchinson J. (1969). Stability of natural slopes and embankment foundations. Soil mechanics & foundation engineering conference proceeding/Mexico/ (pp. 291-340). Berkshire: TRID.

Skempton, A. (1960). "Terzaghi's discovery of effective stress." in from theory to practice in soil mechanics. New York: John Willey and Sons.

Smith, D. C. (1978). Shore erosion control demonstrations in Florida. Gainesville, Florida: USDA Soil Conversation Service.

Stokes A. and Guitard D. (1997). Tree root response to mechanical stress. In A. A. Waisel, Biology of Root Formation and Development (pp. 227–236). New York: Plenum Press.

Stokes A., A. H. Fitter, M. P. Coutts. (1995). Responses of young trees to wind and shading: effects on root architecture. Journal of Experimental Botany 46 , 1139-1146.

Stokes A., Berthier S., Sacriste S., Martin F. (1998). Variations in maturation strains and root shape in root systems of Maritime pine (Pinus pinaster Ait.). Trees Struct. Funct. 12 , 334-339.

Stokes, A. (1999). Strain distribution during anchorage failure of Pinus pinaster Ait. at different ages and tree growth response to wind induced root movement. Plant and Soil 217 , 17-27.

Sweeney, D. (1982). Some in situ soil suction measurements inHong Kong's residual soil slopes. 7th Southeast Asia Geotechnical Conference.vol.1 (pp. 91-106). Hong-Kong: SEAGS.

Tobias S. (1995). Shear strenght of the soil root band system. In D. Barker, Vegetation and slopes, Stability, Protection and Ecology (pp. 280-287). London: Thomas Telford.

Tang C., Shi B., Gao W., Chen F., Cai W. (2007). Strength and mechanical behavoir of short polypropylene fiber reinforced and cement stabilized clayey soil. Geotextiles and Geomembranes , 194-202.

Terzaghi, K. V. (1943). Theoretical Soil Mechanics. New York: John Wiley and Sons.

Tezcan S.S. and Ozdemir Z. (2011, 5). A Refined Formula for the Allowable Soil Pressure Using Shear Wave Velocities. The Open Civil Engineering Journal, 1-8.

Tsaparas, H. Rahardjo, D. G. Toll, E. C. Leong. (2002). Controlling parameters for rainfall-induced landslide. Computer and Geotechnics, vol. 29, no. 1 , 1-27.

Waldron L. J.and Dakessian S. (1981). Soil Reinforcement By Roots: Calculation of Increased Soil Shear Resistance From Root Properties. Soil Science ;An Interdisciplinary Approach to Soil Research , 387-449.

Weimin Wu and Roy C. Sidle. (1995). A distributed slope stability model for steep forested basins. Water Resources Research Vol.31 No.8 , 2097-2110.

Wu, H. (2007). Root reinforcement: analyses and experiments. Eco-and Ground Bio-Engineering: The Use of Vegetation to Improve Slope Stability"Proceedings of the First International Conference on Eco-Engineering 13–17 September 2004" (pp. 21-31). Dordrecht: Springer.

Zienkiewicz O.C. and Taylor R.L. (2000). Finite Element Method (5th Edition) Volume 1 - The Basis. Barcelona: Butterworth-Heinemann.